Vibration fatigue testing and modelling for identification of damage initiation and propagation in fiber reinforced plastics

T.C.P. Masmeijer
July 2021
University of Twente
Engineeringing Technology
Mechanical Engineering
Dynamic Based Maintenance

Master Thesis

Graduation committee

Chairman:	dr.ir. R. Loendersloot
Supervisor:	dr. D. Di Maio
External member:	dr.ir. W.J.B. Grouve

SUMMARY

This thesis investigates the crack initiation and propagation of interlaminar delamination of thermoplastic PEEK cross-ply components. One of the main objectives is to understand the rate of delamination carried out under fatigue vibration testing. The experimental methods encompass several different measurement techniques such as Experimental Modal Analysis, High Cycle Fatigue, and Continuous Scanning Laser Doppler Vibrometry.

This thesis proposes a new workflow to breakdown the experimental procedure in set of blocks. The ambition is to overcome time-consuming transient analysis to investigate how the interface forces at the delamination crack tip develops under fully reversible loading conditions such as R=-1.

Several results will be presented and discussed throughout the thesis, each time indicating advantages and disadvantages of the proposed framework to analysis fatigue crack growth.

Nomenclature

α	Displacements scaler of the Numerical ODS
β	Scan path length scaler of the experimental ODS
η	BK-powerlaw coefficient
γ	Shear strain
μ	Friction coefficient
ν	Poisson ratio
Ω	Scan Rate of Line Scans
ω	Excitation frequency in Rad
Ω_d	Dimensionless frequency
ϕ	Dynamic Phase of response
ϕ_{lim}	Minimum phase before updating the excitation frequency in the Numerical Model
ϕ_{ref}	Reference phase of each segment in the endurance test
σ	Stress
σ_{max}	Maximum stress during cyclic loading
σ_{min}	Minimum stress during cyclic loading
CFRP	Continuous Fiber Reinforced Plastics
CSLDV	Continuous Scanning Laser Doppler Vibrometry
EMA	Experimental Modal Analysis
FRF	Frequency Response Function
MAC	Modal Assurance Criteria
ODS	Operating Deflection Shape
SDOF	Single Degree Of Freedom
SSD	Steady State Dynamics
ε	Strain
ζ	Damping ratio
a	Crack Length

b	Width of the numerical model
C	Intercept of Paris-Erdogan law
c	Damping coefficient
d	Horizontal distance between the nodes
d_s	Nearest distance between the fixture and the scan path
E	Young's Modulus
$F(t)$	External force on SDOF system
F	Forces on node at crack tip
f	Fracture criterion
F_0	Amplitude of external force on SDOF system
f_{exc}	Excitation frequency in Hertz
f_n	Natural frequency
G	Shear Modulus
G	Strain Energy Release Rate (SERR)
G_I	Opening component of SERR
$G_{eq,c}$	Critical Equivalent Strain Energy Release Rate
G_{eq}	Equivalent Strain Energy Release Rate
G_{II}	Shearing component of SERR
k	Stiffness
K_{max}	Maximum stress concentration at the crack tip
L	Length of specimen
L_p	Scan path length of Line Scans
m	Total mass in Equation of Motion of SDOF system
N	Number of cycles
n	Slope of Paris-Erdogan law
R	Loading Ratio
T_{cycle}	Duration of one oscillation during cyclic loading
v	Velocity of vibration
V_A	Measured ODS
V_I	Imaginary displacements of ODS
V_R	Real displacements of ODS
V_X	Polynomial fit of ODS (or some other reference ODS)
X	Displacement of the SDOF system in the free direction
z	Thickness coordinate of plate

Contents

1 INTRODUCTION

It is essential in the aviation industry to design lightweight structures to reduce the required fuel for flight. For this reason composite materials are widely used for their extreme high stiffness. To achieve a minimal mass the industry pushes the composites to their mechanical limit. However, in aviation, where failure of components can have catastrophic impacts, the need for safety is paramount. So, in order to design efficient and reliable components it is of the utmost importance to be able to predict the total life of a component. For this, an engineer needs a thorough understanding of the fatigue behaviour of materials. Extensive research is done on fatigue to achieve this. It seems unquestionable that a certain amount of damage accumulates in composites laminates during the operational conditions, but in many practical cases that accumulation is not critical for the structural integrity. Nevertheless, design criteria are still based on no-damage growth simply because any uncertainty of damage growth cannot be tolerated. One of the main complications of fatigue testing is its time consuming nature. In standard fatigue testing the loading rate is low, generally five to ten cycles per second, with the goal to annihilate the inherent self-heating. The material properties of visco-elastic material are time-temperature dependent and the damage growth would be biased by the effect of the inherent self-heating. Additionally, the higher frequencies come with a low-transfer of forces onto a specimen, making conducting the tests more challenging. Furthermore, the material testing is based on coupons which are never representative of the true behaviour of component responses, as reported in [1].

Nevertheless, Di Maio et al. [2, 3, 4] have proved in several researches that harmonic tests allow investigating the fatigue damage growth with high accuracy. In their work the resonant features of coupons are exploited. Allowing for tuning the loading frequencies to more than 10 times faster. This has an immediate effect on the total required testing time and on the required input energy to achieve a high amplitude vibration that will induce fatigue. A main cause of fatigue failure in components are resonant vibration, for example in helicopter rotor blades or aero-engine blades. This makes testing under resonant conditions the logical next step. The major innovation of Di Maio et al. [2] was to exploit the monitoring of the harmonic response phase between the input excitation and output response to evaluate the level of damage accumulation in composite component subjected to fatigue throughout a test. A breakthrough not presented anywhere before. Most of the research was focused on thermosets, but it is assumed that the same testing methodology can be applied to thermoplastics. On top of that has the method shown that the damage propagation stays at the fibre-matrix interface, making it an especially consistent testing method.

This thesis will elaborate upon this vibration fatigue testing by applying it on a continuous fibre reinforced plastic. In these tests the dynamic parameter phase, which is highly sensitive to a reduction of stiffness, is traced throughout an endurance test. Classically failure stages in fatigue is split into initiation, propagation and final failure [5]. In this thesis it was found that the distinction between initiation and propagation was especially vague. This thesis will investigate the effect of self-introduced damage on the damage development during fatigue tests. Furthermore, this thesis will investigate the development of the damage initiation and propagation by tracing the dynamic property phase during a fatigue test and relating it to a reduction of stiffness. Separately, the damage propagation will be modeled with a numerical framework, with the goal to eradicate the need for any highly time consuming transient analysis. The framework will find a relation between the measured phase drop and crack propagation. From classical fracture mechanics it is known that the crack propagation rate is greatly influenced by the strain energy release rate at a crack tip [6]. The mixed mode characteristics of this parameter are of interest to understand the underlying physics of crack propagation. Therefore, this parameter will be modeled throughout an endurance test in a numerical framework. On top of that will this thesis further develop an experimental approach to determine the strain energy release rate, with the goal of eliminating the need for numerical models. Separately, this thesis will investigate the feasibility of using modal tests to find non-linearity in the vibration response, which could be an indicator of damage in the material.

1.1 Goal of the study

Based on this introduction the following research question is established:

Can we characterize the crack initiation and propagation during vibration fatigue loading in Continuous Fibre Reinforced Polymers and can we understand the underlying physics behind this?

In order to give more detail on this question, it is split up into sub-questions. The sub-questions, along with the approach to answer these question, are established as:

1. *What is the damage initiation and propagation in cross-ply components made of PEEK materials during vibration fatigue?*
   How the damage initiation phase shifts into the propagation phase is currently unknown for cross-ply components made of PEEK materials. It is unknown if the harmonic-driven fatigue tests are valid for thermoplastic material. The question will be answered by conducting endurance tests on coupons. During the development of damage in the tests, both initiation and propagation, the dynamic parameter phase is tracked. The phase is an especially sensitive parameter to a reduction of stiffness. A numerical framework will establish a relation between this phase and a crack length.

2. *What is the effect of a defect introduced by the manufacturing process in terms of damage growth?*
   In accordance to the HEGEL CS2 Grant, Agreement no: 738130 [7], specimens are produced made with a cut ply, which fixes the damage location to one specific place. During testing a first initiation of the damage will occur, before shifting to damage propagation. The differences in phase development during endurance tests that had low and high initial damage will be compared to answer the question.

3. *Can we exploit modal test methods to evaluate change of surface strain caused by delamination growth?*
   A parameter heavily related to the damage initiation and propagation is found in the strain energy release rate at the crack tips. Usually, this parameter is calculated. Enabling the possibility to determine this parameter with experiments would make these calculations unnecessary. A step towards determining this parameter is by determining the surface strain along the beam.

4. *Can we detect a delamination in the material directly from modal tests?*
   It is suspected that under a vibration load a delamination in the material will cause a non-linear harmonic vibration. By detecting this non-linearity the crack length in the material could be determined. This question will be answered by analysing the results of modal tests conducted on coupons.

5. *What are the interface forces acting at the crack tip while the delamination is artificially propagated?*
   The forces governing the crack propagation will give insight in the underlying physics behind crack propagation. Mode mixity caused under fully reversible and high frequency conditions is investigated by setting up a numerical framework. The underlying physics behind the initiation phase is out of the scope of this thesis.

1.2 Outline

The thesis is outlined as follows. The theoretical background in chapter 2 will go through the main references about fatigue damage growth testing and analysis methods, vibration fatigue, visco-elasticity, the fracture mechanics modelling technique: Virtual Crack Closure Technique (VCCT), and the modal test method: Continuous Scanning Laser Doppler Vibrometry. In chapter 3 the design and manufacturing of the thermoplastic laminates will be presented indicating the challenges to achieve adequate cross-ply configuration and their effect in terms of vibration response. The harmonic test method will be described and some preliminary results are discussed, highlighting the sensitivity of the response phase to the damage growth. Furthermore, modal measurements will be presented and discussed. Next, in chapter 4 the numerical framework will be presented. The FEM model and the types of analysis are discussed. Some preliminary results of the frameworks components are presented as well. In chapter 5 the results of both the experimental and numerical investigation are investigated. Finally, conclusions will be discusses on the basis of the research questions and recommendations will present the shortfalls in the choice of the material selection (PEEK), the chosen lay-up, the use of optical microscope, and non-steady state testing conditions.

2 THEORETICAL BACKGROUND

As this thesis reports on fatigue damage growth of thermoplastics composites subjected to harmonic oscillations a general understanding of these topics are required. Therefore this chapter will discuss all necessary subjects point by point. An introduction to composite materials is given, including their characteristic linear solid mechanics. Then, to understand crack growth in composites the fracture mechanics of composites are discussed. The fracture mechanics are numerically modelled in this thesis using the Virtual Crack Closure Technique (VCCT). The theory of this technique will be discussed.
The failure mechanisms behind fatigue in composite materials are described. An increased loading rate of the fatigue testing causes the visco-elasticity of the thermoplastic to play a role, so a section is dedicated to this topic.
A brief account of structural dynamics will be given to introduce the non-expert readers to the most relevant theories exploited during both the simulations and experiments. The major relevant testing methods and measurement parameters will be discussed as follows: Response phase sensitiveness to the damage onset, experimental modal analysis and Continuous Scanning LDV.

2.1 Introduction to composites

Composite materials are produced from multiple constituents. Its constituents have distinct different material properties. Combining the properties of each material enhances the properties of the combined part. Composites exists naturally in nature in the form of for instance wood. It consists of cellulose fibers in a lignin and hemicellulose matrix. However this thesis will focus on the man manufactured Fiber Reinforced Plastic.

2.1.1 Continuous Fiber Reinforced Plastic

This thesis focus on Continuous Fiber Reinforced Plastics (CFRP's). These types of material get their stiffness and strength from their fibers, which form the backbone of the structure. The fibers are packaged in the compliant and formable plastic, also called the resin or matrix material. The combination forms the best of both worlds: a material that is very stiff and is very formable. The application of the material can be found mainly, but not exclusively, in aviation, sports and the automotive industry. The main difference between a thermoplastic and a thermosets is that a plastic consists of unlinked chains of molecules and thermosets are a network of linked chains of molecules. Where a thermoplastic can be reformed after reheating, the manufacturing process of the thermoset is irreversible.
CFRP's can be arranged into composite laminates, into which fibers are orientated in specific directions. This provides required engineering properties in different directions, or more specifically, the individual laminates have orthotropic mechanical properties, as discussed in section 2.1.2. The arrangement can be achieved by just laying the fibers parallel in a single direction, called unidirectional plies, or specific weaves can be used to achieve varying properties. In this thesis unidirectional tapes made from standard modulus carbon fiber in a PEEK plastic were

provided by TPRC. These tapes are designed to be used with the in situ consolidation, press molding, and autoclave manufacturing processes. The specimens in this thesis are manufactured with the press molding process. With this process unidirectional tapes are stacked in a mould in the described stacking sequence. The tapes are already surrounded with the plastic filler material. The plastic consolidates when the mould is heated and pressurised, forming the part. The chosen manufacturing process caused problems in the specimen, which are discussed in the experimental investigation in section 3.2.
According to the manufacturers' specifications as set out in Appendix A PEEK is a thermoplastic with excellent mechanical properties, making it an attractive material in demanding applications, such as aviation. The semi-crystalline nature of the resin gives PEEK an excellent resistance to chemicals and solvents, and an excellent performance in flammability properties. PEEK is also exceptionally resilient [8].

2.1.2 Orthotropic Linear Solid Mechanics

Orthotropic materials are characterized by the fact that in a point in the material properties are different for three orthogonal axes. The linear solid mechanics of orthotropic materials used in this thesis are set out. First the stress-strain constitutive equations, followed by strain relations for thin plates.
The individual laminates in composite materials have three symmetry planes, i.e. they are orthotropic properties. This symmetry greatly reduces the constitutive equations. This relation is set out as the compliance matrix, which is the matrix that links the strain and stress as

$$\varepsilon_{ij} = \begin{bmatrix} \frac{1}{E_{11}} & \frac{-\nu_{12}}{E_{11}} & \frac{-\nu_{13}}{E_{11}} & 0 & 0 & 0 \\ \frac{-\nu_{21}}{E_{22}} & \frac{1}{E_{22}} & \frac{-\nu_{23}}{E_{22}} & 0 & 0 & 0 \\ \frac{-\nu_{31}}{E_{33}} & \frac{-\nu_{32}}{E_{33}} & \frac{1}{E_{33}} & 0 & 0 & 0 \\ 0 & 0 & 0 & \frac{1}{G_{12}} & 0 & 0 \\ 0 & 0 & 0 & 0 & \frac{1}{G_{23}} & 0 \\ 0 & 0 & 0 & 0 & 0 & \frac{1}{G_{31}} \end{bmatrix} \cdot \sigma_{ij}. \tag{2.1}$$

Note that ν_{ij} and ν_{ji} are not the same. However they are related with the symmetric properties of the compliance matrix as:

$$\frac{\nu_{12}}{E_{11}} = \frac{\nu_{21}}{E_{22}}; \frac{\nu_{23}}{E_{22}} = \frac{\nu_{32}}{E_{33}}; \frac{\nu_{31}}{E_{33}} = \frac{\nu_{13}}{E_{11}}. \tag{2.2}$$

These constitutive equations will be used in the numerical model. This model represents a thin beam subjected to bending. Using the plane stress conditions, the constitutive equations reduce to a 2D model. Plane stress can be applied when the stress vector along a particular plane approximates zero, which is the case in thin flat plates that are acted upon only by load forces that are parallel to them. When applying the plane stress conditions, the plane stress compliance matrix reduces to

$$\begin{Bmatrix} \varepsilon_1 \\ \varepsilon_2 \\ \gamma_{12} \end{Bmatrix} = \begin{bmatrix} \frac{1}{E_{11}} & -\frac{\nu_{12}}{E_{11}} & 0 \\ -\frac{\nu_{21}}{E_{22}} & \frac{1}{E_{22}} & 0 \\ 0 & 0 & \frac{1}{G_{12}} \end{bmatrix} \begin{Bmatrix} \sigma_1 \\ \sigma_2 \\ \sigma_{12} \end{Bmatrix} \tag{2.3}$$

and

$$\frac{\nu_{12}}{E_1} = \frac{\nu_{21}}{E_2}. \tag{2.4}$$

The strain can be determined from the displacements of a system using the displacement-strain relations. From classical theory [9] the following relation connects the displacement to strain for thin plates subjected to a bending load.

$$\varepsilon_x = z\frac{\partial^2 w}{\partial x^2}, \quad \varepsilon_y = z\frac{\partial^2 w}{\partial y^2}, \text{ and } \quad \gamma_{xy} = 2z\frac{\partial^2 w}{\partial x \partial y}. \tag{2.5}$$

Where for the top plate z is the thickness coordinate of the beam. The maximum strain is found at plus and minus half of the plate's thickness.
From classical theory [9] the strain energy is calculated according to

$$\begin{aligned} U =& \frac{D}{2}\int_A \left\{ \left(\frac{\partial^2 w}{\partial x^2} + \frac{\partial^2 w}{\partial y^2} \right)^2 \right. \\ & \left. -2(1-\nu)\left[\frac{\partial^2 w}{\partial x^2}\frac{\partial^2 w}{\partial y^2} - \left(\frac{\partial^2 w}{\partial x \partial y} \right)^2 \right] \right\} \mathrm{d}A \end{aligned} \tag{2.6}$$

2.2 Fracture Mechanics

Fracture mechanics is the field of mechanics concerned with the study of the propagation of cracks in materials. In 1957 Irwin [6] found a model to predict growth of a crack by partitioning the total energy in the material in two contributions, the stored elastic strain energy and the dissipated energy, comprising of surface energy and plastic deformation energy. He stated that the strain energy at the crack tip is released in order to create a new surface. Where a new surface means a propagated crack. This occurs when the strain energy at the crack tip exceeds the critical energy (G_c) of the material.
This insight was used later in the Paris-Erdogan research [10] where Irwin's Stress Intensity Factor K_{max} at the crack tip is used to predict the crack growth rate as:

$$\frac{da}{dN} = CK_{max}^n \tag{2.7}$$

Where the crack growth rate defines how much the crack length increases over each cycle and C and n are material properties found from experiments.
When referring to cracks the separation modes are distinguished as mode-I to III, where mode-I is opening, II is sliding and III is shearing. Parton [11] associates the separation modes for a practical case in wood, as depicted in figure 2.1. Here mode-I corresponds to the chopping of wood, II to planing, and III to cutting. Materials, especially if anisotropic, respond differently to these three modes. The importance of separating these separation modes, will be elaborated on with modelling of the fracture mechanics in section 2.3.4.

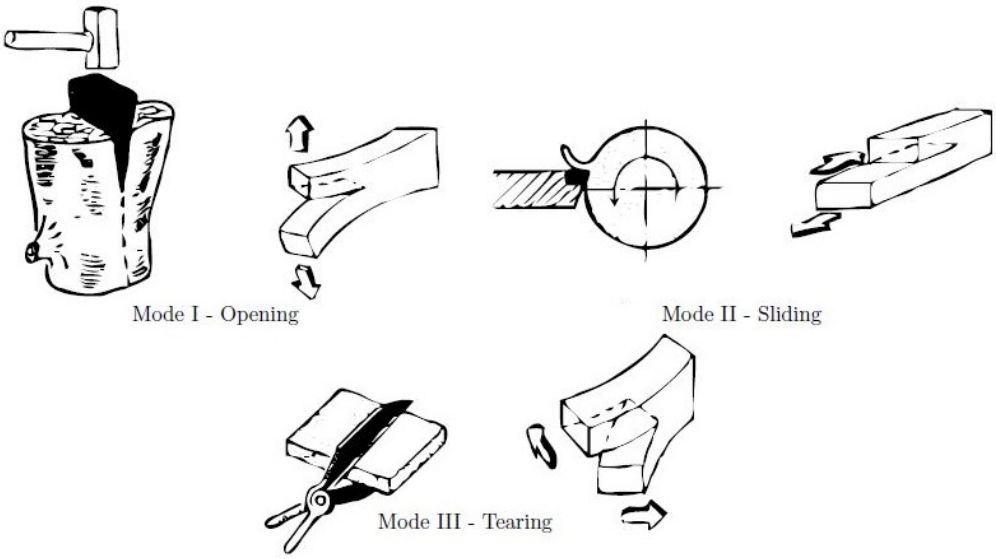

Figure 2.1: Schematic depiction of the three modes of crack separation as described by Parton [11].

2.3 Fatigue in Composites

Research on fatigue in composites is mainly an extension of the fatigue theory of metals. A summary of this theory and how it deviates from fatigue in material will be described.

2.3.1 Fatigue Process

Previously researchers used what was known about fatigue in metals and polymers to compare the fatigue damage behaviour of CFRPs. Plumbridge [5] identified the three stages of fatigue in metals as:

- **Crack initiation**. Locally the yield stress of a material is exceeded. This leads to dislocations in the crystalline structure, forming slip bands where the atomic layers are aligned.
- **Crack growth**. The atoms in near slip bands completely debond under cyclic loading. A crack now grows in a specific direction. The local stress becomes so high at some point that the grain alignment is ignored and the crack growth direction becomes normal to the main stress plane.
- **Final Failure**. Final failure occurs when the remaining load bearing material becomes so small that the stress in this location exceeds its ultimate strength.

The fatigue process in composites varies from this process. Since composites do not have a crystalline structure no crack initiation like this occurs. The initial cracks are formed due to pre-excising flaws or by reorganization of the molecular chains. A series of steps for the fatigue process in composites was proposed by Reifsnider [12] in 1980 which is more based on the anisotropic behaviour of the material rather than the stresses in the material. The consecutive phases of the fatigue process are described as:

1. Nucleation of the crack in off-axis plies (fig. 2.2a).
2. Saturation of the number of cracks at the Characteristic Damage State (CDS).

3. Coupling of cracks due to debonding at the fiber-matrix interface reaching the interface (fig. 2.2b).
4. Formation of a wider damaged region by the above process.
5. Crack growing through the thickness by crack coupling.
6. Final fractures of fibers in the direction of the load.

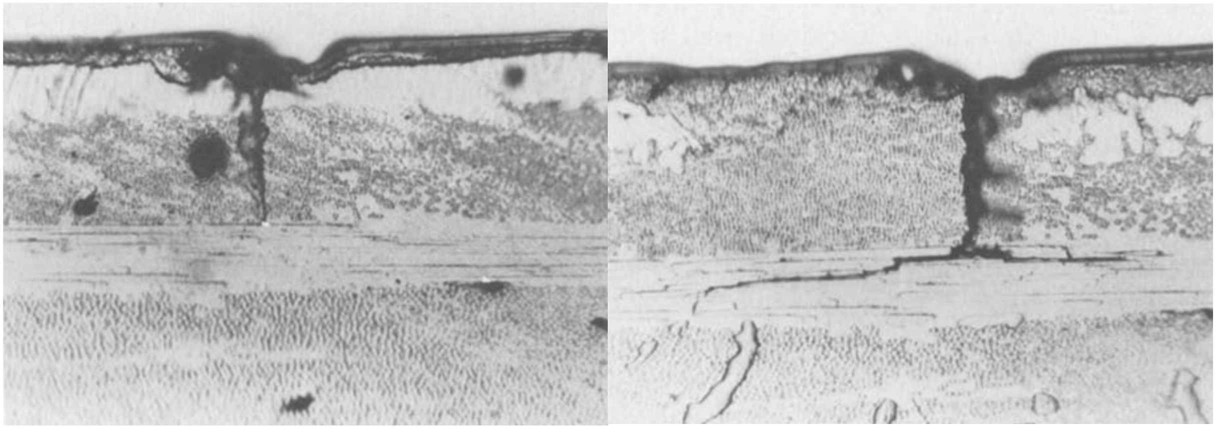

(a) (b)

Figure 2.2: (a) The nucleation of a transverse crack in the off-axis ply. (b) Coupling of the cracks due to debonding at the fiber matrix. Figures by Reifsnider [12].

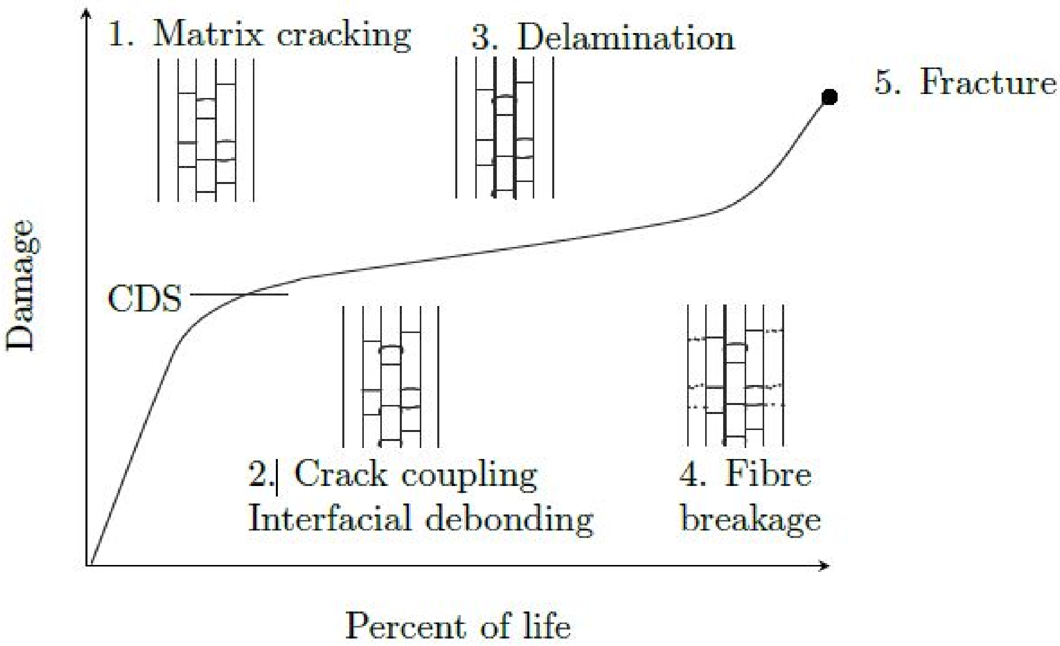

Figure 2.3: Development of damage in composites, as depicted by Stinchcomb [13].

The process is depicted schematically in figure 2.3. Mirco-cracks form in the weaker resin material. The crack propagates until it reach the stiffer fiber material. Since the cracks arrest at the fiber a concentration of smaller cracks occur, instead of one larger crack. After a number of cycles the concentration of micro-cracks saturates. This state is called the Characteristic

Damage State (CDS). The matrix material then debonds from the fiber material at the fiber matrix interface, called delamination. The maturing of the delamination will cause an increase in the stresses in the fiber, causing fiber breakage, after which final failure will occur.
Typically the fatigue life in metals is described by S-N curves. Where the ultimate strength of the material is related to the total number of cycles. Rather than stresses, Talreja [14] made use of the strain to get rid of the differences between the elastic modulus between of fibers and matrix material. A certain load subjected to a composite will cause different stresses throughout the different constituents, whereas the strain will be equal. This leads to Talreja modifying the typical S-N curves, to contain the maximum strain instead of the ultimate strength. A general Strain-Cycle curve is depicted in figure 2.4.

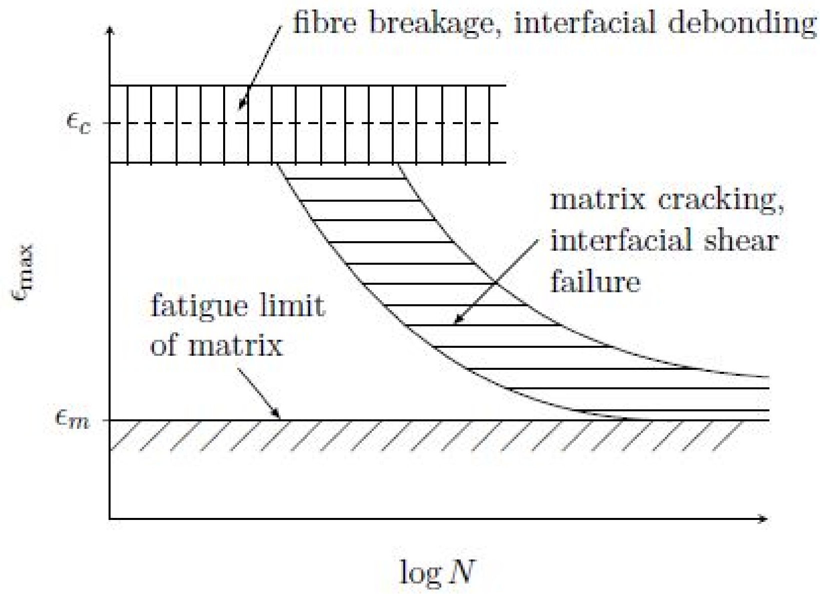

Figure 2.4: Schematic of the fatigue Life of composites as proposed by Talreja [15].

2.3.2 Cyclic Loading

During fatigue testing a specimen in subjected to a cyclic load. Loading conditions are usually described as the Loading Ratio R and the Excitation Frequency f_{exc} defined as

$$R = \frac{\sigma_{min}}{\sigma_{max}} \tag{2.8}$$

and

$$f_{exc} = \frac{1}{T_{cycle}} \tag{2.9}$$

respectively. Where σ_{min} and σ_{max} are the minimum and maximum stresses in the component and T_{cycle} the duration of one oscillation. Both parameters influence the total life of CFRP materials greatly. A high excitation frequency can heat the specimen, which affect the material properties of the thermoplastic material causing a decrease in life expectancy. More on the self-heating effect is described in section 2.4. On the other hand does a high excitation frequency cause an increase in life expectancy, since the material will endure a high stress state for a shorter time period, resulting in a lower load.

The stress ratio indicates how a specimen is loaded:

- $(R > 1)$: Compression-compression.
- $(0 \leq R < 1)$: The specimen is loaded with tension-tension.
- $(R < 0)$: Compression-tension.
- $(R = 1)$: $\sigma_{min} = -\sigma_{max}$. The load is fully reversed.

In this thesis a fully reversed cyclic load is subject to the specimen by means of vibration.

2.3.3 Initiation

The initiation part of a composite total life span is considered to be a large part. However, its characteristic features are difficult to define. For composites no general definition for crack initiation is available.
The crack initiation is often related to a subjective crack dimension. Bhattacharya et al. [16] found that these dimensions can vary widely in different materials, from micrometers to a few millimetres. In composite materials damage is often identified as a complex status of the material rather than a single crack, as is the case for metals. According to the Reifnsiders [12] sequence of events, as set out in section 2.3.1 the damage initiations should be identified as the nucleation of a transverse crack in the off-axis ply. In this thesis this definition will be followed as well. The starting position of all tests needs to be as consistent as possible in order to isolate the effects of the endurance test. Therefore a transverse crack is self-introduced in order to always have a fixed initiated crack. Some problems occurred in this step, as a consistent initial crack could not be created. This will be discussed later on.

2.3.4 Propagation

The definition of initiation of damage in CFRP's might be difficult to define, the propagation of damage is more straightforward to understand and predict.
A model is provided by Magi [17] in his PhD Thesis for crack growth in composites based on the Linear Elastic Fracture Mechanics. Recall from section 2.2 that a crack grows when the Strain energy at the crack tip exceeds the critical value, i.e. $G \geq G_{\text{c}}$. In fatigue this condition is almost never met, as the severity would break the component in the first few cycles. Therefore again the Paris-Erdogan Law is used (eq. 2.7). Where previously the stress intensity factor K_{max} is used now the Strain Energy Release Rate (G) is used. Where the Strain Energy Release Rate is calculated as

$$G = \frac{\delta U}{\delta a}. \tag{2.10}$$

And the modified Paris-Erdogan Law becomes

$$\frac{\text{d}a}{\text{d}N} = C(\Delta G)^n. \tag{2.11}$$

With again C and n as material properties, but also the intercept and the slope of the Paris-Erdogan law on a log-log plot, as depicted in 2.5.

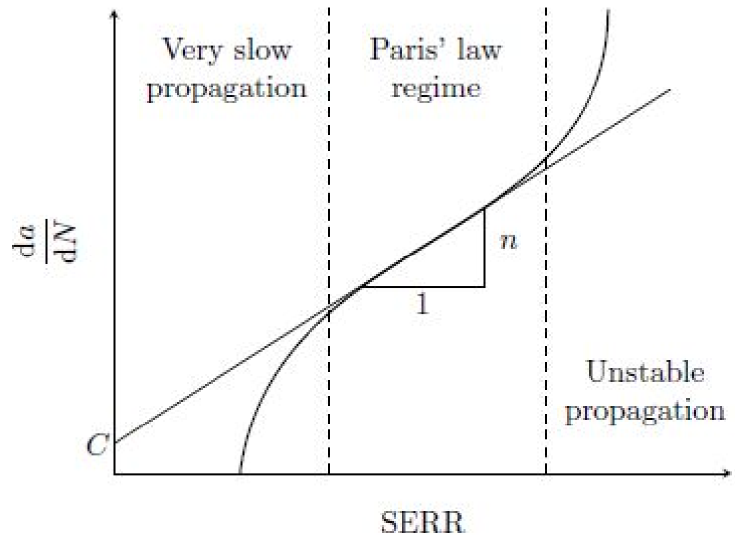

Figure 2.5: General Paris-Erdogan law with Strain Energy Release Rate instead of the Stress Intensity Factor as described by Magi[17].

Modelling of crack propagation

The Virtual Crack Closure Technique (VCCT) is a type of modelling used to investigate the crack propagation along a selected surface, which uses the Strain Energy Release Rate. So the VCCT is based on the insight that the strain energy released when a crack is extended by a certain amount is the same as the energy required to close the crack by the same amount. The Strain Energy Release Rates can be calculated for each separation mode separately, as:

$$G_{\text{I}} = \frac{v_{1,6} F_{v,2,5}}{2bd} \tag{2.12a}$$

$$G_{\text{II}} = \frac{u_{1,6} F_{u,2,5}}{2bd} \tag{2.12b}$$

The symbols in this equation use figure 2.6 as a reference. So G_{I} represents the crack opening and G_{II} represents sliding. $v_{1,6}$ is the displacement in y-direction in the node just before the crack tip. $F_{v,2,5}$ are the forces acting upon the nodes at the crack tip. d is the length between the nodes and b is the width of the element.

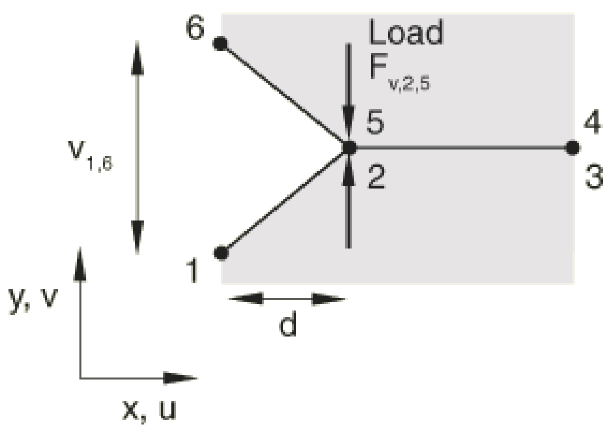

Figure 2.6: Situation before a crack opens for mode-I. [18]

A crack progresses when equivalent Strain energy (G_{equiv}) reaches the Critical Strain energy ($G_{\text{equiv,C}}$). Or defined with the fracture criterion f as:

$$f = \frac{G_{\text{equiv}}}{G_{\text{equiv,C}}} \geq 1.0 \tag{2.13}$$

Where the G_{equiv} is defined as:

$$G_{\text{equiv}} = G_{\text{I}} + G_{\text{II}} \tag{2.14}$$

$G_{\text{equiv,C}}$ is calculated with the BK law model as described in Benzeggagh [19] by the following equation:

$$G_{\text{equiv,C}} = G_{\text{I,C}} + (G_{\text{II,C}} - G_{\text{I,C}}) \left(\frac{G_{\text{II}}}{G_{\text{I}} + G_{\text{II}}} \right)^{\eta} \tag{2.15}$$

The coefficient η is found by curve fitting over experimental results. Note that the critical strain energy in the BK law is not a constant, since it depends on the ratio between the two strain energies. This model can be expanded for a three dimensional case, but this is out of the scope of this research, since only a 2D case is modelled.

2.3.5 Final Failure

Similar as to crack initiation the definition of final failure is not unique in composites. The definition also depends on the application of the material. When a component is subjected to harsh conditions, a single crack in the surface can be sufficient in to characterize the component as failed. On the other hand in some application some degradation is allowed and the part is only classified as failed when a certain drop of stiffness is reached. In order to keep this thesis as general as possible no state is defined for final failure.

2.4 Visco-elasticity

The resin component in the composite used in this thesis is PEEK, which is a thermoplastic. Thermoplastics behave visco-elastically. These materials differ from elastic materials in the sense that their behavior is affected by the loading rate. These effect can be negated by doing fatigue research on low frequencies that the visco-elasticity becomes insignificant. Due to the time expensive nature of these low frequency tests, high frequency tests are investigated anyway.

The endurance tests in this thesis are conducted at the near-resonance frequency to amplify the specimen with relatively low input power into a high enough strain region to enter the fatigue zone. An unwanted side effect is the self-heating effect.

The self-heating effect of resin is characterized using Dynamic Mechanical Analysis (DMA). In DMA a sinusoidal strain is applied to a resin specimen and the relative stress is measured. This allows for calculation of the complex elasticity modulus, where the complex elasticity consist of the storage modulus in phase with the sinusoidal strain and the loss modulus $\pi/2$ out of phase. This complex elasticity is investigated for varying temperatures and loading rates. The loss factor, the storage modulus over the loss modulus, is depended on the loading rate. Due to this effect the results of near resonance fatigue testing will vary with the loading rate. A method for characterizing the behaviour is by conducting tests with varying loading rates and applying Time-Temperature Superposition. The Time-Temperature Superposition is the observation that a master curve at a given temperature can be used as the reference to predict curves at various temperatures by applying a shift operation. This visco-elastic behaviour are out of the scope of this thesis, i.e. only the effect of one loading condition will be investigated.

2.5 Vibration induced Fatigue testing

The majority of fatigue tests are carried out at frequencies below 10Hz. However, vibration fatigue tests are used for certain metallic aerospace components [20, 21]. These tests could not be replicated in composites because of the failure criteria for stopping a test were not known. Di Maio et al. [2] proposed a method for composites which is also patented [22]. The novelty of the new test method was tracing the response phase, instead of the frequency over the cycles. The main motivation was a much higher sensitivity of the phase to the onset of damage. Such a method applied to components featuring ply-drops revealed a peculiar characteristic in the response phase trace, which was then used as failure criterion. This thesis will not elaborate on this criterion interested readers can find adequate reading in [3].
What Magi [17] and Voudouris [4] discovered about the damage growth was a relationship with the delamination length and delamination area respectively. It was reported that the linear decrement of the response phase, which was associated with the change of stiffness, could actually be related to the delamination growth. Hence, if failure criteria were one of the needs for stopping High Cycle Fatigue (HCF) test, the recent observation was indicating that the response phase could be exploited for investigating the fatigue crack growth with high level of accuracy. The testing set-up as used by Magi [17] is schematically depicted in figure 2.7. A specimen is placed into a fixture and vibrated with a shaker. A Laser Doppler Vibrometer (LDV) continuously measures the response of the specimen, The LDV is described more closely further in the section 2.7.1. A strain gauge is placed near the delamination area. The testing methodology consists of using MONTEVERDI and by acquiring a thermal image of the specimen every two seconds. MONTEVERDI is a LabVIEW coded program to automatically conduct fatigue tests. MONTEVERDI uses the LDV signal for displacement control of a location on the specimen using a PID-controller. This ensures a consistent loading condition during the fatigue tests.
The test set-up of Voudouris is very similar, but includes an environmental chamber to investigate the visco-elasticity as well.

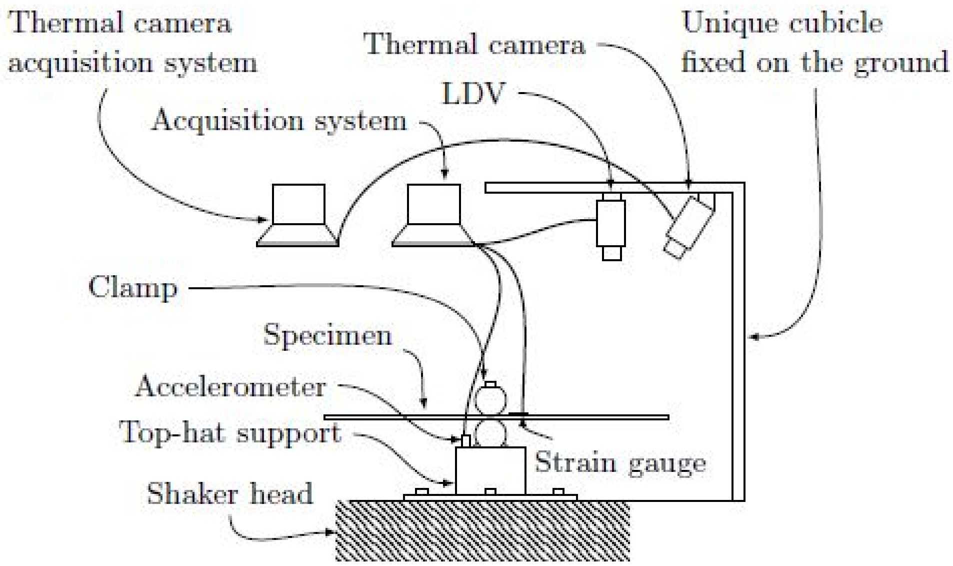

Figure 2.7: Schematic test set-up for composite endurance testing as used by Magi [17].

The specimens Magi and Voudouris [17, 4] used was a composite plate with a sudden ply-drop. They traced the phase response of the structure, since they found that it is directly related to the stiffness of the structure. Magi et al. [17] described that a critical event in the early stage of damage propagation can be captured by a sudden change in the decay rate of the response phase. This critical event corresponds to a transverse crack in the material turns interlaminar, thus shaping an actual delamination. The critical event is depicted in figure 2.8. Here the crack shifts from the initiation phase (a) to crack propagation phase (b). This critical event proved to be difficult for the PID controller to handle. This problem will be negated in this thesis by modifying their geometrically complicated specimens. The specimens will consist of the specific stacking sequence described by the HEGEL CS2 Grant Agreement no: 738130 [7]. Consisting of 10 unidirectional plies of which the top three have a pre-made transverse crack. This transverse crack is thought to push the endurance tests into the propagation phase immediately and no critical event will be detected.

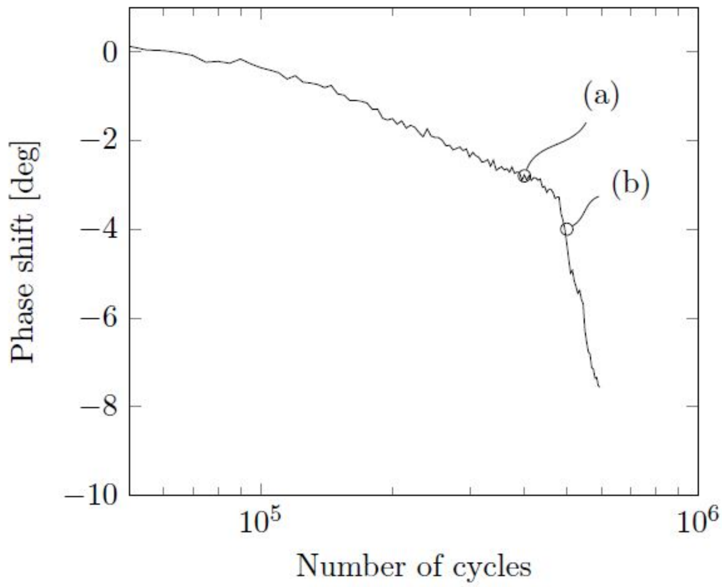

Figure 2.8: Critical event: Crack initiation changes to crack propagation. As shown by Magi [17].

Voudouris [4] continued the search for extracting important information from vibration testing. He conducted interrupted vibration tests to relate a certain damaged area to its respected phase drop. He utilized CT scans to measure the size of delaminated area after a fixed number of cycles. One of the results is depicted in figure 2.9, from which it is apparent that the relation is linear. This thesis will try to set-up a similar relation using the crack length using measurements with an electronic microscope.

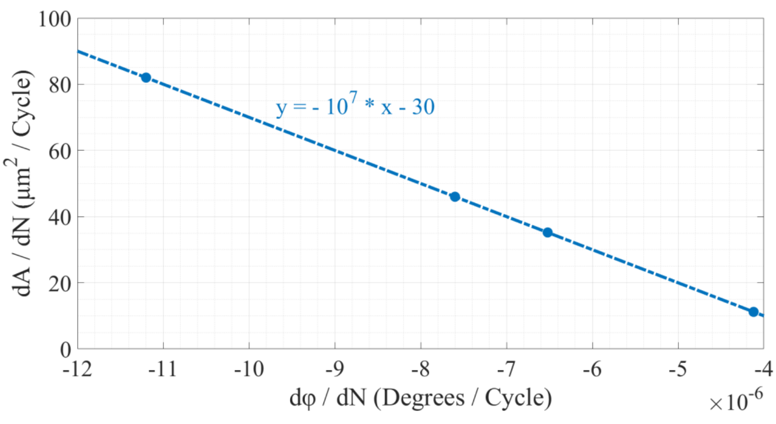

Figure 2.9: Damage Growth Rate against Response Phase Decay as related by Magi [17].

Magi [17] and Voudouris [4] both applied the VCCT modelling method to support their experimental work. The main goal of the VCCT analysis was to set-up a relation for the phase drop rate over the crack growth. Magi [17] investigated why the critical event occurs during testing, and he showed that a 3D model showed very close results to a 2D model. Voudouris [4] investigated the effects of varying ambient temperatures.
In both researches the VCCT was applied without the simulation of friction near the delamination. This interaction property is regarded as an important parameter in the crack growth. However, Voudouris [4] matched experiments to numerical models to determine the friction coefficient near the delamination. These experiments consisted of measuring the increase of temperature near the delamination. Parallel to this he set up a numerical model with varying friction coefficient. The numerical model with a value of 0.75 matched experiments the closest. The work of Magi and Voudouris will be extended in this thesis by setting up VCCT models that includes this friction coefficient.

Separately, research by Cole et al. [23] analysed vibration fatigue tested steel coupons by probing them with micro-indentations. What they found is a reduction in the elastic response in the coupons near the fixture. This can influence the dynamic properties of the coupons to some degree.

2.6 Experimental Modal Analysis

Experimental Modal Analysis (EMA) is an instrument used for describing, understanding and modelling of the dynamic behaviour of a structure. Ewins [24] concisely described the main objectives of experimental modal analysis as:

> ”Experimental observations have been necessary for the major objectives of determining the nature and extent of vibration response levels in operation and (b) verifying theoretical models and predictions of the various dynamic phenomena which are collectively referred to as ’vibration’. There is also a third requirement, (c), which is for the measurement of the essential material properties under dynamic loading, such as damping capacity, friction and fatigue endurance.”

The third goal is most applicable in this thesis since, the modal parameters will be extracted before and after the introduction of damage. This way EMA can give information about the change in the state of the structure.
By subjecting some kind of harmonic excitation leads to a main method for describing the dynamics: The Frequency Response Function (FRF). Which is the ratio of some kind of output over input, such as response velocity over input force. Such a FRF is depicted in figure 2.10. The dynamic parameters, the natural frequency and damping, are retrieved from such an FRF by curve-fitting the retrieved FRF with an FRF-function, which will be explained in the next section.

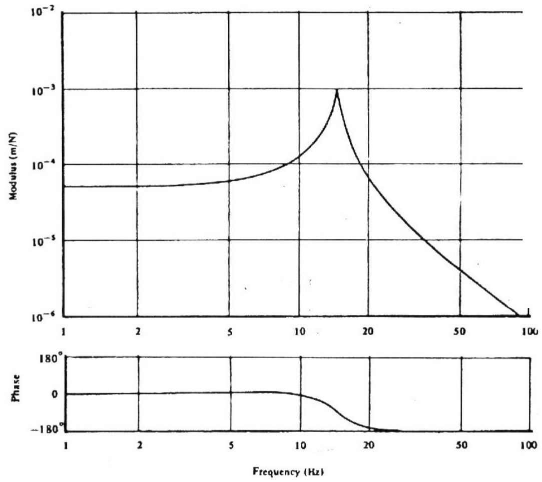

Figure 2.10: Display of frequency response function on a logarithmic scale.

Measuring the FRF is to gain information about a specific frequency range at a location. Measuring the Operating Deflection Shape (ODS) is done to gain information about the response of a range of location at a single frequency. ODS measurement can visualize the vibration pattern of a structure. An object in Steady State vibration is scanned over a line where time is used as a direct measure of spatial position on the structure so that spectral analysis of time varying signals translates directly into spatial descriptions of the vibrating structure [24]. Scanning the structure is typically done with an Laser Doppler Vibrometer, as will be introduced in section 2.7.1.

2.7 Natural Vibrations

The simplest mathematical description of a dynamic system comes from a Single Degree Of Freedom (SDOF) mass-spring damper subjected to a harmonic force as in figure 2.11a. According to theory can the amplitude and phase of Frequency Response Function (FRF) be defined as:

$$|\alpha(\omega)| = \frac{|X|}{|F_0|} = \sqrt{\frac{1}{\left(1-\Omega_d^2\right)^2 + (2\zeta\Omega_d)^2)}} \tag{2.16}$$

$$\varphi(\omega) = \tan^{-1} - \frac{2\zeta\Omega_d}{1-\Omega_d^2} \tag{2.17}$$

In which the natural frequency (ω_n), damping ratio (ζ) and dimensionless frequency (Ω_d) were rewritten to standard notation from the SDOF systems mass, damping and stiffness:

$$\omega_n = \sqrt{\frac{k}{m}}, \quad \zeta = \frac{c}{2m\omega_n} \quad \text{and} \quad \Omega_d = \frac{\omega}{\omega_n} \tag{2.18}$$

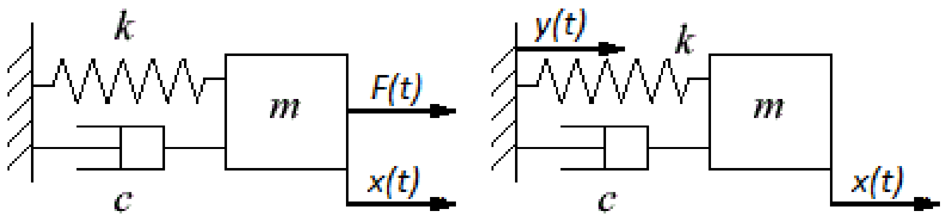

(a) (b)

Figure 2.11: SDOF systems with a harmonic force (a) and a moving base (b).

However, in this thesis a specimen is not subjected to a harmonic force, but to a base acceleration, as in figure 2.11b. The derivation of the amplitude and phase of the FRF of such a system starts with setting up the equation of motion:

$$m\ddot{x}(t) + c\dot{x}(t) + kx(t) = c\dot{y}(t) + ky(t) \tag{2.19}$$

Again using the relation above makes the standard notation:

$$\ddot{x}(t) + 2\zeta\omega_n\dot{x}(t) + \omega_n^2 x(t) = 2\zeta\omega_n\dot{y}(t) + \omega_n^2 y(t) \tag{2.20}$$

Considering that both the base motion and response are harmonic they can be expressed as

$$x(t) = X\mathrm{e}^{i(\omega t)}; \quad y(t) = Y\mathrm{e}^{i(\omega t)}; \tag{2.21}$$

$$\dot{x}(t) = i\omega X\mathrm{e}^{i(\omega t)}; \quad \dot{y}(t) = i\omega Y\mathrm{e}^{i(\omega t)}; \tag{2.22}$$

$$\ddot{x}(t) = -\omega^2 X\mathrm{e}^{i(\omega t)}; \quad \ddot{y}(t) = -\omega^2 Y\mathrm{e}^{i(\omega t)}. \tag{2.23}$$

Substituting the harmonic motions into the standard notation yields:

$$\left[\omega_n^2 - \omega^2 + 2\zeta\omega\omega_n i\right] X\mathrm{e}^{i(\omega t)} = \left[\omega_n^2 + 2\zeta\omega\omega_n i\right] Y\mathrm{e}^{i(\omega t)} \tag{2.24}$$

Both sides of the equation contain $\mathrm{e}^{i(\omega t)}$, which is removed from the equation. The Frequency Response Function can then be written as

$$\alpha(\omega) = \frac{X}{Y} = \frac{\omega_n^2 + 2\zeta\omega\omega_n i}{\omega_n^2 - \omega^2 + 2\zeta\omega\omega_n i} - \frac{1 + 2\zeta\Omega_d i}{1 - \Omega_d^2 + 2\zeta\Omega_d i}. \tag{2.25}$$

The magnitude of the FRF is found by taking the complex conjugate of α and the phase by taking the arc-tangent of the real part of the FRF over the imaginary part:

$$|\alpha(\omega)| = \frac{|X|}{|Y|} = \frac{\sqrt{k^2 + (\omega c)^2}}{\sqrt{(k - \omega^2 m)^2 + (\omega c)^2}} = \sqrt{\frac{1 + (2\zeta\Omega_d)^2}{(1 - \Omega_d^2)^2 + (2\zeta\Omega_d)^2}} \tag{2.26}$$

and

$$\varphi(\omega) = \tan^{-1} - \frac{2\zeta\Omega_d^3}{1 - \Omega_d^2 + (2\zeta\Omega_d)^2}. \tag{2.27}$$

During the endurance tests the systems phase response is measured continuously. In the phase equation 2.27 the stiffness of the system is in the denominator to the power two. When the damage in the specimen progresses during the endurance test, the stiffness slowly deteriorates. The phase also is an especially sensitive parameter, due to the characteristic shape of the arctan function that contains an especially high slope near the resonance.

2.7.1 Laser Doppler Vibrometry (LDV)

Experimental work is a fundamental activity to understand the underlying physics of fatigue. The change in a structure is quantified by using detection techniques. Martirelli [25] describes the need for non-contact measurement devices in order to get a non-invasive measuring technique. This means that the sensor does not influence the mass and inertia of a specimen. A type of non-contact measuring of a vibration response is the Laser Doppler Vibrometry (LDV) technique. This technique is suggested as a replacement for the classical accelerometer, a contact method. The accelerometer is attached to a vibrating component of interest and tracks the acceleration. Both the LDV and accelerometer are used in this thesis. The LDV to track the very lightweight specimen and the accelerometer to track a base acceleration of a heavy electromagnetic shaker. The Laser Doppler Vibrometry (LDV) method is based on sending out a laser light onto a surface

and measuring its reflection with a detector. Due to the Doppler effect the wavelength of the sent signal is either compressed or stretched depending on the speed difference between the source and the receiver. The detector measures this wavelength and relates it to the specimen's velocity. Note that only the surfaces velocity normal to the laser can be detected. Using the LDV detection technique to map a specimen over multiple positions is called Scanning LDV (SLDV). This mapping can done by scanning discrete points on a specimen, which is called Stepped SLDV (SSLDV). The positioning of the laser is time intensive. For this reason the Continuous SLDV (CSLDV) is regarded as the more efficient approach to get spatially dense measurements. A mirror will continuously direct the laser over a specified path using a mirror. In practice this means that a very high number of discrete points is investigated. The CSLDV technique will be used in the experimental investigation. Therefore will the mathematical approach to extracting the spatial and temporal data will be elaborated on.
The CSLDV detection technique can extract spatial and temporal data of a specimen. The ODS of an object can be retrieved by vibrating the object with a fixed frequency and directing a laser over the object with a specific path. Various lines or areas can be described, but since this thesis utilizes a straight line scans, only this path will be elaborated upon.
Note, that when utilizing the LDV like this to retrieve an ODS only the signals velocity in-line with the laser can be retrieved from the signal. This means that the mirror angles should be minimized, such that most of the specimen's vibration is in-line. This is achieved by positioning the LDV as high as possible. According to [26] CSLDV measurements is affected by noise. A laser light reflects on the rough surface of a specimen, parts of the reflected light will interfere constructively or deconstructively. This will cause some dark and bright regions in the laser path, known as the speckle pattern. As the laser moves continuously over the specimen the Speckle Pattern produces pseudo-random vibrations in the signal, which are difficult to distinguish from the true signal and introduce some error in the signal. The noise will increase when the laser is positioned far away. A laser distance of $\sim$1 m has provided good results in previous work [25].

2.7.2 Line Scan

The Continuous Scanning LDV method scans the specimen over a specified path. The test is schematically depicted in figure 2.13. During the test the frequency and amplitude needs to be kept constant. Both these parameters will influence the shape of the ODS, and if it changes during a test the result will be corrupted. The most basic method for specifying this path is the constant rate method.

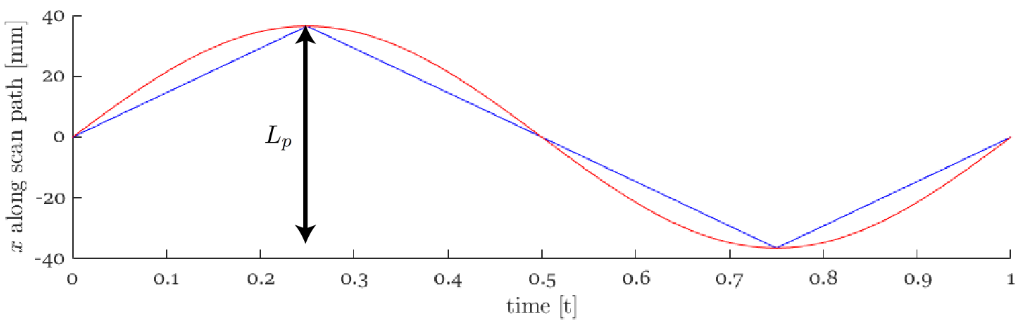

Figure 2.12: Investigated scan paths. Constant rate in blue and sinusoidal in red.

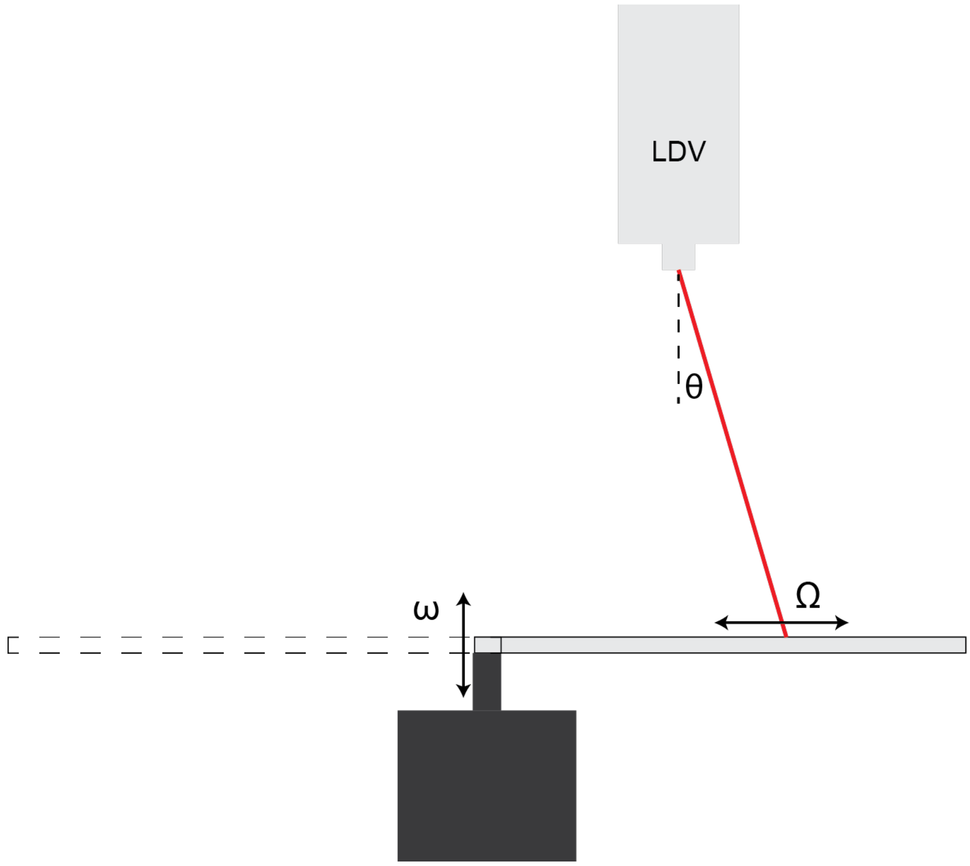

Figure 2.13: Schematic depiction of utilizing the Continuous Scanning Laser Doppler Vibrometry technique with a line.

The laser moves over the specimen with a constant speed, when the end of the specimen is reach the scan speed is inverted, resulting in a triangle path, as depicted in figure 2.12. When looking at the CSLDV signal the general shape of the amplitude of the ODSs can already be distinguished to some degree from the envelope of the signal. A disadvantage of this scan type is the instantaneous reversal in velocity [25]. Due to the mass and inertia of the mirror and its driver components distortions when the mirror changes direction.
This disadvantage is solved by introducing a sinusoidal path. The idea of the sinusoidal is that the velocity of scanning point at the ends of the specimen is reduced to zero smoothly. No instantaneous reversal of direction is present, which allows for the scan path to be traced very closely by the LDV mirror. For completeness, the two types of scan paths are defined as:

$$x(t) = 2L_p\Omega t \tag{2.28}$$

$$x(t) = \frac{L_p}{2}\sin(2\pi\Omega t) \tag{2.29}$$

Where $x(t)$ is the position along the scan path, L_p is the length of the scan path and Ω is the scan rate. The direction of the continuous rate path changes each time the end is reached, which is left out of the equation for simplicity.

The specimens can be considered to be undergoing a sinusoidal vibration at a frequency ω. This vibration can be expressed as the velocity in z-direction, measured at point x in time as:

$$v_z(x,t) = V_R(x)\cos\omega t + V_I(x)\sin\omega t \tag{2.30}$$

Here $V_R(x)$ and $V_I(x)$ correspond to the real and imaginary components of the amplitude at a specific point along the specimen. Taking V_R and V_I over the complete specimen yields the real and imaginary ODSs. The general composition of a CSLDV is achieved by substituting the described scan paths, equation 2.28 and 2.29 in this equation. Now the challenge is to retrieve the ODSs from this general composition, which is found in the demodulation method, as described in the next sub-section.

2.7.3 Demodulation Method

The challenge of the CSLDV theory is finding an efficient method of retrieving the ODSs from the signal. Simply taking the envelope of the curve does not cut it, since it only yields the amplitude of the ODS and not the real and imaginary ODSs. The real and imaginary ODS can be retrieved from the measurement by demodulating the CSLDV signal, as first described by Stanbridge et al. in [27]. Their convenient method is to multiply the output signal by an in-phase and a quadrature signal at the excitation frequency, yielding equation 2.31.

$$V_R(t)\cos^2\omega t + V_I(t)\sin\omega t\cos\omega t = \frac{1}{2}V_R(t) + \frac{1}{2}V_R(t)\cos 2\omega t + \frac{1}{2}V_I(t)\sin 2\omega t \tag{2.31a}$$

$$V_R(t)\sin\omega t\cos\omega t + V_I(t)\sin^2\omega t = \frac{1}{2}V_I(t) + \frac{1}{2}V_R(t)\sin 2\omega t - \frac{1}{2}V_I(t)\cos 2\omega t \tag{2.31b}$$

The real and imaginary amplitudes of the, $\frac{1}{2}V_R(t)$ and $\frac{1}{2}V_I(t)$, can be isolated from the signal by applying a Low Pass Filter. In order for this to be successfully Ω needs to be sufficiently smaller than 2ω. It is advised to set the pass frequency of the low pass filter well below the ω, since frequencies lower than interferences can 2ω can be included in the signal due to crosstalk interference [25]. Important to note that no windows can be applied on the amplitude signal. A signal is usually multiplied with a windowing function to make sure that the signal is zero-valued at the beginning and end. This negates errors in the results due to spectral leakage. Windows will influence the amplitudes of the signal, which are used to determine the amplitudes of the ODS, as is depicted in figure 2.14. Here the demodulation method is applied on a signal with and without a window.

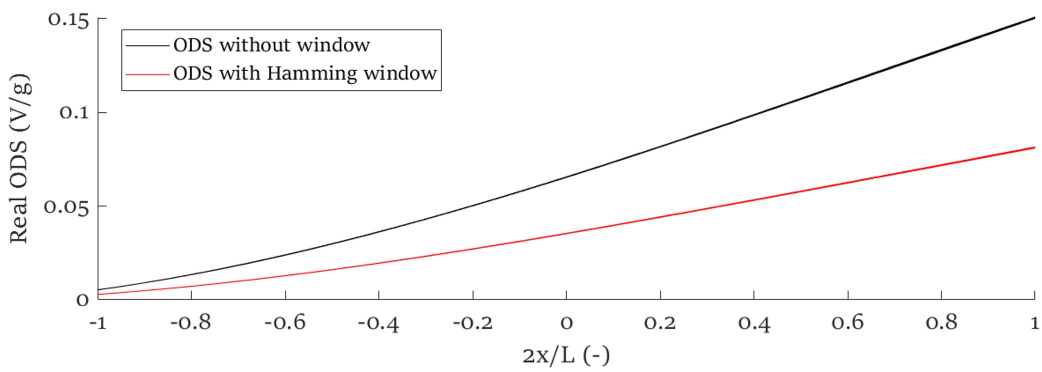

Figure 2.14: real part of the ODS retrieved with the demodulation method. With and without applying a hamming window.

2.7.4 Polynomial fit of the ODS and the MAC score

When the Operating Deflection Shapes are determined with the demodulation method the shapes are first fitted with a polynomial in order to gain a continuous function. This leads to the following definition of the vibration:

$$v_z(x,t) = \sum_{n=0}^{p} V_{Rn}x^n\cos(\omega t) + \sum_{n=0}^{p} V_{In}x^n\sin(\omega t) \tag{2.32}$$

The fit function helps negate any measured noise in the results and can be used for differentiation of the ODS later on. The quality of the fit is quantified using the Modal Assurance Criterion (MAC) [28], defined as:

$$\text{MAC} = \frac{\left|\{V_A\}^T \{V_X\}^*\right|^2}{\left(\{V_A\}^T \{V_A\}^*\right)\left(\{V_X\}^T \{V_X\}^*\right)}. \tag{2.33}$$

The MAC is used as a correlation constant between two vectors. Here the measured ODS, V_A, is compared with the polynomial ODS V_X. The superscript $\{\}^*$ denotes the complex conjugate of the function. Thus the resulting score is a scalar even for real or imaginary inputs. The order of the polynomial is increased until the MAC score exceeds 0.999. The max order is set to 8 to prevent any overfitting problems. In literature the approach with MAC scores is usually extended by also comparing all investigated modes with each other. However in this thesis only the first mode is of interest, yielding this redundant.

3 EXPERIMENTAL INVESTIGATION

This chapter will explain the entire experimental procedure carried out for testing the samples. The procedure will include how the test was set up and how the sample were tested, furthermore it will discuss the effects of the manufacturing process on the experimental data.

3.1 Experimental measurement procedure

The main type of test in the experimental investigation is the high frequency endurance test. Before conducting this test several tests are required to prepare the specimen and to characterize the specimen before damage is introduced. This section will go through the flow diagram of the experimental procedure which is rather elaborated as shown in figure 3.1.

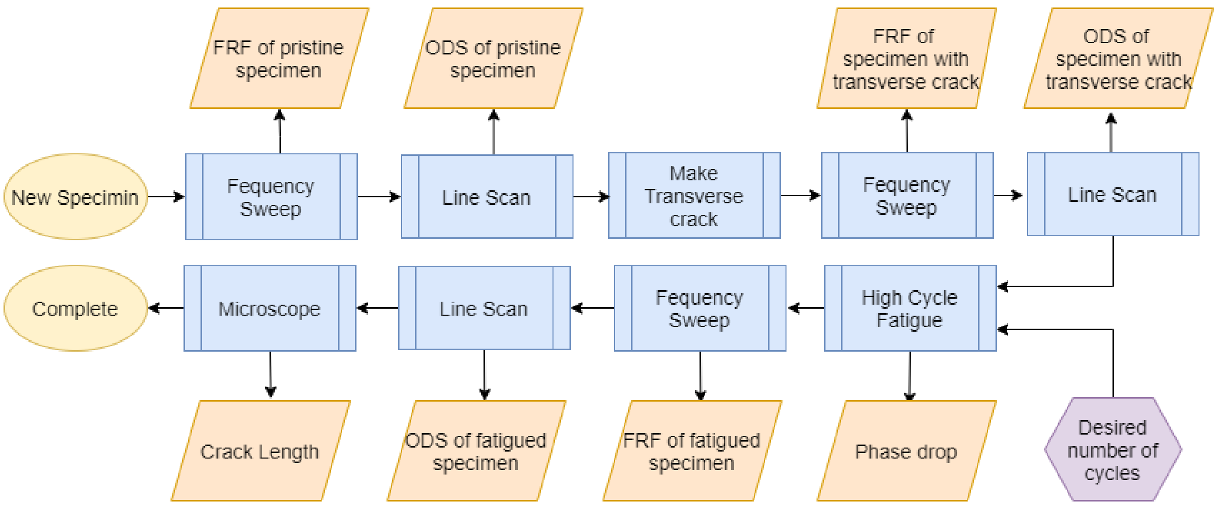

Figure 3.1: Overview of Experimental approach

The steps presented in figure 3.1 can be summarized as follows. Every specimen is subjected to modal tests before the endurance test to measure the resonance phase and also to characterize the dynamics before damage is created by fatigue. Next, the specimen is scanned with the Continuous Scanning LDV technique to characterize the Operating Deflection Shape (ODS) of the pristine sample. Previous research on thermosets has shown that the maturing of transverse crack through the matrix material near the preprocessed crack happens instantly. Therefore is it an important task to create the transverse crack before the endurance test to avoid the PID controller being unable to control the test. A new modal analysis is carried out again to identify the frequency shift caused by the transverse crack and the new resonance phase. This latter parameter is fundamental for monitoring the crack growth from near resonance conditions. Also the specimen is scanned again with the CSLDV technique to find the ODS of the transversally cracked specimen. The endurance starts after these preliminary tests are conducted. In the endurance tests again the specimens are vibrated, meaning that a fully reversible load ($R = -1$) is used. The endurance test lasts a fixed number of cycles. The number of cycles that are

investigated is 50.000, 75.000, 100.000, 125.000, and 180.000 cycles. Here the initial excitation frequency is chosen at the found resonance frequency. At the end of the HCF, a modal analysis is carried out again to characterize the dynamics of the fatigued specimen. The modal analysis consists again of a frequency sweep and of scanning the specimen to find the ODS.
The last task is to remove the sample from the fixture and proceed with the optical inspection with the digital microscope to identify the crack lengths. This step also requires several preliminary actions, such as surface polishing.

3.2 Samples and manufacturing process

This section first describes the used specimens and then discusses the procedure to manufacture these specimens. For the the thermoplastic specimens the material carbon fiber cross-ply thermoplastic PEEK material was used. The specimens are cut to a size of 179 mm by 25 mm and have a thickness of 1.4 mm. While the initial plates had a size of 12 inch ($\sim$0.3 m), the full lengths were not used in order to increase the resonant frequency (from 80 Hz to 150 Hz). This will decrease the required time of the endurance tests. On top of that requires the longer specimens a tip-displacement up to 100 mm to get strains near the crack in the fatigue region. The engineering intuition told that this would prove difficult for the PID controller in the endurance tests.
The lay-up sequence of the beam is [90/0(cut)/90/0/90/90/0/90/0/90], which is depicted in figure 3.2. The fibers of the upper 0-degree ply was cut 10 mm off center. This cut fixes the nucleation point for the delamination for all conducted tests.
The specimens used in this investigation were manufactured with press molding. The pressing process is performed by the TPRC staff according to their standard steps.

1. Heat up with 10°C/min at 19 kN, heat up to 385°C, then at dwell 10 min at 385°C 2 bar (19 kN).

2. Dwell 20 min at 385°C at 186 kN (20 bar).

3. Cool down to 60°C with 5°C/min at 186 kN (20 bar).

After curing the specimens were removed from the mold. The sides of the newly manufactured plate are trimmed and 11 specimens are cut out.
The major challenges of manufacturing the specimens is firstly to assure that the fibers are indeed orthogonal to each other, meaning that no steering occurs during the allocation of the layer. Secondly, the two sides of the cut ply need to be kissing each other and need to be parallel to the other plies. And thirdly, that all manufactured specimens are as identical as possible. Micro-imperfection will cause specimens to never be completely identical the goal is to get as close as possible. It was critical that the samples' characteristics, such as geometry, are as consistent as possible to reduce any undesired test-to-test variability. The results of optical inspection of the cut-ply region will be discussed in more details in the next section. A cross section of the stacking sequence zoomed in on the pre-made cut in the top 0-ply is depicted in figure 3.3.

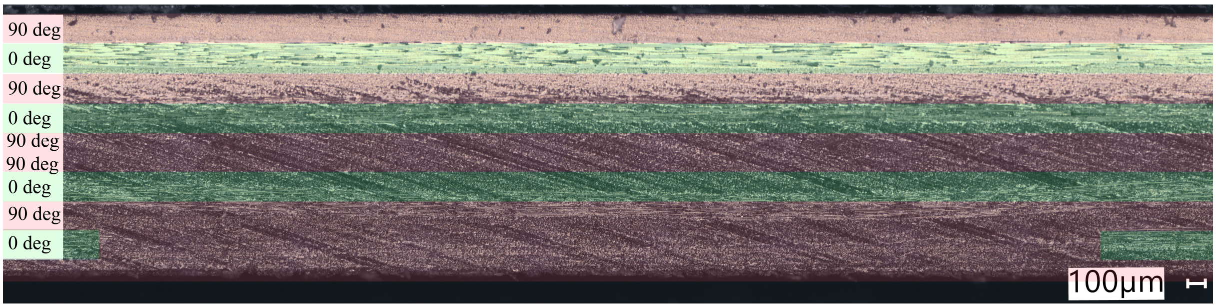

Figure 3.2: Stacking sequence of specimen. With the 90 degree plies highlighted in red and the 0 degree plies in green. The pre-made crack can be found in the extra 90 degree section.

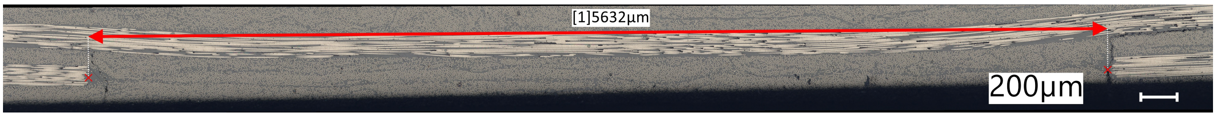

Figure 3.3: Zoom of pre-made cut in specimen 5 (Plate 1).

3.2.1 Cut-ply gap

In order to have a representative specimen of how a real-life transverse crack would appear in parts the two sides of the cut ply need to be just touching each other. From figure 3.3 it becomes clear that a resin pocket is introduced near the cut-ply. This is mainly attributed to manufacturing process. During the pressing of the material, when the resin has not completely consolidated, the fibers in the unidirectional tapes start to steer. Resin is pushed into the created cut and forms a pocket, which we call the resin pocket. Very important to note is that the creation of the resin pockets is not as constant throughout the plates as it was expected. The resin pockets throughout plate 1 range from 4.6 to 7.1 mm and in plate 2 from 3.3 to 6.0 mm. From the 22 specimens from plate 1 and 2, five were selected that were as close as possible. The resin pocket in these specimens ranges from 5.3 to 5.5 mm. All zoomed cross sections of the Resin Pockets with their lengths from side A and B are set out in Appendix C.

3.2.2 Fiber waviness

In some of the other cross sections of the lay-up, like figure 3.4a it is noted that some of the fibers of the 0-degree plies are not perfectly 0-degrees. A perfect 0-degree fiber would be perfectly perpendicular to the plane of view. However, they seem to go inside and outside the plane of view. Most prevalent on the left bottom side of figure 3.4a where the 0-degree fibers only have a length $\sim 50\mu$m. This effect is present to a different level of severity for the different specimens. The cause of this effect is mainly attributed to fiber waviness. This effect was not taken into account when selecting the top 5 specimens since the effect is only visible after an extensive polishing procedure, which was conducted after the tests. This observed effect mean that the specimens vary from each other.
Another observation from the cross section in figure 3.3 is how the 0-degree ply beneath the cut ply is pushed inside the resin pocket created by the cut-ply. Some of the specimens show more of this effect then others. The top 5 selected specimens show the effect to the minimal extend. Due to this fiber flowing the specimen is expected to behave differently when subjected to a bending moment, such is the case in the endurance tests. The cut-ply already introduces a stacking configuration which is not balanced, because it occurs on one side only, and the fiber waviness will only add to this complexity.

3.2.3 Fiber bridging

Very interesting to note is that research from Johnson et al. [29] declare this rotated ply as a major cause for fiber bridging. The fiber bridging phenomena being the bridging of fibers between adjacent plies over the delamination plane to act as a crack arrestor [30]. This phenomena causes the delamination resistance and fracture toughness to increase. This bridging effect is very prevalent in figure 3.4a, where the delamination can be seen going into the 0-ply instead of staying between the main 90-ply/0-ply interface. This effect is likely to show up in some of the samples, but it will prove to be difficult to predict to what degree. Different methods of observations are required to investigate the complete damaged area.

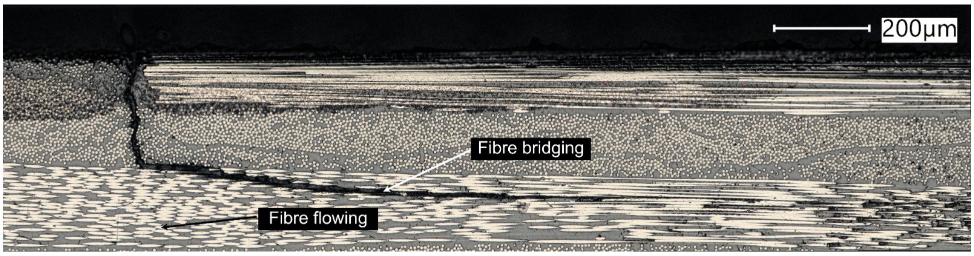

(a)

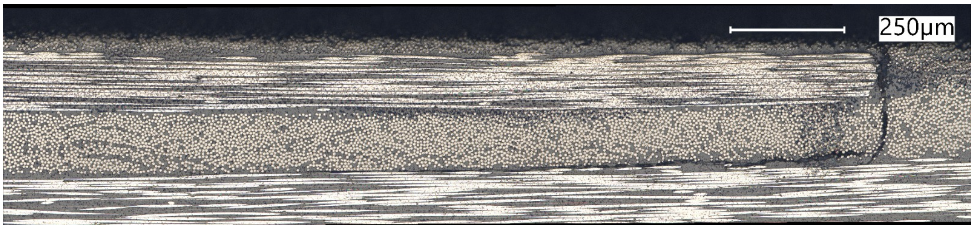

(b)

Figure 3.4: Cross section of specimen 5 plate 2 from side A (a) and B (b).

3.3 Test set up

This section will describe the designed test set up with all its components. For clarity is the test set up first set out schematically in figure 3.5.

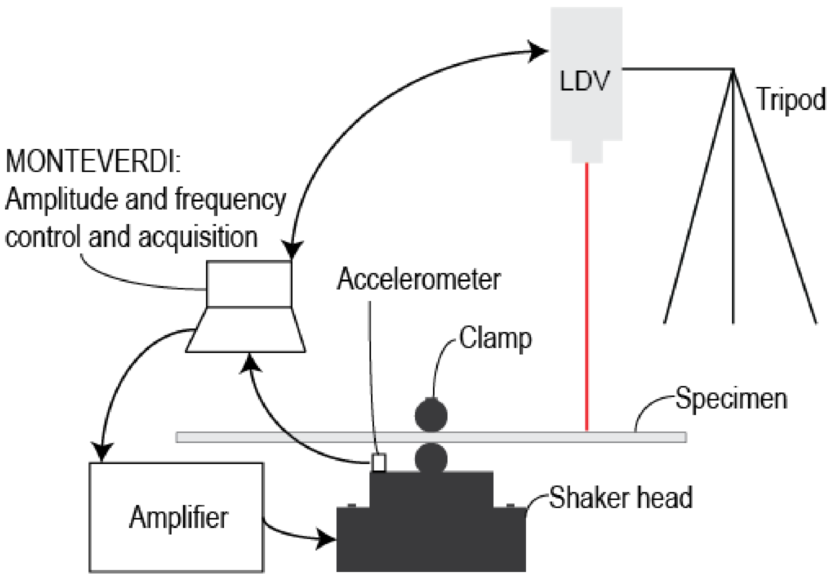

Figure 3.5: Schematic test set up

The set up and its constituents are depicted in figure 3.6. The added labels in this text correspond to the labels in the figure. A specimen (1) is fixed into a fixture (2). A predictable and consistent fixture is ensured using a knife edge clamping conditions and with the procedure described later on in this section. The top and bottom bars of this fixture are manufactured from a solid round bar. This round bar causes the contact between the fixture and the specimen to be a line contact. The total mass of the fixture, including all attached bolts and sensors, is weighed to be 2.4kg. This fixture is attached with bolts on top of a V300 SignalForce electromagnetic Shaker (3). The armature of the shaker is 1.7kg according to its Datasheet. The total mass of the armature and the fixture is 4.1kg. According to the specification of the shaker it is rated up to accelerations of 98g at 4700Hz, which is well within the test requirements set for this research work. The base acceleration is measured using an one-axis analogue accelerometer (5), with a $\pm$50g range and a sensitivity of 40mV/g. The specimen's velocity response is measured with A Polytec PSV-I-560, a Laser Doppler Vibrometer (6). The full scale value (peak) of the laser is set to 2500 mm/s which corresponds to a sensitivity of 95 μm/s.

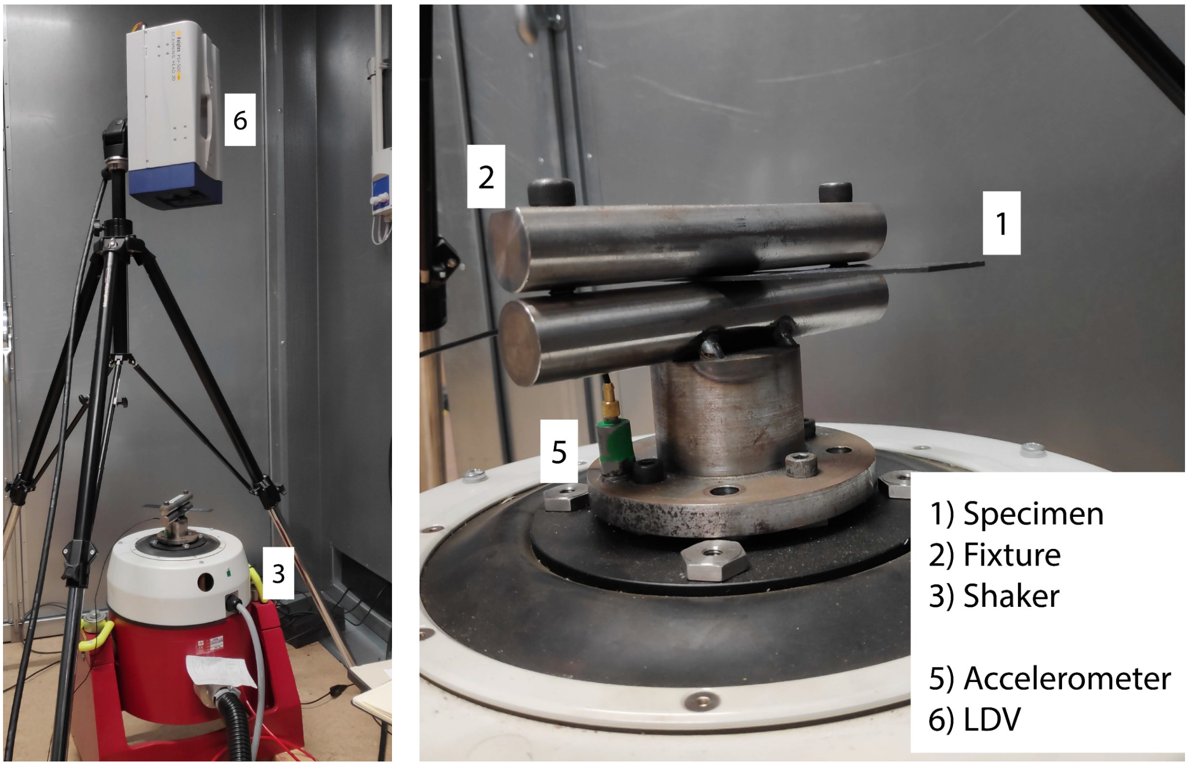

(a) (b)

Figure 3.6: Experimental Set up (a) and zoomed in on the fixture (b). The labels in this figure can be found in the corresponding text above.

The LDV is positioned on a tripod 0.74m above the specimen. It is important that the laser is orientated as vertical as possible, since a small angle can have relatively large deviations in the results. This is achieved using a levelling tool. The LDV is aligned exactly parallel to the specimen such that only one mirror is required to scan parallel to the specimen. It is positioned exactly 52 mm off center in the length direction. This position, from now called the LDV position, is seen in figure 3.7 as the green dot. This spot is chosen in the middle from the furthest positions the laser can see on both sides of the specimen. Which on one side is where the fixture covers the specimen and on the other side the tip of the specimen. During the construction of the testing approach and the test set up two problems concerning the modal line scans occurred. One being that the cracked area could not be fitted into a line scan, due to the fixture obstructing the field of vision, and the other being that loading conditions of the endurance tests

could not be replicated during the line scan without propagating the delamination. This could influence the results of the endurance test. The goals of the line scans are therefore updated. Only the feasibility of using the line scans to determine the strain throughout the specimen will be investigated. The LDV position is located at the cracked side of the specimen. This decision is motivated by the fact that the SSD analysis in the numerical investigation has shown that when applying displacement control on the cracked side, that the amplitudes of the pristine side still changes significantly as the delamination progresses, as will be shown in the numerical investigation (sec. 4.4). So setting the displacement constant on one side, will not set the other side constant, as previously assumed.
The specimen is placed with the cracked side downward. The static analysis in the numerical investigation has showed a relatively large strain at the bottom surface near the delamination. It is suspected this will be easier to measure.
A PC is used to control the shaker and the LDV mirrors. The same PC is used to acquisition data from the accelerometer and the LDV.

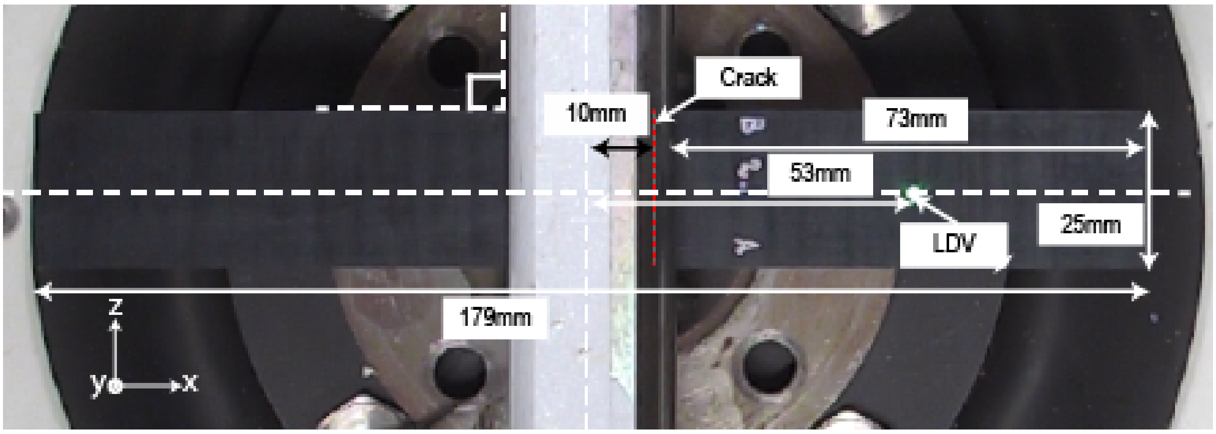

Figure 3.7: Properly aligned specimen. Note the LDV position as the green dot 53 mm from the center. The crack location is marker as the dotted red line. The scan path length L_s is measured to be 73 mm

To get valuable data from experiments is important to keep the testing conditions as consistent as possible. For instance, any misalignment of the test sample installed onto the fixture will influence the results. The procedure for this installation is as follows. Using a ruler the specimen is first placed in the middle of the fixture. Then, the ruler is used to center the specimen along the length of the specimen. Next, an angle tool is placed between the specimen and the fixture to orientate the specimen as straight as possible. These steps are repeated until all three parts are aligned to the best extent. Finally, the bolts on both sides of the fixture are torqued incrementally in turn in steps of 1 Nm up to 6 Nm. Due to the big difference in hardness between steel of the fixture it is highly important that the bolts are not torqued any higher to prevent any damage to the specimen.
These steps need to be followed very carefully, but a human error is always possible. Therefore the importance of three steps are quantified by conducting several modal tests to set up the Frequency Response Function. The tests are an indication of how much the results can reasonably change due to human error.

1. A good alignment of the specimen is compared with a bad one. The bad alignment has the specimen placed off center with $\sim$1 mm and showed a frequency shift of the resonant frequency of -0.5Hz.

2. A specimen aligned straight is compared to a specimen placed under an angle of $\sim$0.5°. The resonant frequency shifted with -0.3Hz.

3. The effects of an unevenly torqued fixture is investigated. One side of the fixture is torqued completely first and then the other side completely. The resonant frequency is found to shift +0.3Hz due to this.

A frequency shift of this order of magnitude is to be expected when replacing a specimen in the fixture. The complete FRF results are set out in appendix B. No other changes in the FRF's could be identified.

3.4 Modal testing

Modal tests are conducted before and after opening the transverse crack and after the endurance tests in order to characterize the dynamics of the system. The modal tests consist of a frequency sweep in order to retrieve the FRF and a line scan to retrieve the ODS. Both are discussed in the next subsections.

3.4.1 Frequency sweep

Modal tests are conducted to measure the resonance phase and also to characterize the dynamics of the specimen. These modal tests consist of an upward frequency sweep over a selected frequency ranges divided into a certain number of steps. The tests measuring the range around the resonant frequency have a set range length of 2 to 3 Hz, divided in 40 equal frequency steps. An accelerometer at the base of the fixture provides the reference for the test, since the control panel allows setting the voltage to the shakers' amplifier only. The resonance can be scanned at various level of vibration amplitudes. The amplifier increases this voltage to the shaker to a certain extent by tuning a physical knob. This knob is set manually, therefore the exact amplification might vary for each test and causing the exact base acceleration to vary slightly. Therefore the base acceleration, measured with the accelerometers, is used instead. During the tests the velocity of the LDV position is measured. Finally, the Frequency Response Function is set up as the LDV velocity over the base acceleration. The resonant frequency of the tests are used as an initial frequency of the endurance test. The results of these frequency sweeps are set out in 5.1.1.
Since the frequency sweeps are meant as a non-destructive testing method they are conducted with low acceleration levels of approximately 0.1g. This level is negligible compared to accelerations used in the High Cycle Fatigue (up to 15g).
The transverse crack is made by conducting a high acceleration frequency sweep. The higher acceleration causes larger stresses in the specimen causing the matrix material to break. These FRFs were conducted with approximately 3g, which is described in more detail in section 3.5.
The linearity of the input acceleration to the response velocity is investigated on a dedicated sample. This linearity is of importance since modal tests are conducted with low input acceleration and the endurance test on a relative high acceleration. These test will give insight on whether the modal tests will give a representative insight on the systems dynamic properties during the endurance tests. The results are set out in chapter Results in section 5.1.2.

3.4.2 Line scan

Modal tests are conducted to investigate the Operating Deflection Shapes (ODSs) of the specimens in its natural frequency. These modal tests consist of utilizing the Continuous Scanning Laser Doppler Vibrometry (CSLDV) technique, from section 2.7.1 along the centerline of the cracked side of the specimen. The specimen is vibrated in the investigated frequency at a low acceleration of $\sim$0.1g in order to not progress or introduce any damage in the material. During the line scans it is important that the specimen vibrates in a steady state. In a non-steady state

the ODS will not be constant. When retrieving the ODS from the signal, the result will be corrupted. As described in section 3.3 the LDV-position was chosen such that most of the cracked side of the specimen can be scanned without having to move the LDV. This results in a total line scan of 73 mm, as depicted in figure 3.7. The LDV-position is chosen along the centerline of the specimen such that the data is not corrupted by any torsion components, which are expected to be small for the narrow specimens. The scan rate (Ω) is chosen to be 1.1Hz.
The results of the different line scans will be discussed together with the corresponding results from the numerical investigation in chapter Results in section 5.2.

3.5 Opening the transverse crack

The specimens used in this thesis have been manufactured with an embedded 0-deg cut-ply which would create a weak resin region allowing a transverse crack to travel up to the 0-deg pristine ply from which the delamination starts. This transverse crack is filled with resin during the manufacturing process. Since, this thesis initially investigated the crack propagation of a delamination, this transverse crack needed to be opened first. It is suspected that the PID-controller will struggle during the transition between transverse crack and delamination when the transverse crack snaps open. Therefore, the practice to initiate the transverse crack at the outset was planned before running the delamination growth.

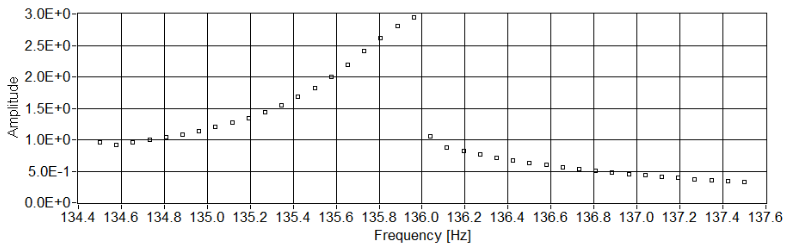

(a)

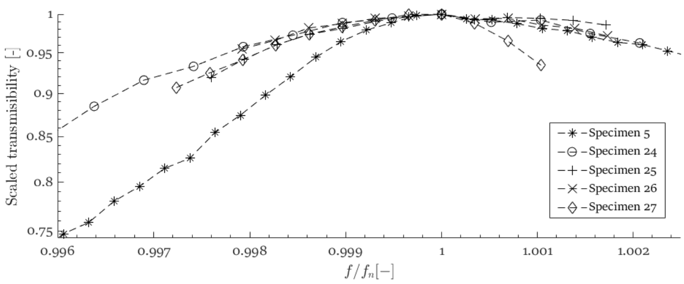

(b)

Figure 3.8: Creating the transverse crack in a thermoset (a) and in the used thermoplastic specimens (b). A separate test was conducted on a thermoset to show this behaviour.

Therefore an initial high acceleration (∼3g) frequency sweep around the first mode is conducted to break the matrix material in the transverse crack. This process is used successfully previously on thermoset composites. During the Frequency Sweep the amplitude of the response increases since the excitation frequency get increasingly close to the specimens resonance. Due to the increasing displacement the load on the transverse crack increases. At some point during the test will the stresses become too large for the local matrix material. The transverse crack is known to open extremely fast. Since the load bearing cross section is suddenly diminished, the dynamic properties will change. Due to this the excitation frequency will not be near the resonance any more. The amplitude, and thus the stress around the crack, drops

significantly. This drop off is depicted in figure 3.8a. Due to this instant reduction of stress and strain it is ensured that no damage is added to the system from then on, making sure that only a transverse crack is introduced in the system and nothing more.
When applying the same process in this research with a thermoplastic, a distinct tinking noise can be heard when exciting the system near the resonance. This indicates some kind of failure is introduced in the specimen. However, when inspecting the corresponding Frequency Response Function in figure 3.8b the immediate drop off is not present. Some smaller deviations near the peak do indicate some change in stiffness. It is likely that due to more resilient nature of thermoplastics [8] the transverse crack does not snap open at once, but gradually grows. It can be seen from the FRF that not all specimens give the same response. It is likely that the due to this the initial damage to the specimen is not completely consistent. This uncertainty has to be taken into account when analysing the results of the tests. In order to compare the FRF in one figure the transmissibility is scaled to its peak and the frequency is scaled to the resonance frequency.

3.6 High Cycle Fatigue test

When the preparatory tests are conducted the High Cycle Fatigue (HCF) endurance test can be started. The specimen is excited in the resonant frequency found in the modal tests. By conducting several trial tests the decision was made to apply this displacement control at an amplitude of 3.78 mm. In order to not immediately break the specimen when starting the endurance test the acceleration is delivered gradually, causing between 3.000-13.000 cycles to be required to set up the test. These cycles are not counted in the total number of cycles subjected upon the specimens since they deliver much less energy into the delamination.
During the endurance tests the LDV measures the specimen's velocity with a sample rate of 10 kHz. After every 30 samples Fast Fourier Transformation is applied. This allows for continuously tracking the phase of the response with a rate of 333 Hz. During the tests the mean amplitude, acceleration and excitation frequency are saved. An example of these results are depicted in figure 3.9.

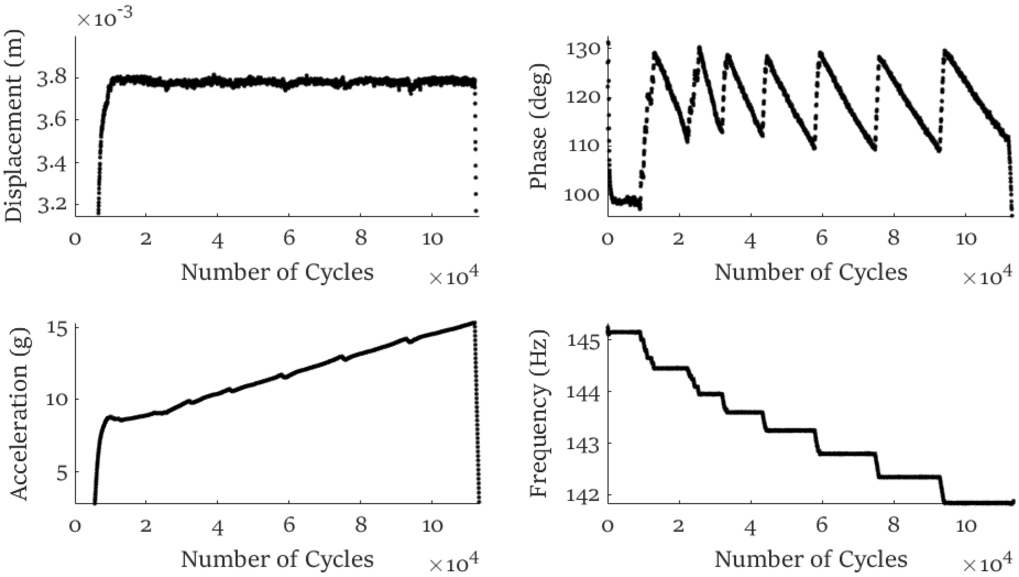

Figure 3.9: Displacement, required Acceleration, Phase and excitation frequency during the HCF sequence for specimen 5 from plate 1. Note how the characteristic phase hikes corresponds to the frequency updates.

In the top right a drop in phase can be distinguished over when the test develops. As explained in section 2.7 is the phase extremely sensitive to the stiffness of the system. A measured phase drop with f_{exc} constant indicates a reduction in stiffness, meaning a propagating delamination. The characteristic 180° drop of the phase of the FRF is in narrow frequency range ($\sim$0.1Hz). To make sure the phase remains within this sensitive are during the complete endurance tests, the excitation frequency is updated when the phase drops with 8-14°. Updating is done manually by incrementally reducing the frequency with steps of 0.01Hz. This splits the endurance tests into multiple segments. Between each segments the PID controller required some steps to settle at the correct displacement. This requires approximately 500 steps. The endurance test is continued until the desired number of cycles is reached. The number of cycles for the 5 best specimens are 50.000, 75.000, 100.000, 125.000, and 180.000 cycles. The results of these tests will be discussed together with the corresponding results from the numerical investigation in Chapter Results in section 5.3

3.7 Microscope measurement of crack length

After the modal tests and the endurance test is complete the specimen is removed from the fixture. The delaminated region is cut from the specimen. The cross sections are polished using automatic polishing equipment. After which they are placed in the corresponding fixture first. A mount is used to ensure that the specimens are fixed exactly parallel in the polisher. The automatic polisher exerts a constant force during operations of 30 N divided over three specimens. The polishing scheme is as follows: 1:30 min with grain 1000, 2000 and then 4000 and final etching is achieved by polishing with OP-S on a cloth for 3 min. The surfaces are treated with isopropyl alcohol and dried with a hair dryer to ensure no residue from water is left on the surface. Then the surfaces are inspected and photographed with a Keyence VHX 7000 Digital Microscope. The attached lens has a magnification of times 1000. The complete procedure is repeated on both side A and B of the specimen and for some case as well after polishing off $\sim$1mm of the sides. This final step allow to get a small insight as to what is happening with the delamination deeper into the specimen.
Note that in preparation of the experimental investigation the gap near the cut-ply was measured using the same microscope. The resulting images are of poor quality, because complete specimens do not fit in the automatic polisher. Therefore, the specimens were polished by hand. The polishing step with grain 1000 was skipped in order to not damage the specimens. No etching was applied.

4 NUMERICAL INVESTIGATION

This chapter is dedicated to describing the numerical approach and all its components. An extensive numerical approach was set up to investigate beyond the experimental capacity. The results will be discussed together with the results of the experimental investigation in the Results chapter.
A specific approach is set up that reinforces the experimental investigation. The approach matches the experimental High Cycles Fatigue endurance tests as closely as possible. This includes displacement control and updating the excitation frequency. Where the experiments will show a relation for in the phase drop over the number of cycles ($\frac{\Delta\varphi}{\Delta N}$). The numerical framework can give insight in the phase drop over the crack growth ($\frac{\Delta\varphi}{\Delta a}$). During a vibration the loading conditions on the specimen change between a positive and negative deflection. The numerical framework investigates the mixed mode loading conditions for both directions, giving insight in how each of these modes contribute to the fatigue failure.
In this chapter the approach is described first. In the upcoming section the components of the approach will elaborated on, where the components consists of the FEM model itself and the different types of modelling. The frequency analysis will be used for a sensitivity analysis of the element size to check the viability of the mesh of the model. A goal of the modelling approach is automation. The approach that is set up requires several analysis types on a lot of separate models, where each model represents a different crack size.

4.1 Modelling approach

The modelling approach is set out in figure 4.1. The red arrows indicate the flow of the analyses and the black lines the flow of required data for these analyses. The approach is designed to follow the experimental High Cycles Fatigue tests as closely as possible. The complete process is automated in Python using Abaqus scripting. Important features of the model are parametrized, most importantly its dimensions. Resulting in a very flexible model. This allows for the model to be used in later research as well and allows for modelling different set ups quickly.

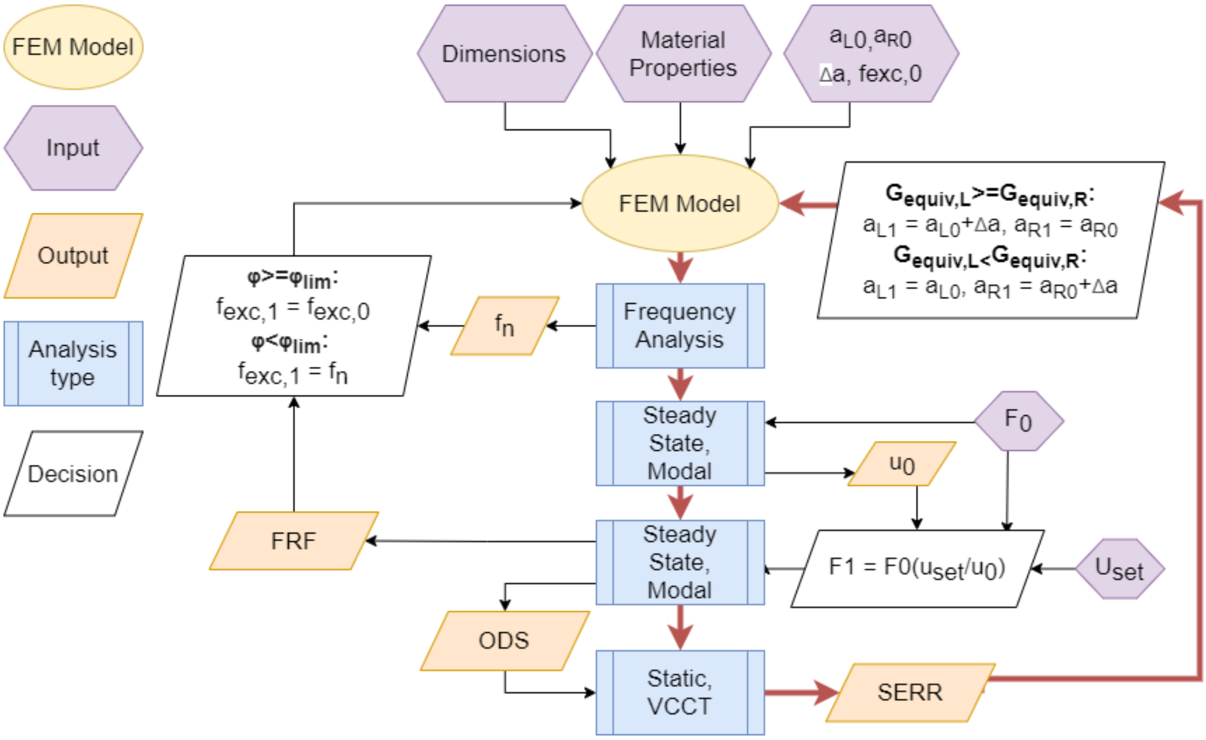

Figure 4.1: Modelling approach. The red arrows indicate the flow of the analyses and the black lines the flow of required data for these analyses.

The composite cantilever beam is modelled in Abaqus matching the material properties and dimensions of the physical specimen as closely as possible, as more closely described in section 4.2. The numerical investigation starts with the transverse crack and follows the effects of the growth of a delamination. This is done by incrementally releasing a contact constraint near the crack tip. The delamination then grows as depicted in figure 4.2, which is similar as found in the experimental work. In the schematic overview this process is depicted as the right outer loop. So for every time the loop is passed a new FEM model is set up. For each loop an excitation frequency is used to focus on, just as in the experiments. When the phase drops below a set level (φ_{lim}), the excitation frequency for the next step ($f_{exc,1}$) is updated to the current first natural frequency f_n. Represented as the outer loop on the left in the schematic modelling approach. In each loop first a frequency analysis is conducted, as described in section 4.3. This step is used to perform eigenvalue extraction to calculate the natural frequencies and corresponding mode shapes of a system. Then, a steady-state dynamic analysis is conducted based on the systems eigenfrequencies and -modes, as described in section 4.4. This type of modelling is used to calculate the steady-state dynamic linearized response of a system to a harmonic excitation. This harmonic excitation is achieved by applying a harmonic input force (F_0) of a fixed magnitude onto the tips of the specimen. In the experimental endurance tests displacement control was applied on the LDV-position. To investigate a situation similar to this in the numerical model, the displacement at the LDV position (u_0) is exported from the SSD analysis. A second SSD model is then set up where the input force (F_0) is scaled such that the displacement at the LDV position will result in a set fixed displacement (u_{set}). Simply scaling the input force is possible due to the purely linear nature of this type of analysis. In order to save on time the first SSD analysis only save u_0. From the second SSD analysis the Operating Deflection Shape (ODS) of the specimen is saved for the current excitation frequency and the Frequency Response Function is saved of the LDV-position. Since the SSD analysis shows the specimen's vibration based on the specimens eigenmodes following a sine based path it cannot take the local behaviour around the delamination into account. In order to investigate this local region the complex ODS of the specimen in the excitation frequency is imported as a displacement boundary condition into a static model. This is done for two time instances of the complex ODS: When the LDV-position is at its maximum position, so the delamination is closing and when the LDV is at its minimum position, so the delamination is opening. The Virtual Crack Closure Technique is then applied on both orientations, as described in section 4.5. The Strain Energy Release Rates at the crack tips are saved. These SERR's are used to investigate the mode mixity of the cyclic load. The SERR at the left and right crack tips are compared as the crack propagates in the direction where the SERR is highest. The process stops after a set number of iterations pf 30.

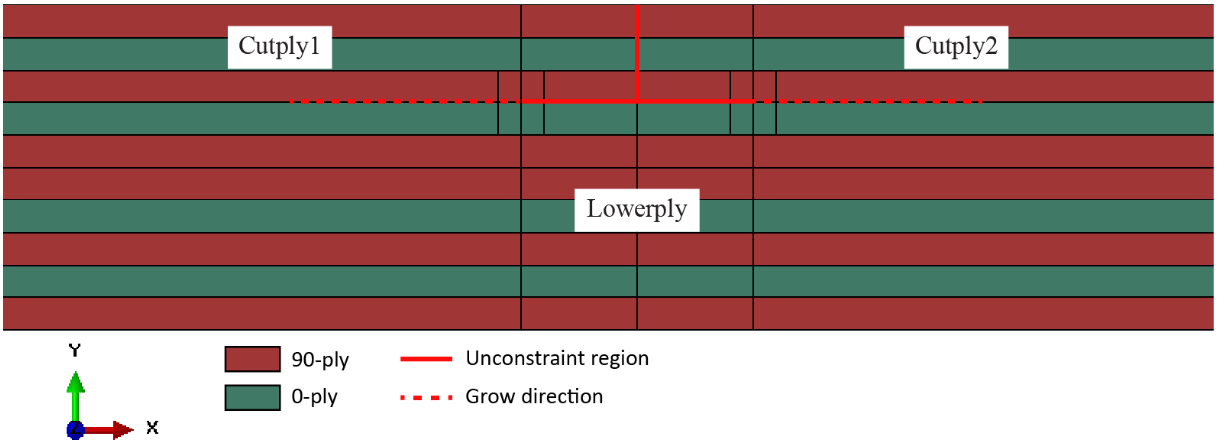

Figure 4.2: Schematic depiction of modeled specimen with delamination grow directions.

4.2 FEM model

This section will describe the set up FEM model. First the geometry in the model is discussed. Followed by the element selection. Next the material properties are discussed. Then the set boundary conditions are described and the interactions during the static analysis. Then the described analysis types will be discussed. The mesh that was set up will be described in the subsection about the frequency analysis, since a sensitivity analysis of the element size will be part of this.

4.2.1 Geometry

A numerical model is set up in Abaqus FEA and is depicted in figure 4.3. The specimen was modeled as a 179 mm long and 25 mm wide and 1.4 mm cantilever beam. The complete specimen consists of 10 0.14 mm thick plies. The lay-up sequence of the beam is [90(cut)/0(cut)/90(cut)/0/90/90/0/90/0/90]. Where these cuts are located 10 mm off center to the right. The crack is modelled as a gap of 0.01 mm width, in order to prevent any problems with buckling in the static analysis step. By cutting the first three layers a transverse crack is created in the model, similar to the physical specimens. The LDV-position is located 52 mm off center to the right, similar to the physical specimens. Section 3.2 is described how the physical manufactured specimens have imperfections. The described imperfections were resin gaps, fiber flowing around the resin gap and the plies not being exactly 0-, or 90-degrees. None of these imperfections were included in the numerical model, causing the models to represent a slightly different situation. Differences in test results between the two can be attributed to so some degree to this decision. It is chosen to not include these imperfections in the model in order for the model to remain as general applicable as possible and because matching the real specimens would prove to be very difficult.

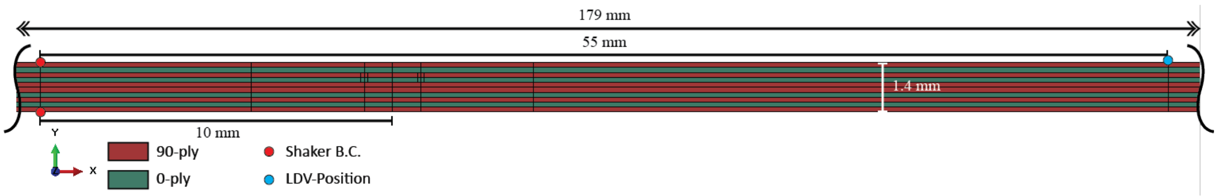

Figure 4.3: The FEM model with dimensions.

4.2.2 Element selection

The specimen are simplified to a 2D model by taking plane stress conditions into account. This will be accurate for thin structures, like composite plates, under a transverse load. By reducing the model to a 2D model computation times will be significantly reduced. Therefore plane stress beam elements are used.
In the static model relatively large deflection are subscribed to the specimen. A simple four-node quadrilateral plane stress element is not applicable for large deflections, since they are susceptible to hourglassing, an effect that is observed in earlier trial analysis. Therefore the 8-node biquadratic plane stress element is selected. In order to prevent any locking behavior this element is used with reduced integration.

4.2.3 Material properties

The anisotropic behaviour of the composite beam is modelled by attributing the 90 degrees plies different material properties from the 0 degree plies. This is done according to orthotropic constitutive equations, in equations 2.3 and uses the fact that they are symmetric, e.g. equation 2.4. The material properties of the carbon fiber and PEEK resin are set out in table 4.1 and are provided by the materials manufacturer TPRC. The name of the material is Toray Cetex TC1200 PEEK and its data sheet is added as appendix A. The out-of-plane Shear modulus was not provided. With out-of-plane shear a load is applied parallel to the fibers, the fibers will not add stiffness in this direction. Therefore the shear modulus of the matrix material PEEK is used, which will be close to reality since the fibers do not add any stiffness in this direction.

Table 4.1: Material properties of Toray Cetex TC1200 PEEK

Property		Units	[0] Plies	[90] Plies
Density	ρ	kg/m^3	1590	1590
Young's Modulus	E_1	GPa	135	10
	E_2	GPa	10	135
Poisson ration	v_{12}	-	0.28	0.0208
Shear Modulus	G_{12}	GPa	5.20	1.45
	G_{13}	GPa	5.20	1.45
	G_{23}	GPa	1.45	5.20
Critical SERR	G_{Ic}	kJ/m^2	1.6	
	G_{IIc}	kJ/m^2	2.3	
BK-power law coefficient	η	-	0.63	
Friction coefficient	μ	-	0.75	
Damping ratio	ζ	-	0.01	

4.2.4 Boundary conditions

At the middle of the specimen a displacement boundary conditions is included on two nodes, as depicted in figure 4.3. The two nodes are located where the electromagnetic shaker would be attached in the experimental work. The boundary condition consists of setting the displacement to zero for both x- and y-direction.

4.2.5 Interactions

During the VCCT analysis in the static model the delamination acts upon the base structure. This is achieved by defining interaction properties in the model. The interactions with labels are depicted in figure 4.4. The interaction between the two parts normal to each other is achieved by setting a hard limit. When the positive ODS is subjected onto the static model the delamination shears over the base structure. The tangential behaviour of the interaction model is created by setting a friction coefficient of 0.75, in accordance to [4]. In this research on the same material the friction coefficient is matched to an increase in temperature around the delamination.
So an interaction is created between the delamination and the base structure. Parallel to this an interaction between the two tips of the delamination is created, called the Tip interaction. The interaction is modelled as a hard contact and without any tangential properties. Note that these interactions can only be taken into account in the static analysis.

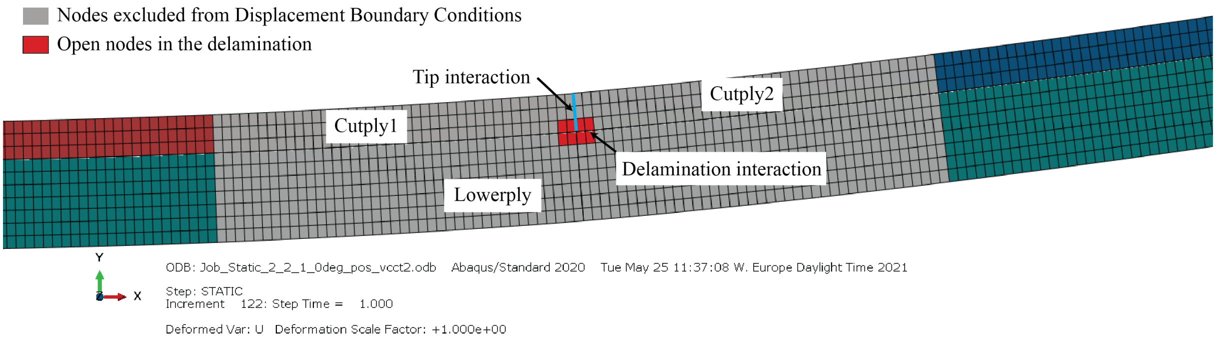

Figure 4.4: Interactions and boundary conditions in the numerical model. The tip interaction is marked with the cyan line. The delamination interaction is between the red nodes.

4.3 Frequency and sensitivity analysis

The numerical frequency analysis performs eigenvalue extraction to calculate the natural frequencies and the corresponding mode shapes of a system. The analysis type is a completely linear step. This means that the effects of the interactions will not be taken into account, even though the opening and closing of the delamination might influence the dynamic properties of the system.
The number of natural frequencies to be investigated is chosen to be 10. The higher frequencies will only have a minor influence on the steady-state response at the excitation frequency of approximately 150 Hz. The tenth mode has a frequency of 9 kHz which will have negligible effect near the investigated region.

The frequency analysis is used as a sensitivity analysis of the element size to validate the models mesh. A model is set up with a mesh of 5 mm and is incrementally reduced to 0.05 mm. The resulting resonant frequency and the required CPU time is plotted for each step, as depicted in figure 4.5. The model has a delamination of 0.2 mm both left and right.
As becomes clear from the analysis does the resonance not change as much anymore after 0.2

mm. The required CPU time drastically increases above 0.1 mm. Based on this analysis the element size can be chosen. The element sizes are special case mesh where the element size is set to 0.5 mm, but the mesh is refined near the shaker to 0.1 mm. The refined region includes the crack. The strains near the refined area are relatively larger, requiring a smaller element to calculate accurately. This results in an accurate and time efficient mesh. The chosen mesh is added to figure 4.5.
An additional motive of the refined mesh is that the delamination opens node by node. An element size of 0.1 mm allows for investigating many crack sizes, while keeping the calculation times manageable.

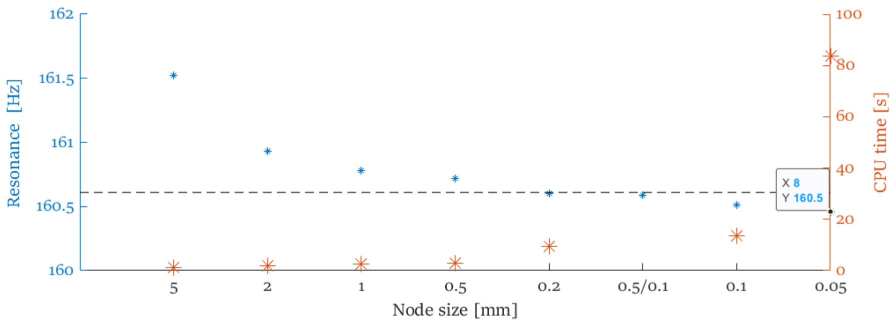

Figure 4.5: Resonant Frequency and required CPU time for the Frequency Analysis dependent of the element size. The black dotted line indicates the set acceptable level.

4.4 Steady-State Dynamics analysis

The Steady-State Dynamics (SSD) analysis provides the steady-state amplitude and phase response of a system due to a harmonic excitation. This analysis type uses the dynamic properties of the current model found in the frequency analysis. A damping ratio (ζ) of 0.01 is set over all found modes. This value was not matched to the experimental investigation, since the conducted experimental showed a nonlinear damping over the input acceleration.
As described in the numerical approach is the SSD conducted twice for each model, first to displacement control the system and next to investigate the FRF around the excitation frequency and Operating Deflection Shape in the excitation Frequency.
The first time the SSD analysis is conducted an initial load (F_0) of -0.025N is applied in y-direction at both free ends of the cantilever beam. This allows for the displacement control at the LDV-position for the second analysis. The displacement was set to 3.78 mm (u_{set}) in order to match the displacement in the experimental investigation.
Most importantly the SSD analysis is used to save the phase in the current excitation frequency. Since the phase is regarded as a very sensitive parameter to a reduction of stiffness, i.e. a propagating delamination. The development of the phase through the modelling approach is set out in section 5.3.5. The effect of updating the exciting frequency, like in the experiments, is investigated. The excitation frequency is updated when the phase drops below the limit (φ_{lim}) of -3 rad. This values is chosen such that the frequency is updated once in the framework, approximately in the middle. The resulting FRF of the computational approach can be set to have very dense data points, meaning that it would be possible to get a very exact phase development even outside the sensitive area. However, updating the frequency anyway can give insight of its effects of the phase drop and the Energy Release Rates later on.
This approach gives insight in the development of the FRF and ODS of the approach, which are depicted in figure 4.6 and 4.7 respectively. The completely right FRF functions correspond to the pristine model. For each model the FRF shifts to the left, so the FRF completely left corresponds to the fully propagated crack. The vertical lines in the FRF plot indicate the inves-

tigated excitation frequency. Also, note that all amplitude functions meet at u_{set}, marked with the horizontal line.

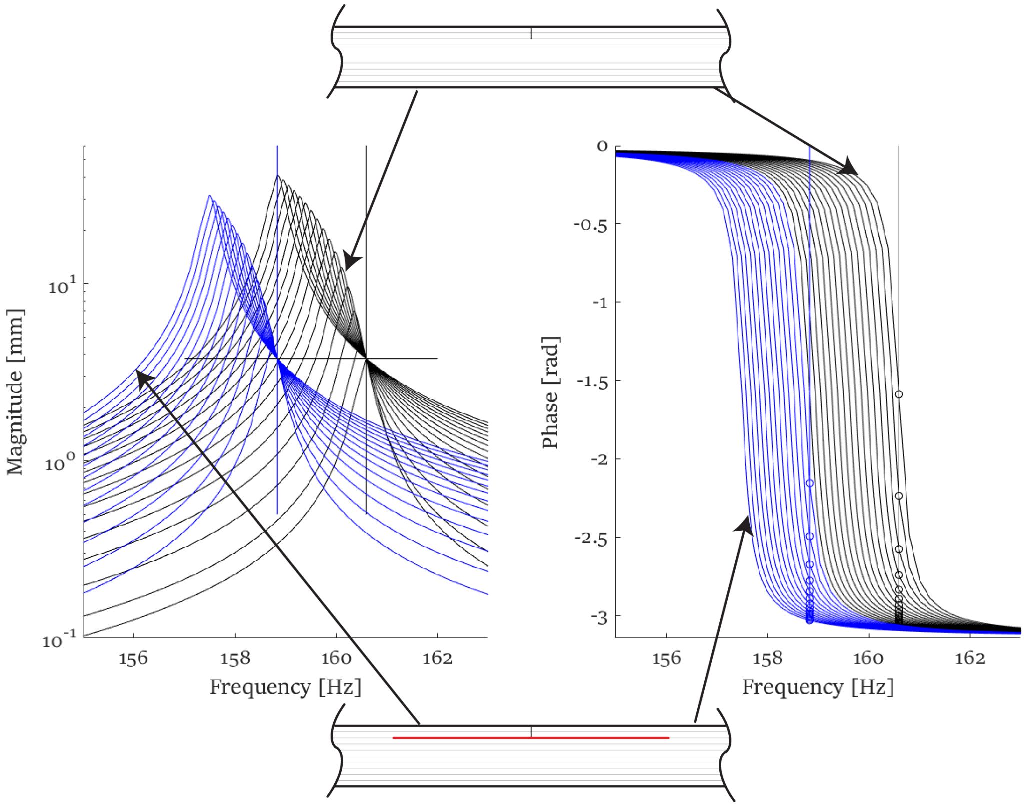

Figure 4.6: Frequency Response Functions for each investigated crack size. When the excitation frequency is updated the line color is switched from black to blue. The vertical lines indicate the excitation frequency and the horizontal line indicated the displacement of 3.78 mm.

The figure depicting the ODS shows that the LDV-position is constant throughout all tests. The pristine side (left) however, does deviate largely. This was the motivation to change the LDV-position to the cracked sided in the experimental investigation.

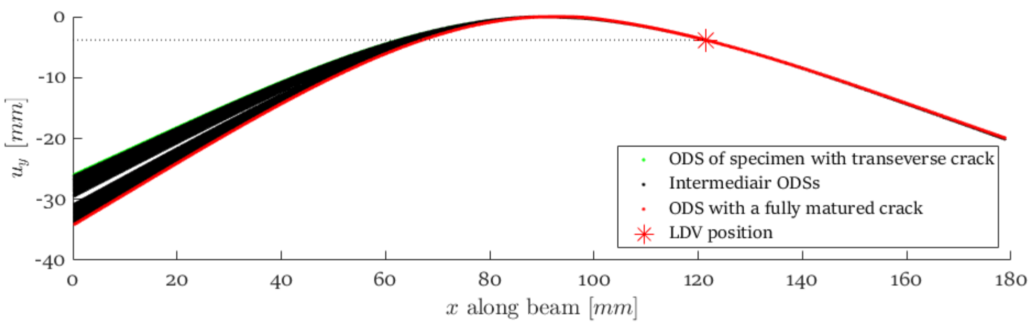

Figure 4.7: Operating Deflection Shapes for each investigated crack size.

4.5 Static model with the Virtual Crack Closure Technique

From the previous analysis step the complex Operating Deflection Shapes are found for current excitation frequency. Two specific orientations in time are selected to be of special interest: When the crack tip is at the maximum and minimum. Here the strains energies near the crack tips will be highest. The ODS with the tip at the max is called the positive ODS, and the other

way around is the negative ODS. The positive ODS is characterized by the delamination being compressed together, so this corresponds to crack closing. The delamination shears along the base structure. The negative ODS is pulling the delamination from the base structure, so it corresponds to crack opening. The VCCT analysis is performed on the two cases separately. The general specific interactions properties and the interactions were set out in section 4.2.5.
The two ODS's orientations are imported in a static model as a displacement boundary condition. The nodes near the delamination are excluded from the boundary conditions, as depicted in figure 4.4. These nodes should not be described by the SSD analysis since this analysis type is not able to predict the ODS near any interactions. This is due to the complete linear nature of the SSD analysis.
As described in the theoretical background in section 2.3.4 can the VCCT analysis be used to investigate the crack propagation along a defined surface. This will be applied on the delamination with the imported deflections. During the analysis the boundary conditions are applied incrementally for each step. The model is subjected fully to the boundary conditions only at the final time step. The analysis is split up into increments. For the initial time step in the analysis all nodes part of the delamination start as bonded to the base structure. Then for each increment the Strain Energy Release Rates (G_I and G_II) are calculated for these nodes. When the equivalent Strain Energy Release Rate (G_equiv) exceed the critical equivalent Strain Energy Release Rate ($G_\text{equiv,C}$) the node is released. All according to equations 2.14 and 2.15. Note that in fatigue a crack can progress even if the critical G has not been exceeded, all according to the modified Paris-Erdogan law in equation 2.11. In order to ensure that the crack propagation in the numerical framework does not settle to soon, $G_\text{I,C}$ and $G_\text{I,C}$ are reduced with a factor ten thousand. The $G_\text{equiv,C}$ is calculated using the BK power law (eq. 2.15). As explained in the theoretical background in section 2.3.4 is the coefficient η in this equation material depended and found from experiments. For the carbon fiber PEEK composites literature was found that have conducted these experiments on a similar material and found the coefficient value of 0.63 [31]. The similar material is unidirectional AS4/PEEK. Where AS4 is a standard modulus carbon fiber, which is the same classification as the carbon fiber in this thesis. The BK-powerlaw coefficient was taken after the specimens were pre-cracked under 20% mode II loading, which is a difference that can cause some deviation from the found value. This value will be used in the numerical framework.
For each loop in the numerical approach a VCCT analysis is conducted for a growing delamination with one node added to the delamination region. For each loop it has to be decided towards which direction the delamination matures. Therefore the G_equiv is calculated for both sides of the delamination. A node will be released at the side with the highest Strain Energy Release Rate. Note that the $G_\text{equiv,C}$ is in this case *not* used to decide whether a crack propagates at all. From the theory of fatigue in section 2.3.4 it is clear that in fatigue a crack can mature even if the critical value is not exceeded.

5 RESULTS

With all described tests in the experimental approach conducted and the numerical framework completed, the results can be analysed. This section will discuss notable feature of the measured signals. All analyses and their goals are summarized as:

- The shift in resonance frequency of the pristine, the transversally cracked and the fatigued specimen will be used to find an initial indication of the introduced damage into the specimen. The resonant shift before and after opening the transverse crack will indicate how consistent this opening is.
- The (non-)linearity of the input acceleration to the response amplitude will be investigated in order to determine if the dynamics from the modal tests are representative of the specimen during endurance testing.
- The ODS from the experimental approach before and after the endurance tests will be compared to investigate the change in dynamic properties.
- The ODS from the experimental approach will be compared to the ODS from the numerical approach in order to determine how representative the numerical model is of the experiments.
- The strains will be determined and compared to the numerical model to investigate if retrieving ODSs with line scans is a feasible method for estimating surface strains.
- The resulting signal of the line scans are demodulated separately for the positive part (crack closing) and negative part (crack opening) to investigate if the line scans are appropriate to investigate any non-linear harmonics. The positive and negative envelope of the line scan signal will be investigated with the same goal.
- The phase drop over the number of cycles will be set up as an indicator of the reduction of stiffness, i.e. the propagation of the crack.
- The total drop in phase will be used as an indicator of the total reduction of stiffness. This will be related to the crack lengths in the material. A relation like this will be powerful for predicting the crack lengths in future tests.
- A relation will be set up for the phase drop over the crack growth from the numerical model. This will show how a relation would look like between the measurable phase drop in experiments would relate to crack growth.
- The mode mixity will be investigated from the numerical investigation. The strain energy release rate at the crack tips will show which mode will be more dominant. Specifically the effects of the novel features will be investigated. Being an interaction property between the tips of the two delamination sides and the inclusion of the friction coefficient in the interaction between the delamination and the base structure.

Finally the most important results will be summarized.

5.1 Frequency Response Functions

As described in section 3.4.1 in the experimental investigation are frequency sweeps conducted to find the dynamics of the systems. Two things are investigated. The next two subsections are dedicated to how the dynamics change due to damage introduced to the system and how the response change with respect to acceleration levels.

5.1.1 Frequency shifts between tests

How much the resonant frequency shifts before and after the endurance tests can be a first indication of the amount of introduced damage. Similarly, the resonance shift before and after making the transverse crack (as described in section 3.5) can be an indication in how well the transverse crack has matured.
The FRFs are depicted in figure 5.1. Note that the pristine FRF for specimen 5 was conducted on 50 mV instead of 100 mV which explains its distinct different response. A frequency shift is observed after the transverse crack is made. How much the frequency shifts is found to vary a lot. The results, including resonance shifts, are set out in table 5.1. Where the resonance of specimen 5 of plate 1 shifts 0.7 Hz, specimen 5 and 6 from plate 2 only shift 0.10 Hz, seven times less. As described in section 3.5 it is suspected that the more resilient nature of the matrix material cause the transverse to not snap open at once, but more gradually mature. Therefore it is suspected that the specimens that show a higher frequency drop already have a more matured transverse crack. The main aspect to take from this is that it is likely that the endurance tests, presented in section 5.3, do not start at the same point. A certain number of cycles of the endurance test of specimen 24, 25 and 26 are used to grow the transverse crack and not to grow a delamination. This impacts the research, since maturing the transverse crack is part of the damage initiation phase, instead of the damage propagation phase. The results in figure 5.1 show an increase in damping for before and after the endurance tests. No change in damping was found before and after making the transverse crack. All pristine specimens have a damping ratio of 0.17 and all fatigues specimens of 0.22.

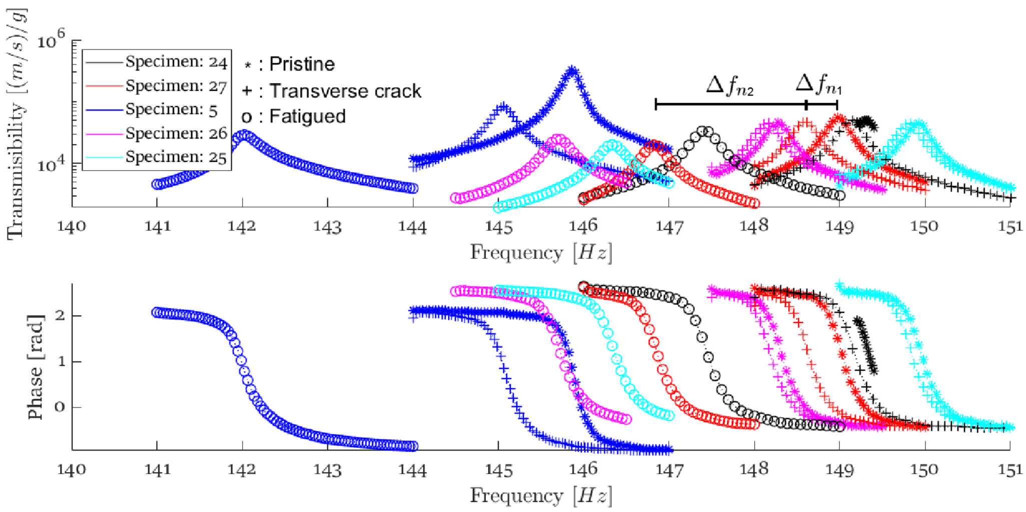

Figure 5.1: FRF's of the top 5 specimens (Pristine, with transverse crack and fatigued).

5.1.2 Non-linearity of the beam structure

Very important to note is that the response of the specimen is not linear to the input acceleration. As previously explained in section 3.4.1 is this behaviour mapped by conducting several FRFs

Table 5.1: Natural frequencies of the pristine, transversally cracked and fatigued specimens. $\Delta f_{n,1}$ shows the frequency shift before and after the transverse crack and $\Delta f_{n,2}$ shows the frequency shift caused by the endurance test.

Specimen	Number of Cycles (#)	f_n pristine (Hz)	$\Delta f_{n,1}$ (Hz)	f_n Transverse crack (Hz)	$\Delta f_{n,2}$ (Hz)	f_n Fatigued (Hz)	Total shift (Hz)
plate 2 spec 4 (24)	50.000	149.31	0.15	149.15	1.76	147.38	1.92
plate 2 spec 7 (27)	75.000	148.97	0.35	148.61	1.79	146.82	2.15
plate 1 spec 5 (5)	100.000	145.8	0.7	145.06	3.03	142.02	3.83
plate 2 spec 6 (26)	125.000	148.26	0.10	148.16	2.48	145.67	2.58
plate 2 spec 5 (25)	180.000	149.92	0.10	149.82	3.48	146.33	3.58

on increasing input accelerations on a dedicated separate sample. The change in transmissibility and phase is set out in figure 5.2. The most important aspect to take from this results is that the damping increases drastically when the input acceleration increases. Which can be seen from the fact that the peak of the amplitude flattens and that the phase drop flattens. During the endurance tests the accelerations are very high relative to the modal tests. Due to this increasing damping do the modal tests not represent the situation during the endurance test very well. The sensitivity of the phase drop is much smaller than initially expected due to the flattened phase curve. However the phase drop during the endurance tests will be constant over a much wider frequency range, which will lead to more consistent results.
Note that these tests were conducted on a specimen of different dimensions. Therefore the first mode is found at a different frequency as before. The damping effects are expected to be similar since the material is the same.

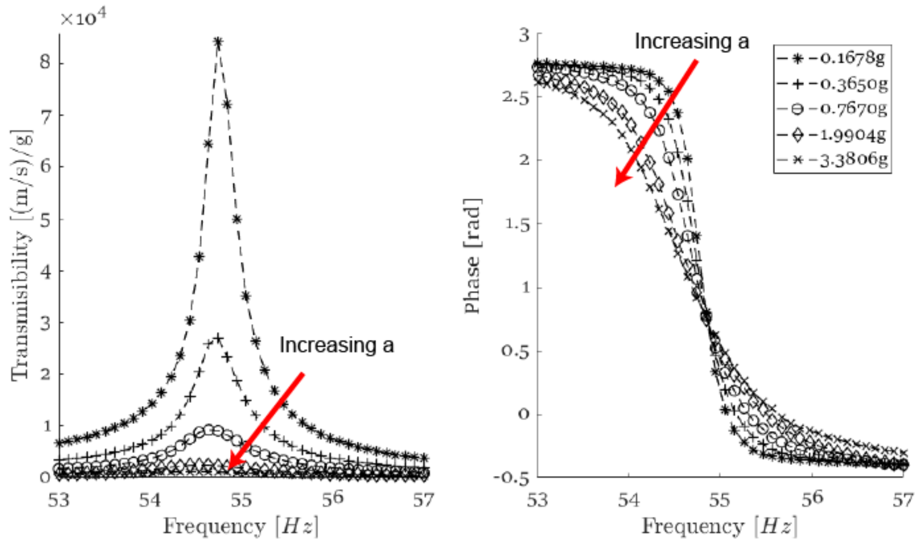

Figure 5.2: Frequency Response Function for varying voltage levels.

5.2 Operating Deflection Shapes (ODS)

The modal characteristics of the specimen were investigated further according to the procedure described in section 3.4.2. The next sub-section will describe the procedure of analysing a typical CSLDV signal and will set out the results of the line scans of the pristine, transversally cracked and fatigued specimens. The next sub-section will compare the found line-scan to the ODSs found in the numerical analysis. In the next subsection the strain will be derived from the experimental ODS and will be compared to the strain found in the numerical investigation. In the final subsection a side-track is investigated: The CSLDV signals will be investigated again to find any non-linearity in the harmonic vibration.

5.2.1 Experimental ODSs

A typical CSLDV result signal is depicted in figure 5.3. The signal in voltage is converted to velocity with the set sensitivity of 2.5 m/sV. The displacement is found by dividing the signal with the current excitation frequency.

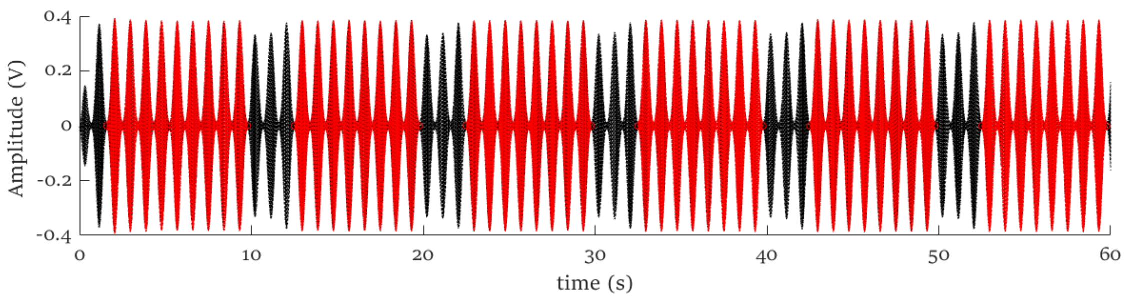

Figure 5.3: Line Scan Response signal.

As described in section 2.7.2 are steady-state conditions required in order to measure a constant ODS. Figure 5.3 shows that in the beginning of the signal the vibration needs to be started first. This part of the signal is removed. A second observation is that after some scan passes the amplitude of the signal drops off to some extent. The cause of this drop off is thought to be in the control program of the test. Some deviation is found in the peak height of all passes, indicating that the signal is never completely steady-state. This causes some error in the resulting ODS. The part of the signal deemed of sufficiently high quality is indicated in red in figure 5.3. This means that the signal is now cut into multiple segments. These segments are treated as individual tests. As explained in section 2.7.2 it not possible to use a window on the segments, since this will alter the resulting ODS. Therefore special care is taken to cut the segments at the data point nearest to zero, to minimize spectral leakage. The segments are demodulated using the theory from section 2.7.3. Each segment now has a corresponding real and imaginary ODS, which is then fitted with a polynomial function. The order of the fit is increased by one until the Modal Assurance Criterion is higher than 0.999. The maximum order however is set to 7 in order to prevent overfitting. Each segment is fitted separately. MAC scores between the fit and the original data are set out in table 5.2. Only the MAC is denoted of the segment with the lowest criterion. The segments with a MAC below .98 were removed from further analysis. Increasing the polynomial order is found to only barely increase the MAC scores, this is likely due to not completely steady-state conditions. Meaning that not one polynomial exists that fits all the data. By setting the derivative of equation 2.32 to zero the time instance for which the velocity at the tip of the specimen is max is found. The ODS corresponding to the complete specimen is found by averaging the results of each segment. The max ODSs of the 5 specimens, for the pristine, transversally cracked and fatigued case, are depicted in figure 5.4. The quality of the found ODS increases by increasing the durance of the tests. The tests in this thesis were conducted for 60 seconds, before removing the bad data.

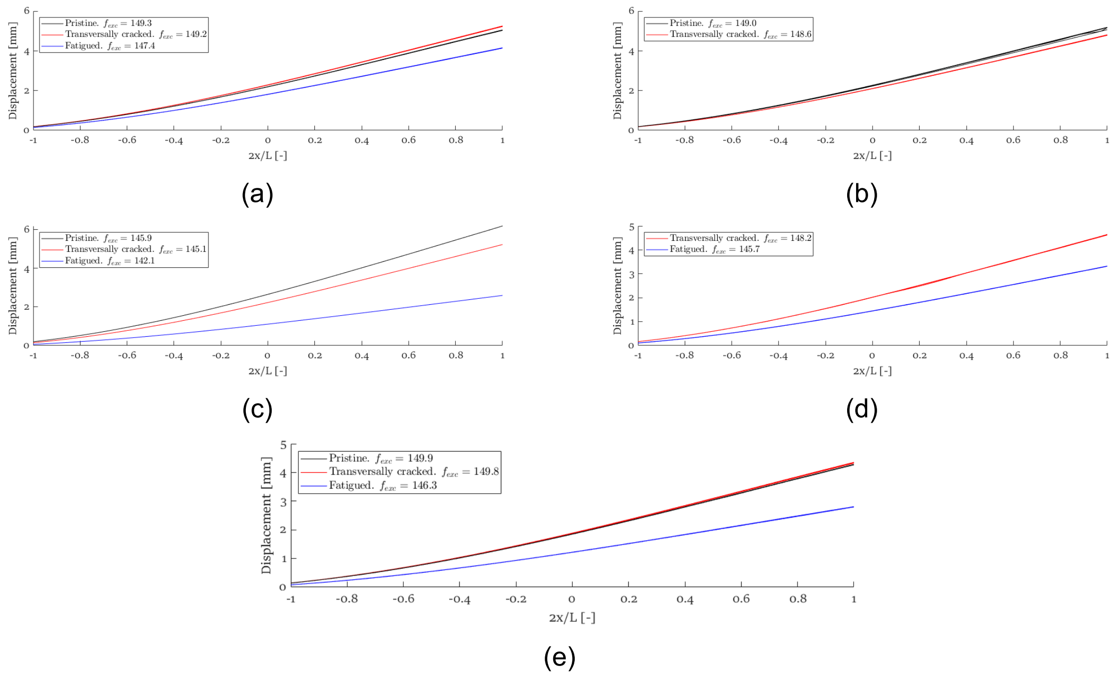

Figure 5.4: Pristine, transversally cracked and fatigued ODSs of the five specimens. (a) Specimen 24: 50.000 cycles, (b) Specimen 27: 75.000 cycles,(c) Specimen 5: 100.000 cycles,(c) Specimen 26: 125.000 cycles and (e) Specimen 25: 180.000 cycles,

The displacements of the fatigues specimens are lower, which can be attributed to the increase in damping.

Table 5.2: Modal Assurance Criterion of the results and its corresponding polynomial fit. For the Pristine (P), transversally cracked (T) and the fatigued (F) specimens. For both the real and imaginary ODS.

	Real			Imaginary		
Specimen	P	T	F	P	T	F
Plate 2 spec. 4 (24)	0.999	0.999	0.999	0.994	0.984	0.988
Plate 2 spec. 7 (27)	0.981	0.999	x	0.989	0.996	x
Plate 1 spec. 5 (5)	0.994	0.988	0.999	0.999	0.988	0.997
Plate 2 spec. 6 (26)	x	0.999	0.999	x	0.980	0.988
Plate 2 spec. 5 (25)	0.999	0.999	0.999	0.986	0.993	0.993

5.2.2 Comparing the numerical and experimental ODSs

The retrieved ODS of the Steady-State Analysis in the Numerical model is compared to the experimentally retrieved ODSs. Specimen 5 is used after the transverse crack is created. The amplitude of the ODS of the Numerical model is scaled with scalar α to fit best over the experimental ODSs, which is possible since the SSD analysis is a purely linear modelling type. The length of the scan path (L_p) was measured to be 73 mm with a ruler. This measurement will not be exact, so the length of L_p will be scaled with scaler β to fit the numerical ODS best. The smallest distance between the fixture and the scan path (d_p) is calculated to be approximately 16 mm from the found scan path length and the specimens length. Since this will not be exact d_p is varied to fit the numerical ODS best. The optimal values for $[\alpha, \beta, d_p]$ are found with a non-linear numerical optimization scheme, based on the interior-point method where the Hessian is estimated using BFGS [32]. The initial guess was set to $[1, 1, 16]$. The optimization goal is to maximize the Modal Assurance Criterion (MAC) between the two ODSs. The max MAC of 0.99 was found with α is 0.12, β is 1.002 and d_p is 14.2 mm. The results are depicted in figure 5.5. The main take from this result is that a great accordance can be found between the numerical and experimental results.

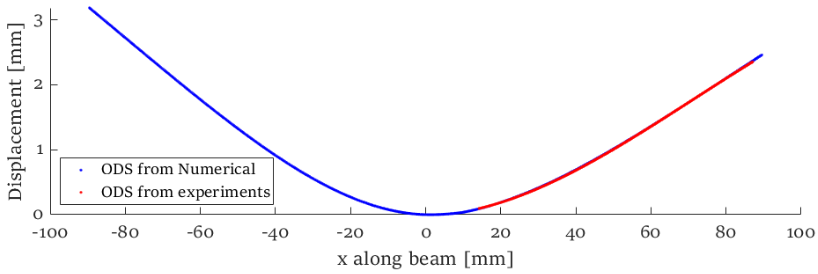

Figure 5.5: The experimental ODS aligned with the Numerical ODS.

5.2.3 Strain from ODS

From the ODS it is possible to determine the strain along the specimen according to the analytical strain equations for plates in equation 2.5. The found relative strains are depicted in figure 5.6. An attempt is made to compare the strains to the numerical. However, due to an as of now unidentified error the strains are of a factor 200 off.

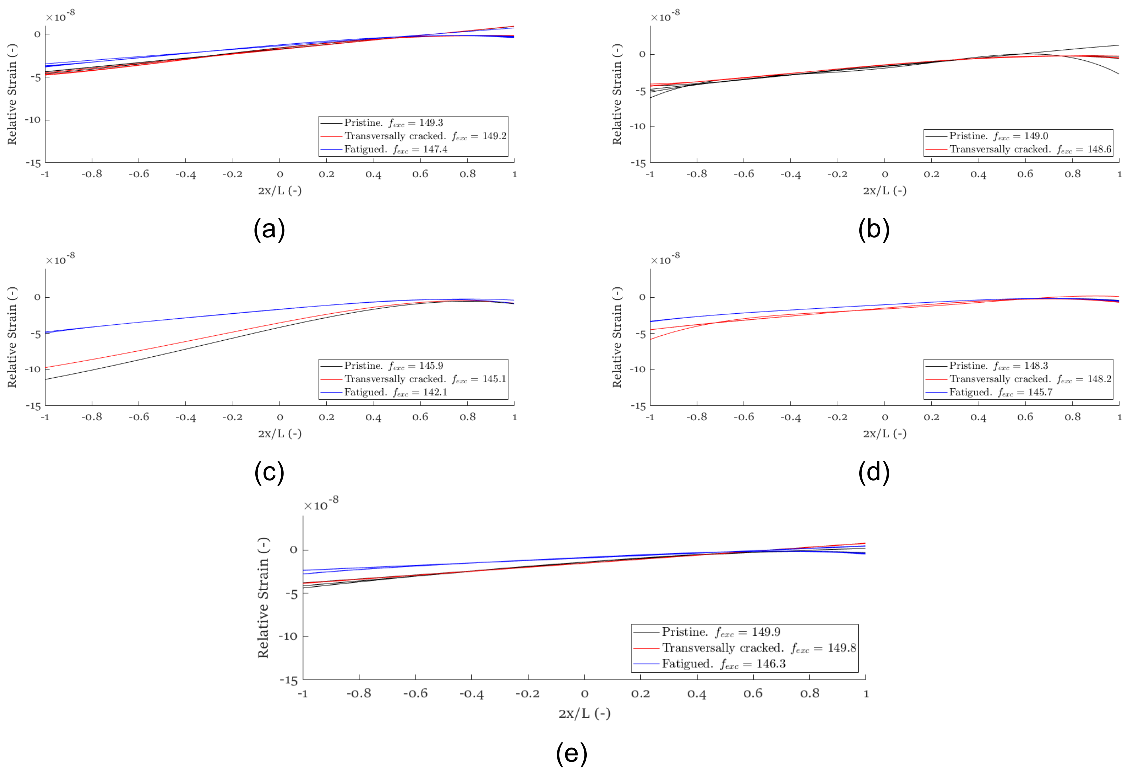

Figure 5.6: Strain along the beam of the pristine, transversally cracked and fatigued cases of the five specimens. (a) Specimen 24: 50.000 cycles, (b) Specimen 27: 75.000 cycles,(c) Specimen 5: 100.000 cycles,(c) Specimen 26: 125.000 cycles and (e) Specimen 25: 180.000 cycles,

5.2.4 Non-linear harmonics

Damage in the specimen because the dynamical behaviour to be different when the specimen is bending positively, i.e. the damage is pushed closed, and when the specimen is bending negatively, i.e. the damage is pulled open. This effect is investigated by manipulating the signal of the pristine and fatigued specimen 5. The effect is expected to be most dominant with the fatigued specimen since here the crack is largest. However, the line scans were conducted on low acceleration levels in order to not propagate damage. Due to these testing conditions the differences due to non-linear harmonics are found to be small.
The crack opening and the crack closing is represented by taking max$([0, V(t)])$ and min$([0, V(t)])$ of the signal respectively, after which the demodulation method is applied on both. The ODS is normalised in order to get a fair comparison between the pristine and fatigued specimen. Figure 5.7 depicts the results. The right figure shows the difference between the positive and negative part for both section. No meaningful difference between the two could be distinguished.

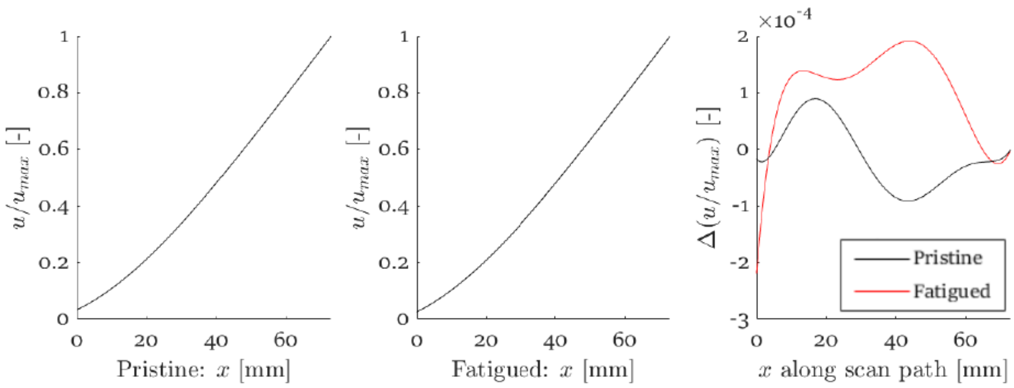

Figure 5.7: Positive vs. negative ODS scaled to the maximum deflection of the pristine and fatigued specimen 5 retrieved with the demodulation method. Note that since the differences are so small only one of the lines is visible in both the pristine and fatigued plots, in fact there are two in each.

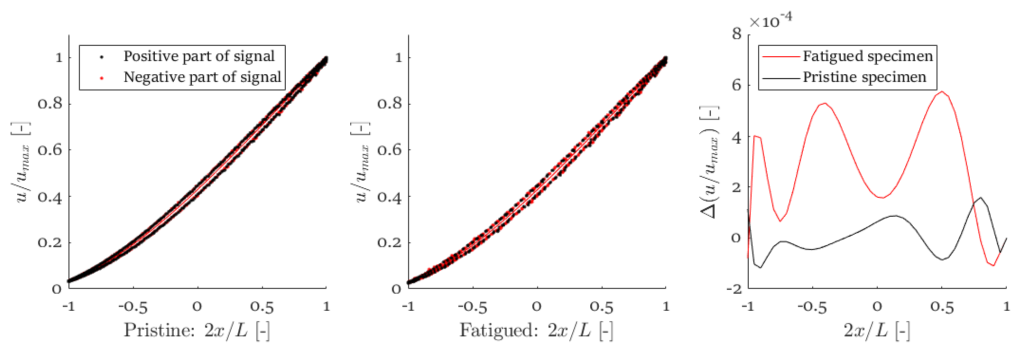

Figure 5.8: Difference between the positive and negative envelope of the signal of specimen 5 normalised to the maximum deflection.

A second method to find any signs non-linear vibrations is by taking the positive and negative envelopes of the signal. Where the envelope of the signal consists of all the maximum or minimum values of each vibration. The envelopes along the scan path are plotted in figure 5.8. The envelopes are taken of a pristine case and of a fatigues case. The envelopes are fitted with a polynomial of order 7. The found differences between the fits for the positive and negative envelopes are plotted separately for both cases. The difference between the amplitude is plotted in the bottom part of the figure. As can be seen is the found difference bigger for the fatigue specimen, which corresponds with the fact that the non-linear harmonics are higher in this case. However, due to the overall small difference that is measured, the method seems insufficient for detecting non-linear harmonics for the current testing conditions.

5.3 Endurance tests and simulations

This section will present a result of a typical endurance test first for clarity. Next, an interesting observation about the required acceleration is discussed. The acceleration required to maintain constant displacement kept increasing during the test. To make sure nothing is going wrong in the tests, the mechanism behind this observation is investigated. Then the sensitive phase drop is related to the number of cycles in the test. This parameter is an indicator of the crack growth rate. Observations about the progression of this parameter are discussed. The relation between the total phase drop and the crack length is investigated. A clear relation between the two could be a powerful tool for prediction the crack length with the phase drop in future work. The endurance test is investigated numerically as well. The phase drop in the numerical model is related to the crack length. Finally the mode mixity during the endurance test will be discussed based on the numerical model. The effects of the new interactions in this thesis are discussed specifically.

5.3.1 Phase drop trace

The phase drop during the endurance tests is depicted in figure 5.9. As stated before, the saw-tooth effects is caused by updating the excitation frequency to a lower setting. All cycles between each frequency update is called a segment. The figure shows that the phase region in which the tests are conducted ranges to up to 50 degrees. This leads to the following observation, which is best explained when taking a FRF such as figure 5.2 as reference. The different phase ranges in the endurance tests correspond to different frequencies in the FRF. As can be seen in the FRF are the slopes of the phase not constant all over. This will result in the fact that the phase drop rates of the five endurance tests do not correspond to the same level of stiffness reduction. It is important to keep this in mind when comparing the results of the five tests later on.

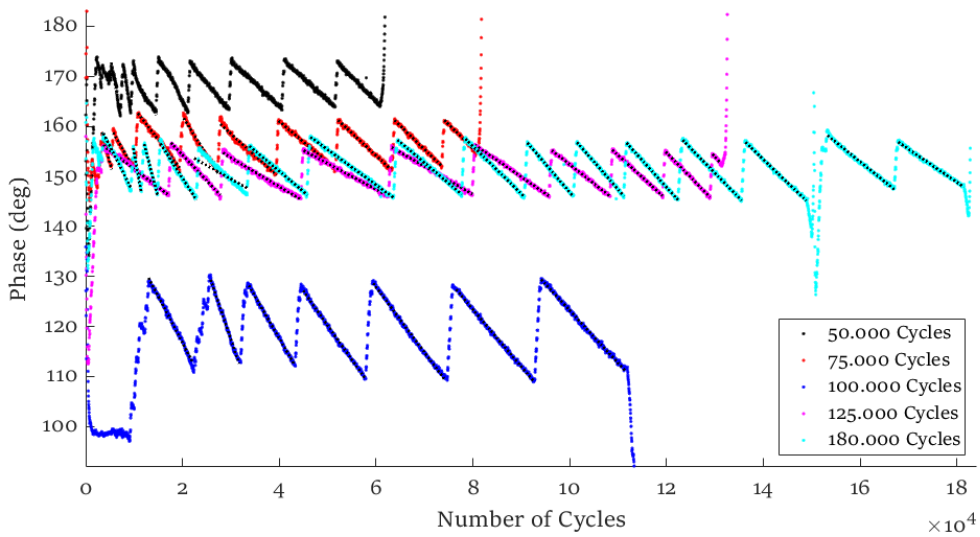

Figure 5.9: Phase drop of the top 5 specimens.

5.3.2 Acceleration Trace

Figure 5.10 depicts the required accelerations during the endurance test to maintain constant displacement at the LDV-position. In section 3.6 it is described how the excitation frequency is chosen at the resonance frequency. The motivation being that the acceleration trace will be monotonically increasing during that segment as the FRF shifts to the left and the excitation frequency drifts from the resonance. When the excitation frequency is updated the acceleration drops again, since the excitation frequency then again matches the resonance. This is the behaviour found in the displacement matched SSD analysis in the numerical investigation, as depicted in figure 4.6. The real acceleration trace of the tests is depicted in figure 5.10. Some changes to this expectation are observed. Firstly, some of the traces, mostly the 50.000 cycles test, show an hike in required acceleration instead of a drop after each segment and secondly, for some reason an all over increase in required acceleration is found, not seen before in previous research [3, 4]. This section will try to find the underlying mechanism of these differences.

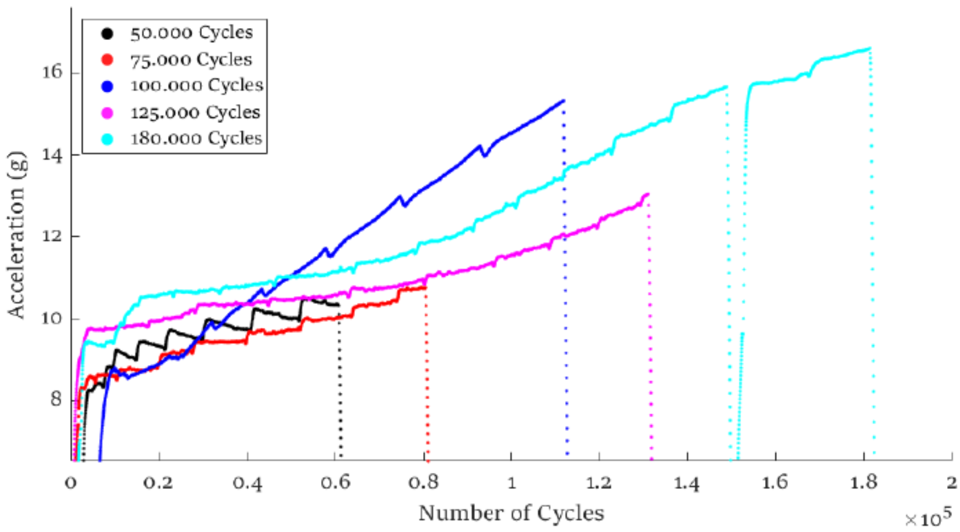

Figure 5.10: Acceleration trace of the top 5 specimens.

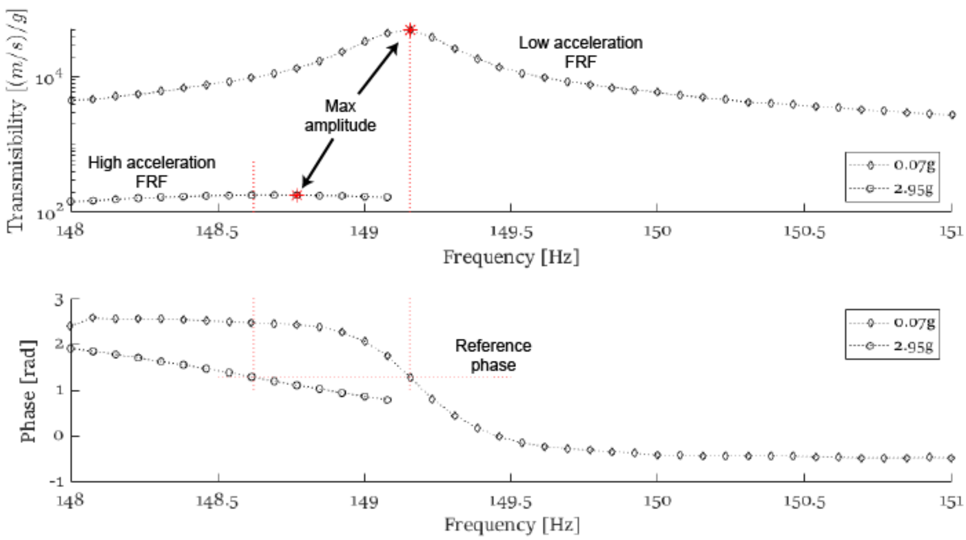

Figure 5.11: Low and high amplitude FRF corresponding to the 50.000 cycles specimen.

First will be set out why the acceleration counter-intuitively spikes after each segment for the 50.000 cycles specimen. As described in section 3.1 an initial low acceleration FRF is conducted to set the excitation frequency to the resonance frequency. The phase level (φ_{ref}) corresponding to this frequency is set as a reference during the endurance test. At the start of each segment the phase is matched to φ_{ref}. Figure 5.11 shows this frequency with the vertical red dotted line on the right. When looking at a high amplitude FRF, the same reference phase corresponds to a frequency somewhat below the resonance. This is represented with the left vertical dotted line. The consequence of this observation is that during the endurance test f_{exc} would drift toward the frequency with max response instead of away. This will cause a spike in the acceleration instead of a drop.

A separate observation of the acceleration trace is a general increasing trend. It was found that increasing the acceleration, causes an increase in damping. Take the analytical equation (eq. 2.26) for the amplitude of the Frequency Response Function for a SDOF system with a moving base from section 2.7. When the damping coefficient c increases the amplification reduces. This is observed in the results of the FRF's on multiple acceleration levels in figure 5.2. For higher accelerations the amplitude not only flattens, but also decreases. It was found in section 5.1 that during the endurance test the damping in the specimens increases, causing a lower amplification and thus a higher required acceleration. As shown in section 5.1.2 will the damping only increase more when the acceleration increases causing the effect to be amplified.

5.3.3 Experimental phase drop rate

The phase drop is post processed by taking the phase drop rates of each segment as $\Delta\varphi/\Delta N$. Since the results in previous work of Di Maio et al. [2] showed a relation best described by a power law, the phase drop rates are plotted on a log-log scale in figure 5.12. The range of each segment was set manually after which each segment was fitted with a linear fit to get the slopes.

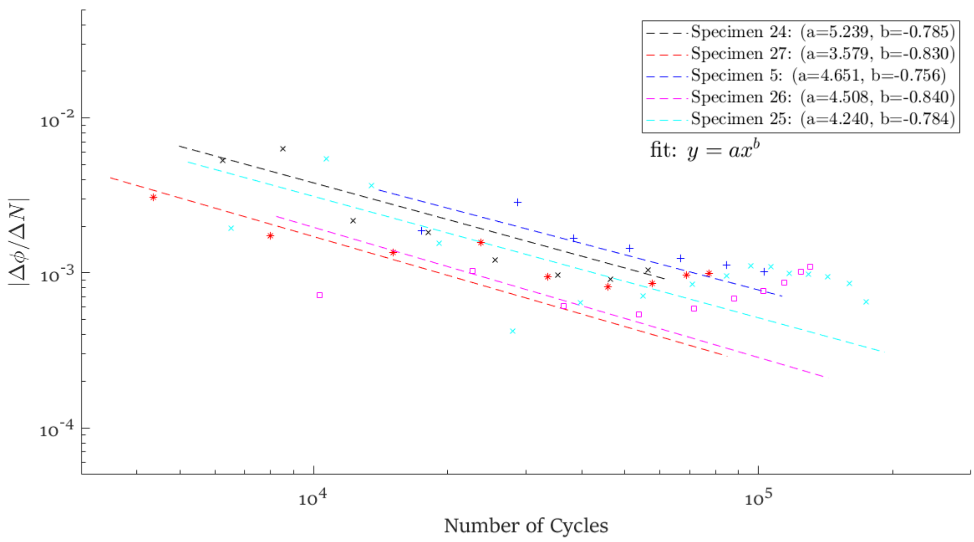

Figure 5.12: $\Delta\varphi/\Delta N$ over N for each segment from the experiments. Each test is individually fitted with a power law.

The results show that generally the phase drop is higher in the beginning of the test. When fitting a logarithmic fit over all results, there could not be found a fit that describes all results very well. The major cause of this is attributed to (i) non-uniformity of the specimens (ii) varying test-to-test conditions and (iii) non-consistent crack initiations, as described in section 3.2, 3.3

and 5.3.1, and 3.5 respectively. Therefore a logarithmic fit is constructed in figure 5.12 for each individual test only.
An important observation about the results is the fact that the data points around the fit are not randomly distributed around the fit, as would be the case with noise. The data points around the fit look like they have a trend in it. One of these trends is made visible in figure 5.13. Note that this trend is meant for visualization only and is not based on any physics based fit or function. The fit can be interpreted as the mean phase drop rate, and the trend around it suggests some oscillation around the mean. The phase shifts caused by making the transverse crack in section 5.1.1 indicated that specimen 24, 25 and 26 had the least progressed transverse crack. Specimen 5 had the largest and specimen 27 something in between. When looking at the progression of the phase drop rates it interesting to note that specimen 5 shows least oscillation. This is an indicator that the cause of the oscillation can be found in the shift in failure mechanism: Going from maturing an initial damage to a progressing the delamination.

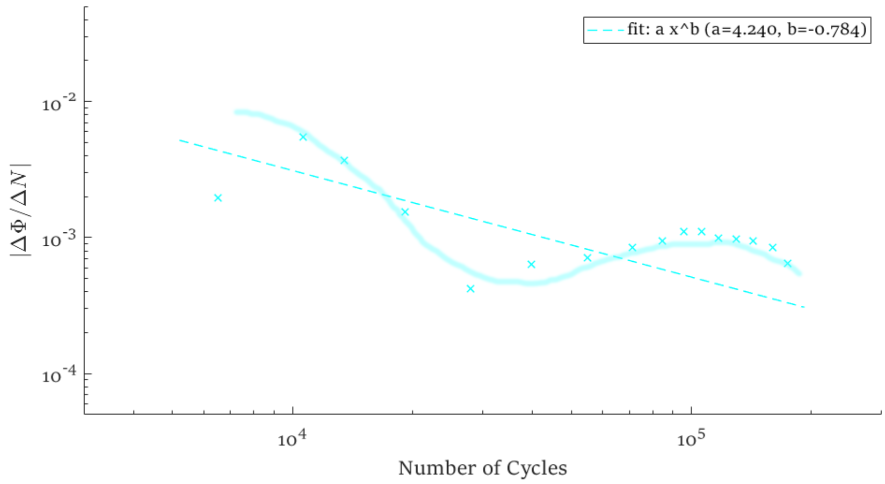

Figure 5.13: Phase drop of specimen 25 with a trend

5.3.4 Correlating the total experimental phase drop to the crack lengths

In table 5.3 the found crack lengths in the five specimens are set out. The crack lengths could be found, using inspection with an electronic microscope, all results are set out in Appendix C for completeness. Both sides of the specimen are recorded since it was found that the crack lengths vary throughout the specimen. Therefore some separate measurements were also made inside the specimen. Approximately 1 mm of one the sides is polished off before re-measuring the crack length. Some of the measurements are inconclusive since it is unclear where exactly the crack ends. In that case a minimum crack length is denoted in the table. Not recorded crack lengths are denoted with a dash in the table.

With the crack lengths set out the total drop in phase can be used as a measure of how much the stiffness in the specimen has reduced, a stiffness reduction caused by the propagation of the crack. The found relation is depicted in figure 5.14. Note, that this is the first type of analysis where the data of all specimens are combined. As stated before, comparing the specimens with each other is not very trustworthy, since the starting point of the endurance tests are not consistent and the tests were conducted around different phase regions. The test conducted on plate 1 is left out, since conditions are suspected to be too different.
Also, note that even for specimen 24, in which a negligible crack length was found, the total phase drop still is 80°. This implies that a lot of the phase drop is connected to the maturing of the transverse crack, i.e. correspond to the crack initiation phase instead of the propagation

Table 5.3: Crack lengths of the 5 specimens.

Specimen	Number of cycles	Crack length A [mm]	Crack length ≈1mm A [mm]	Crack length B [mm]	Crack length ≈1mm B [mm]
Plate 2 spec. 4 (24)	50.000	0.05	No delam.	No delam.	No delam.
Plate 2 spec. 7 (27)	75.000	0.55	-	No delam.	0.21
Plate 1 spec. 5 (5)	100.000	>1.55	3.59	1.64	-
Plate 2 spec. 6 (26)	125.000	0.52	1.10	1.21	-
Plate 2 spec. 5 (25)	180.000	>1.33	2.02	1.29	-

phase. Unfortunately, it is difficult to separate the phase drop corresponding to which part of the fatigue process. For this reason are the results are not used for any further analyses.

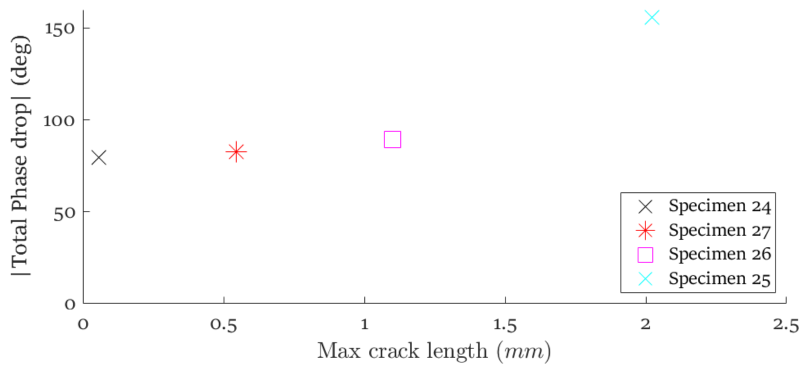

Figure 5.14: Total drop of phase over the crack length.

5.3.5 Numerical phase drop rates

The numerical model has investigated the phase at the current excitation frequency for crack lengths up to 3 mm with steps of 0.1 mm, causing a phase drop for every updated model. It was decided that the excitation frequency would be updated if the phase drops below 3.0 rad (φ_{lim}), which splits the phase drop into two segments. The phase drop rate is calculated as $\frac{\Delta\varphi}{a}$. Similar to the experimental results are the numerical results depicted on a log-log scale in figure 5.15. It should be possible to relate the phase drop rate from the experiments to the crack lengths from the numerical model. However, in the numerical model a fixed damping ratio of 0.01 was set. It was found that this is not in accordance with the tests and the damping ratio will influence the phase drop rate.

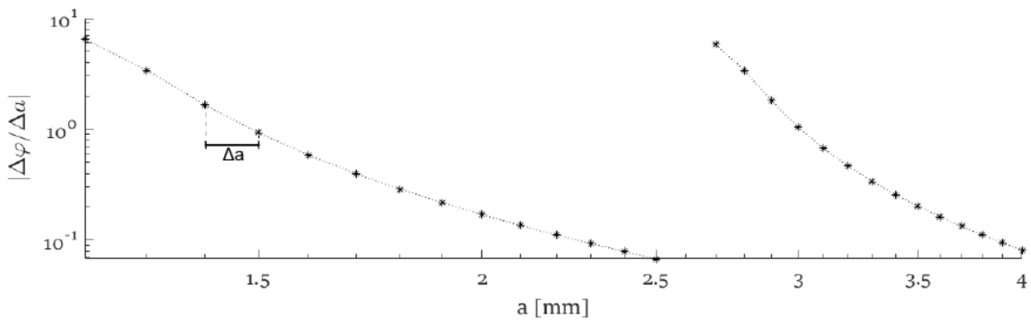

Figure 5.15: Phase drop rate ($\Delta\varphi/\Delta a$) over the crack lengths.

Cole et al. [23] showed that in steel vibration fatigued specimens the elasticity of the material reduces near the cracked region. Currently it is unknown if similar behaviour is present in the CFRP PEEK material. During the endurance tests in this thesis the phase drop indicates a drop of stiffness, which can be related to a propagation of a crack. In order to investigate to which degree a reduction of stiffness near the crack tip influences the phase drop a model is set up. The 4 elements around each crack tip are assigned different material properties. The numerical framework is investigated 5 extra time where these elements are assigned 90, 95, 98, 99, and 99.9 percent of the Young's Modulus. It is found that the characteristic slope of the phase drop rate only changes slightly when the crack tip softens.

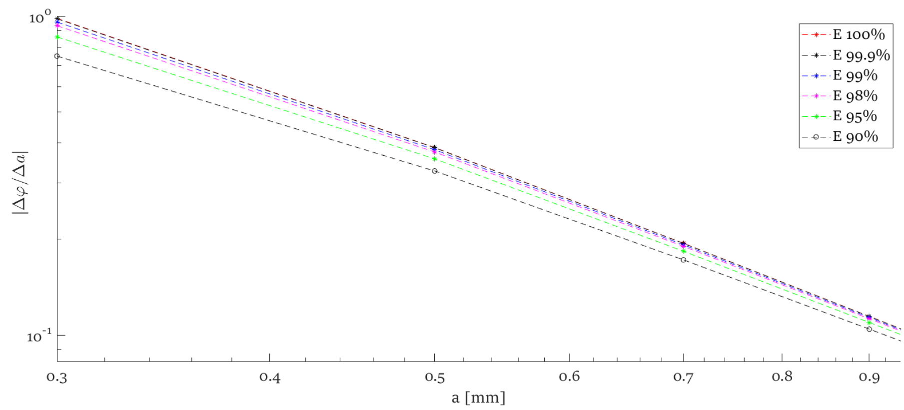

Figure 5.16: Total drop of phase over the crack length.

5.3.6 Mode mixity at the fracture

The Strain Energy Release Rates (G) at the crack tip for each model in the numerical approach was saved. Figure 5.17 depicts the G for each crack length for both deflection directions, i.e. crack opening and crack closing. G is determined separately per mode, yielding mode opening, G_{I}, and mode sliding, G_{II}. As explained in 4.5 are the deflections iteratively subjected to the model, and for each iteration the G is calculated. The final iteration, representing the full ODS, is of most interest since here the most extreme G will be found. However, it is found that the numerical framework stops updating G from the iteration where $G_{equiv},$ surpasses $G_{\text{equiv,C}}$. Therefore, the results in this subsection will quantitatively not represent the final iteration, the qualitative development however does. It is clear that in crack closing mode-II is more dominant than mode-I, while the opposite is true for crack opening. In the vibration fatigue tests the two orientations will subsequently follow each other. So both will influence the crack growth simultaneous. However, due to the fact that the G found during crack closing is an order of magnitude higher than for crack opening, crack closing is deemed dominant. It is likely that it will have more impact on the crack growth overall.
The crack length inspections with the optical microscope showed that only a delamination matured in the direction of the fixture. In the numerical framework the crack progressed either to the left or right based on which crack tip had a higher G_{equiv}. Both crack opening and closing showed crack propagation to the left only, so the model corresponds well to the observations from the test.

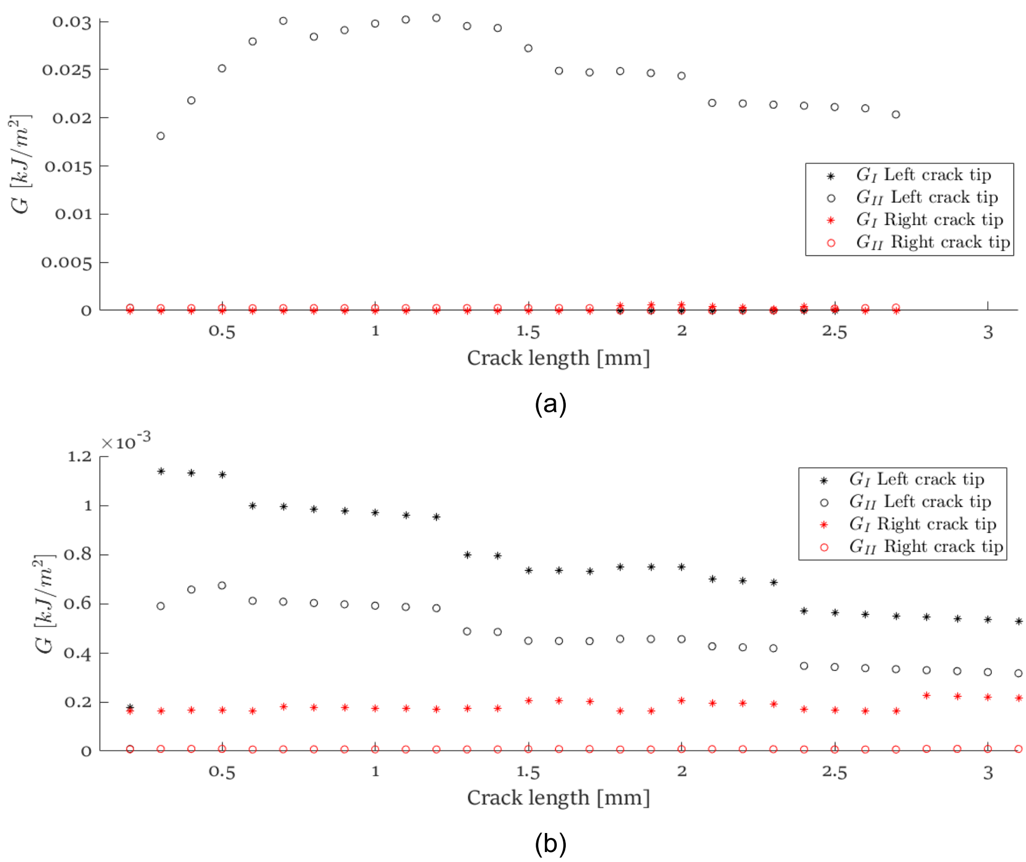

Figure 5.17: Mode-I and Mode-II Strain Energy Release Rates during the modelling approach for crack opening (a) and crack closing (b).

The Paris-Erdogan law is used to relate the strain energy release rate to the crack growth rate da/dN, according to equation 2.11. In this thesis the Paris-Erdogan law could not be set up for the specific specimen and loading conditions, because no consistent relation was found between the crack lengths and the number of cycles. However, from the general progression of the Paris-Erdogan law (as depicted in figure 2.5) it is clear that a lower G corresponds to a reduction of the crack growth rate.

5.3.7 Inclusion of the friction coefficient

As explained in section 4.2.5 is the friction interaction between the delamination and the base structure modeled with a friction coefficient of 0.75. The coefficient was derived from experiments from Voudouris [4]. He did not however include this parameter into any VCCT analysis. In order to determine if friction influences the results of the numerical framework it is investigated without this interaction included. Just the orientation representing the closing of the crack is investigated, since the interaction does not make contact during crack opening. The results are depicted in figure 5.18. It is found that the found G can vary up to 25 percent without the friction coefficient included, making the parameter important for a good model.

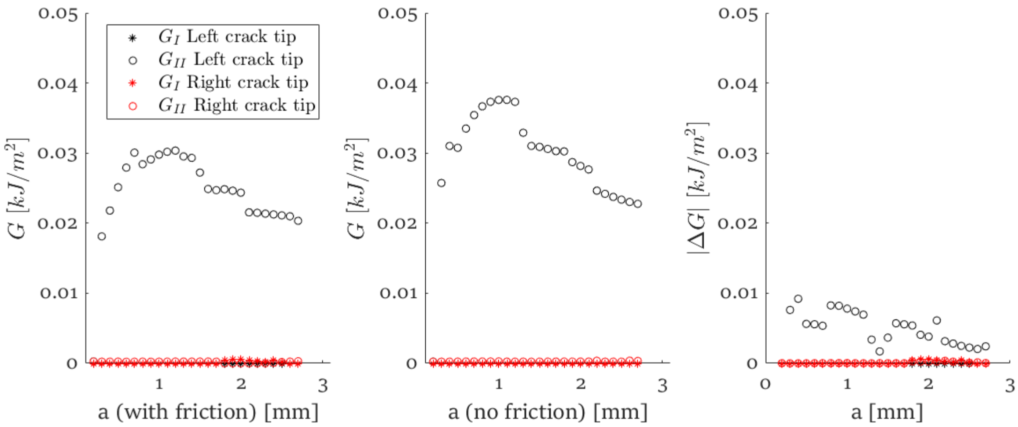

Figure 5.18: SERR at crack tips with and without the friction coefficient included. With on the right the difference in the result. For the crack closing orientation.

5.3.8 Inclusion of tip interaction constraints

As explained in section 4.2.5 is a vertical interaction added to the model between the two delamination tips. Including this interaction will represent the real situation much closer, since without it the nodes can move through each other. In order to distinguish the importance of this interaction, the framework is investigated without it as well. Just the orientation representing the closing of the crack is investigated, since the interaction does not make contact during crack opening. The results are depicted in figure 5.19. Without the interaction the crack propagates towards the right, so incorrectly away from the fixture. This means that the interaction property is essential in characterizing the mode mixity.

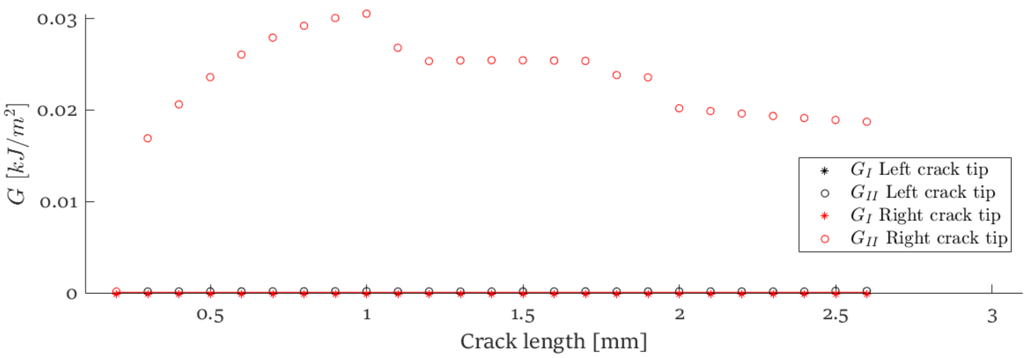

Figure 5.19: SERR at crack tips without the vertical interaction included. For the crack closing orientation.

5.4 Summary of results

The most important results of this chapter are summarised in this section. Varying resonance shifts between before and after making the transverse crack has shown that the transverse crack has not been matured completely for some specimens. Based on this it is inadvisable to compare the results of the specimens with each other. The phase drop was traced during the tests, which is related to the reduction of stiffness. This seems like a successful parameter to track the crack propagation throughout the tests. A very interesting trend is observed in the phase drop rate, where the phase drop rate oscillates around the mean. A possible cause of the oscillation is found in the level of initial damage introduced to the specimens. A trustworthy

relation between the total phase drop to the crack length could not be established, due to differences is testing conditions. The phase drop was related to the crack length in the numerical model. The similarities between the numerical and experimental relation indicate that the approach is successful for thermoplastic materials. The numerical framework has predicted the crack growth direction in accordance to the experiments for both crack closing and opening. For this prediction the interaction property between the delamination tips was found to be essential. The friction coefficient has found to influence G up to 25 percent, also making it a very important interaction property. The strain energy release rate for mode-I is found to be more important for the opening of the crack and the mode-II for the closing of the crack. The closing of the crack is suspected to be dominant, since the found SERR is of a magnitude higher.
Operating Deflection Shapes were retrieved from line scans experimentally. Due to an error the strain was not determined accurately. The ODSs are very close to ODSs of the Numerical model. It was not possible to show any non-linear harmonics in the signal of the line scans using the demodulation method or by investigating the signals envelopes for the current testing conditions.

6 CONCLUSIONS AND RECOMMENDATIONS

This thesis titled ”Vibration fatigue testing and modelling for identification of damage propagation in fiber reinforced plastics” set the following research questions:

Can we characterize the crack initiation and propagation during fatigue loading in Continuous Fiber Reinforced Polymers and can we understand the underlying physics behind this?

Before this question can be answered, the set up sub-questions will be discussed, which were established as:

1. *What is the damage initiation and propagation in cross-ply components made of PEEK materials during fatigue?*
2. *What is the effect of a defect introduced by the manufacturing process in terms of damage growth?*
3. *Can we exploit modal test methods to evaluate change of surface strain caused by delamination growth?*
4. *Can we detect a delamination in the material directly from modal tests?*
5. *What are the interface forces acting at the crack tip while the delamination is artificially propagated?*

From the analysis of the endurance tests crack initiation and propagation was successfully traced with the dynamic parameter phase. However, the parameter showed a wide range of results, which is mainly attributed to (i) non-uniformity of the specimens (ii) varying test-to-test conditions and (iii) non-consistent crack initiations. That the phase drop rate in the damage propagation phase is actually related to a delamination could be determined from the numerical framework. In the models the phase drop rate could be related to crack growth and showed a very similar relation.
The effects of introducing defects to the specimens was investigated by comparing the results between tests with small and big initial damage. How much damage is introduced influences the damage stage during testing: initiation or propagation. Further research is required to specify the effect of the damage initiation completely. However, this thesis could distinguish a very promising feature: it was found that the tests with small damage initiation showed an oscillating behaviour in the phase drop rate per cycle. Discovering this feature in future test can indicate that the damage is not in the propagation phase yet.
The line scan proved very effective in determining the ODSs. Due to this success it is recommended to further develop this method, by including the damaged region into the line scan path. Due to an error in the analysis the strain was not determined accurately in the tests yet. It is recommended to add a strain gauge to the specimens near the fixture, in order to make this analysis simpler. At the damaged area a spike in strain will occur, according to the numerical simulation. A new challenge would be to estimate the strain in that region. It is recommended to conduct the line scans on higher acceleration level to better represent the endurance test

conditions.
An attempt was made to detect a delamination in the coupons directly from line scans. A non-linear vibration would be an indication of this damage. However, this could not be distinguished with either the demodulation method or by inspecting the envelopes of the signal. A main reason for this is likely the lower acceleration levels in the line scans. It is expected that the non-linear harmonics are small for these testing conditions. Therefore, it is recommended to conduct the tests with higher acceleration in future work.
The numerical framework was successful in determining the development of the interface forces during crack propagation at the crack tips in the form of the Strain Energy Release Rate. During dynamic fatigue tests the mixed mode interface force will vary for crack opening and closing. It was found that the G at the crack closing was of much higher amplitude, making this the more important orientation to investigate in future work. In this orientation the sliding mode is more dominant than opening, making this an important feature to model correctly. It was found that the interaction properties between the tips of the delamination is essential for this. Similarly, the friction coefficient influenced the results of the sliding SERR greatly. In the numerical framework the G stopped updating at the iteration where the critical $G$was exceeded. It is recommended to update the model such that the G at the final iteration is saved.
From these conclusions it was found that the crack initiation and propagation could be characterized successfully. The numerical model gave insight in the underlying physics of the crack propagation.
The next sub-section will discuss some additional recommendations to help with any future work.

6.1 Recommendations

6.1.1 Manufacturing the specimens

As explained in section 3.2 did the results of the experimental investigation vary, partly due to non-uniformity in the test specimens. For this reason is a new manufacturing process recommended.
It is recommended to change the manufacturing process from press molding to Autoclave curing. The used method had a big problem with fiber flowing. The Autoclave manufacturing process has produced very consistent specimen in the past with a significantly shorter Resin Gap, as can be seen in figure 6.1.

6.1.2 Stacking sequence of specimens

As described in section 5.1.2 was a high non-linear relation found between the input acceleration and the damping in the specimens. This proved to be a problem, since the phase became a lot less sensitive for the high input forces. The sensitivity of the phase was exactly what made it such an interesting parameter to use. Another downside is that the numerical model does not take this non-linearity into account, so minimizing it would bring the two closer together. It would be possible to include an input force depended damping into the numerical model, but this would require to map the non-linearity for each new material of interest. So a better approach is reducing this non-linearity. A method for achieving this is adding more pristine plies to the stacking sequence.

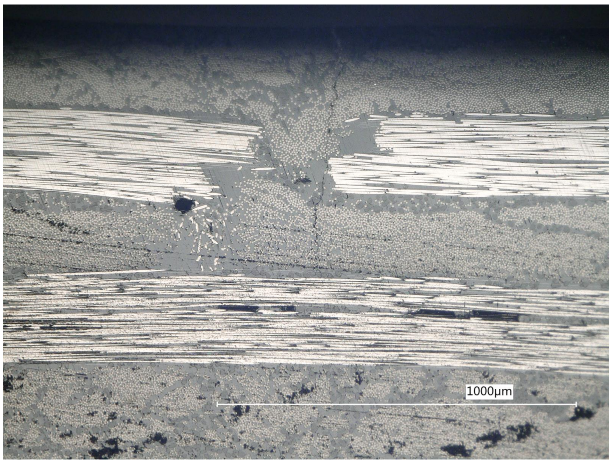

Figure 6.1: Cross section of specimen manufactured in the Autoclave. Note the smaller resin pocket.

6.1.3 Reproducibility of crack initiation

When conducting the endurance tests in the experimental approach it was found that the crack initiation was not instantaneous for thermoplastics, as it was for thermosets. Therefore, the transverse crack was only opened partly in some of the tests. The high amplitude frequency sweep is an insufficient method to get a reproducible starting position for the endurance tests in thermoplastics. A possible approach is to stop with the dynamic method and use a static method. The specimens can be subjected to a bending load using a 3 point bending set-up. Since the location with the cut-ply is weakest a crack will first appear here. A drop in force will indicate that the crack has appeared.
Another method is the use of a zero pressure water cooled saw to make a cut in the material in the cut-ply. A cutting method that does not generate heat is required in order to not alter the micro-structure of the thermoplastic. A side-effect of this method is that it alters the interaction near the crack. A gap is introduced at the crack, so when the crack is pushed closed first this gap is closed before the tips will touch. This change in interaction will have an effect on the crack propagation. Due to this free gap the interaction will be more simplified, which will likely make the crack propagation more predictable.
A different approach can be to make no transverse crack at all. It could be investigated if the phase parameter to track the damage can be used to distinguish between the forming of the transverse crack and damage propagation. It is suspected that the oscillating phase drop rate is related to the damage initiation. This behaviour could be utilized for this goal.

6.1.4 Damaged area from CT-scans

The found crack lengths in this thesis were found to vary widely throughout the specimens. This makes classifying the cracks with a single dimension inappropriate. CT-scans are widely used accurately before to characterize the area of a damage in composites [4]. This method is recommended to be applied to the specimens used in this investigation. Instead of a crack length a damage area is then used. CT-scans can give insight into which specimens were affected most by fiber bridging as well. The experimental crack growth rate $(\Delta\varphi/\Delta N)$ could then be used with the cracked area to set up the Paris-Erdogan law of the specimen.

6.1.5 Continuous scanning LDV

As explained in section 3.4.2 is decided to conduct the line scans on a low acceleration level in order to not progress any damage in the specimen. Now, when trying to estimate the strain energy near the crack tip, the conditions are very different and do not represent the situation during the endurance tests. It is recommended to conduct a high acceleration line scan after the crack length (or area) is measured. In this thesis it was opted to not do this in order to not introduce any error in the system, however since the required number of cycles for these tests are relatively low this effect is expected to be small.
On top of that showed the measured signal of the CSLDV method some drop off during the test, causing a non-steady state testing condition, as explained in section 5.2.1. The cause of this drop off is thought to be in the controller of the test. If a researcher is planning to use this same controller, it is highly recommended to solve this error before conducting more experiments.

6.1.6 Conducting endurance tests

During the endurance tests in this thesis the excitation frequency was updated to remain in the sensitive area of the FRF. The slopes of the descending phases of each segment was related to a certain drop in stiffness and the goal is to relate this to a certain crack growth rate. As the excitation slowly shifts out of the sensitive area of the FRF, the slope of the phase decreases. In order to get a consistent result the frequency needs to be update at the same position in the FRF. In the endurance tests in this thesis this is performed manually. It is recommended to update the controller to update the frequency after a fixed phase drop.

6.1.7 Updating the numerical framework

As explained in section 4.5 is only the final step used of the VCCT analysis. This is the time instance when the complete displacement boundary conditions are subjected to the model. The Strain Energy Release Rate (G) at the crack tips were compared in order to decide the direction of the crack propagation. The crack still progresses even if the found G does not exceed the critical value, because in fatigue a crack progresses even if this limit is not met. This means that a more efficient approach can be set-up instead of the VCCT analysis. The displacements can be applied at once on the model. When the delamination area has settled, G can be calculated manually. This will reduce the total required calculation time greatly.
The framework can be simplified more. In this thesis the modal characteristics of the specimen were modelled using a Steady-State Dynamic analysis. The displacement at the LDV-position was saved. A new SSD analysis was conducted with the input force scaled accordingly. However, this could have been done at once. Since the SSD analysis is a purely linear modelling approach, the resulting FRF and ODS can be scaled to represent the correct LDV displacement. This could save some time in a future framework.

Bibliography

[1] L. Molent and A. Haddad. A critical review of available composite damage growth test data under fatigue loading and implications for aircraft sustainment, jan 2020.

[2] Dario Di Maio and Fabrizio Magi. Development of testing methods for endurance trials of composites components. *Journal of Composite Materials*, 49(24):2977–2991, 2015.

[3] Fabrizio Magi, Dario Di Maio, and Ibrahim Sever. Validation of initial crack propagation under vibration fatigue by Finite Element analysis. *International Journal of Fatigue*, 104:183–194, 2017.

[4] G. Voudouris. *Fatigue behaviour of composites under vibration and thermal loading*. Phd thesis, University of Bristol, 2019.

[5] W. J. Plumbridge. Review: Fatigue-crack propagation in metallic and polymeric materials. *Journal of Materials Science*, 7(8):939–962, 1972.

[6] G. Irwin. Analysis of stress and strain near the end of a crack transversing a plate. *Journal of Applied Mechanics*, pages 361–364, 1957.

[7] High Cycle Fatigue Prediction Methodology for Fibre Reinforced Laminates for Aircraft Structures in CROR Environment – Development and Validation | HEGEL Project | H2020 | CORDIS | European Commission.

[8] A.K Vegt, van der, and L.E Govaert. De belangrijkste kunststoffen. In *Polymeren van keten tot kunststof*, chapter 1, page 16. VSSD, Delft, 5th edition, 2009.

[9] W Leissa, Arthur. *Vibration of plates*. NASA, 1969.

[10] F. Erdogan. Fracture mechanics. *International Journal of Solids and Structures*, 37(1-2):171–183, 2000.

[11] V.Z. Parton. *Fracture Mechanics: From Theory to Practice*. Gordon and Breach Science Publishers, 1998.

[12] Kenneth Reifsnider. Fatigue behavior of composite materials. *International Journal of Fracture*, 16(6):563–583, 1980.

[13] Wayne W. Stinchcomb. Nondestructive evaluation of damage accumulation processes in composite laminates. *Composites Science and Technology*, 25(2):103–118, jan 1986.

[14] Ramesh Talreja. Damage and fatigue in composites - A personal account. *Composites Science and Technology*, 68(13):2585–2591, 2008.

[15] R. Talreja. Fatigue of composite materials: Damage mechanisms and fatigue-life diagrams. *Proceedings of The Royal Society of London, Series A: Mathematical and Physical Sciences*, 378(1775):461–475, 1981.

[16] Gurit Holding AG. Guide to Composites, 2000.

[17] Fabrizio; Magi. *Vibration fatigue testing for identification of damage initiation in composites*. PhD thesis, University of Bristol, 2016.

[18] Michael Smith. Crack propagation analysis. In *ABAQUS/Standard User's Manual, Version 6.9*, chapter Special-Pu. Dassault Systèmes Simulia Corp, 2009.

[19] M. L. Benzeggagh and M. Kenane. Measurement of mixed-mode delamination fracture toughness of unidirectional glass/epoxy composites with mixed-mode bending apparatus. *Composites Science and Technology*, 56(4):439–449, jan 1996.

[20] T. J. Adam and P. Horst. Experimental investigation of the very high cycle fatigue of GFRP [90/0]s cross-ply specimens subjected to high-frequency four-point bending. *Composites Science and Technology*, 101:62–70, 2014.

[21] J Claeys, J Van Wittenberghe, P De Baets, and W De Waele. Characterisation of a resonant bending fatigue test setup for pipes. *Sustainable Construction and Design*, 2(1):424–431, 2011.

[22] Ibrahim A. Sever, D. D. Dario, and M.A.G.I. Fabrizio. Vibration Fatigue Testing, 2019.

[23] D. P. Cole, E. M. Habtour, T. Sano, S. J. Fudger, S. M. Grendahl, and A. Dasgupta. Local Mechanical Behavior of Steel Exposed to Nonlinear Harmonic Oscillation. *Experimental Mechanics*, 57(7):1027–1035, sep 2017.

[24] D. J. Ewins. *Modal Testing: Theory, Practice and Application*. Research Studies Press LTD, 2001.

[25] Milena Martarelli. *Exploiting the laser scanning facility for vibration measurements*. PhD thesis, University of London, 2001.

[26] P. Chiariotti, M. Martarelli, and P. Castellini. Mode matching of Continuous Scanning Laser Doppler Vibration data in the frequency domain, 2018.

[27] A. B. Stanbridge and D. J. Ewins. Modal testing using a scanning laser Doppler vibrometer. *Mechanical Systems and Signal Processing*, 13(2):255–270, 1999.

[28] Miroslav Pastor, Michal Binda, and Tomáš Harčarik. Modal assurance criterion. *Procedia Engineering*, 48:543–548, 2012.

[29] W. S. Johnson and P. D. Mangalgiri. Investigation of Fiber Bridging in Double Cantilever Beam Specimens. *Journal of Composites Technology and Research*, 9(1):10–13, 1987.

[30] Rafiullah Khan. Fiber bridging in composite laminates: A literature review. *Composite Structures*, 229:111418, 2019.

[31] J. R. Reeder. 3D mixed-mode delamination fracture criteria - An experimentalist's perspective. *American Society for Composites - 21st Technical Conference of the American Society for Composites 2006*, 1:129–145, 2006.

[32] R. Fletcher. *Practical Methods of Optimization*. Wiley, 2 edition, jul 2000.

A MATERIAL PROPERTIES OF CARBON FIBRE REINFORCE PEEK

This appendix contains the material properties of the carbon fibre reinforce PEEK as provided by manufacturer Toray. The manufacturing itself was performed by TPRC.

Toray Cetex® TC1200 PEEK

'TORAY'
Toray Advanced Composites

PRODUCT DATA SHEET

DESCRIPTION

Toray Cetex® TC1200 is a high-end thermoplastic composite material, utilizing the semi-crystalline thermoplastic polymer PEEK for excellent mechanical performance.

The long-standing use of PEEK in demanding applications such as aerospace and cutting edge medical applications proves its benefits and versatility. As a composite material it offers outstanding mechanical performance, also at elevated temperatures. The semi-crystalline nature of the resin ensures an excellent resistance to chemicals and solvents, and an equally superior performance in flammability properties.

Toray Cetex® TC1200 is available in UD tape, fabric prepreg, and RTL formats (reinforced thermoplastic laminate). RTLs can be equipped with lightning strike protection, and carbon reinforced RTLs can be supplied with a thin glass top layer to protect a partly metallic assembly against galvanic corrosion. Glass scrim is also applicable in structures made from UD tape.

FEATURES

- **Excellent toughness and impact resistance**
- **Excellent mechanical performance, also at elevated temperatures**
- **Low moisture uptake for good hot/wet strength retention**
- **Fully impregnated low void content unidirectional tapes for robust processing**
- **Inherently flame retardant**
- **Outstanding chemical and solvent resistance**
- **Indefinite shelf life at ambient temperature storage**

PRODUCT TYPE

PEEK (PolyEtherEtherKetone) Thermoplastic Resin System

TYPICAL APPLICATIONS

- Primary and secondary aircraft structure
- Structural aircraft interiors applications
- Access panels, rib stiffeners, brackets, conduit, flooring
- Medical
- Oil and gas

SHELF LIFE

Out Life:	Indefinite at ambient temperature storage
Frozen Storage Life:	Not applicable—product does not require freezing

TYPICAL NEAT RESIN PROPERTIES

Density (specific gravity)	1.30 g/cm³ (81.2 lb/ft³)
T_g (glass transition)	143°C (289°F)
T_m (melt)	343°C (649°F)
T_c (crystallinity)	290°C (554°F)
T_p (processing)	370–400°C (700–750°F)

Contact us for more information:
North America/Asia/Pacific
e **explore@toraytac-usa.com**
t **+1 408 465 8500**
Europe/Middle East/Africa
e **explore@toraytac-europe.com**
t **+31 (0) 548 633 933**

MECHANICAL PROPERTIES

Standard Modulus Carbon 145gsm FAW UD Tape Laminate 34% RC				
Property	Condition	Test Method	Results	
Tensile Strength 0°	RTD	ASTM D 3039	2410 MPa	350 ksi
Tensile Modulus 0°	RTD	ASTM D 3039	135 GPa	19.5 Msi
Tensile Strength 90°	RTD	ASTM D 3039	86 MPa	12.5 ksi
Tensile Modulus 90°	RTD	ASTM D 3039	10 GPa	1.4 Msi
Compressive Strength 0°	RTD	ASTM D 6641	1300 MPa	189 ksi
Compressive Modulus 0°	RTD	ASTM D 6641	124 GPa	18 Msi
Compressive Strength 0°	ETW[(1)]	ASTM D 6641	1210 MPa	176 ksi
Compressive Modulus 0°	ETW	ASTM D 6641	121 GPa	17.6 Msi
In-Plane Shear Strength ±45°	RTD	ASTM D 3518	152 MPa	22 ksi
In-Plane Shear Modulus ±45°	RTD	ASTM D 3518	5.2 GPa	0.75 Msi
Flexural Strength 90°	RTD	ASTM D 7264	152 MPa	22.0 ksi
Interlaminar Shear Strength (SBS) 0°/90°	RTD	ASTM D 2344	96.5 MPa	14 ksi
Open-Hole Tensile Strength	RTD	ASTM D 5766	386 MPa	56 ksi
Open-Hole Compressive Strength	RTD	ASTM D 6484	320 MPa	46 ksi
Compression After Impact Strength 30.5 J (270 in/lb) Impact Energy	RTD	ASTM D 7137	303 MPa	44 ksi
Mode I Interlaminar Fracture Toughness (G_{IC} Strain Energy Release Rate)	RTD	ASTM D 5528	1.6 kJ/m²	9.0 in-lb/in²
Mode II Interlaminar Fracture Toughness (G_{IIC} Strain Energy Release Rate)	RTD	ASTM D 7905	2.3 kJ/m²	13.0 in-lb/in²

Fiber type AS4D
59% fiber by volume (Vf)
[(1)]ETW is tested at 82°C (180°F) after 14 days soaked in 71°C (160°F) water
The mechanical data provided are average values from a limited dataset. For additional data please contact Toray Advanced Composites

MECHANICAL PROPERTIES

Intermediate Modulus Carbon 145gsm FAW UD Tape Laminate 34% RC				
Property	Condition	Test Method	Results	
Tensile Strength 0°	RTD	ASTM D 3039	3100 MPa	450 ksi
Tensile Modulus 0°	RTD	ASTM D 3039	159 GPa	23 Msi
Tensile Strength 90°	RTD	ASTM D 3039	86 MPa	12.5 ksi
Tensile Modulus 90°	RTD	ASTM D 3039	10 GPa	1.5 Msi
Compressive Strength 0°	RTD	ASTM D 6641	1300 MPa	189 ksi

Continued on page 5

B TEST SET-UP ERROR

In section 3.3 the errors due to misuse of the test set-up is investigated. Figure B.1 shows these errors.

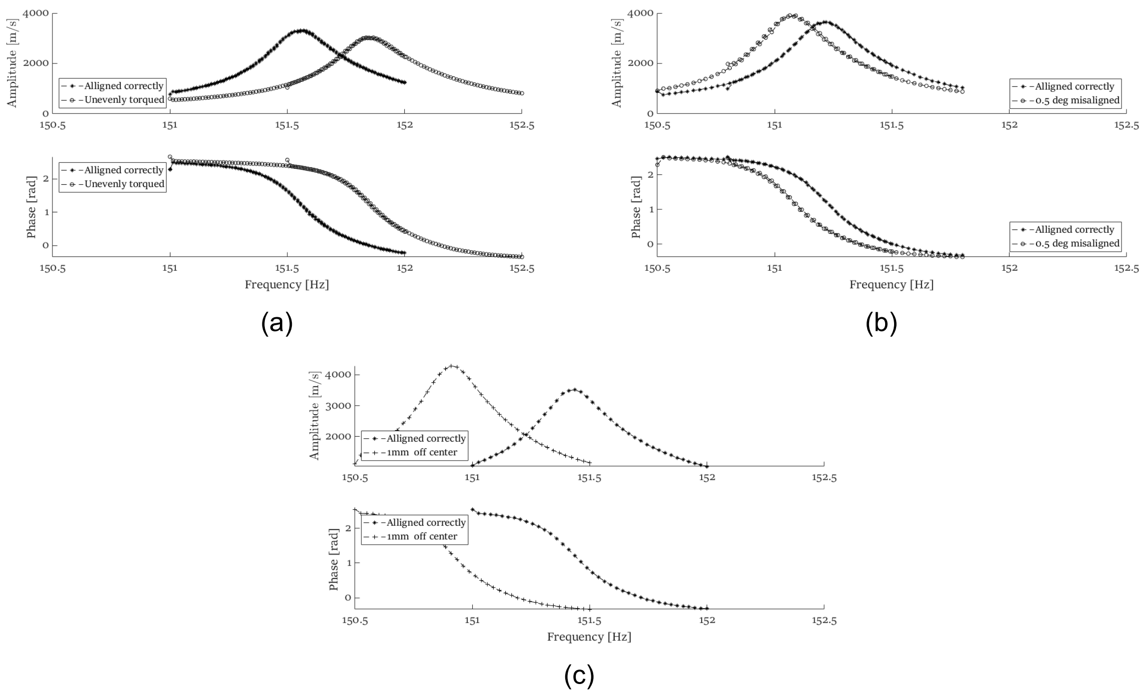

Figure B.1: Change in response due to (a) an unevenly clamped fixture, (b) a 1 deg angled specimen and (c) the specimen being 1mm off center.

C RESIN GAPS AND CRACK SIZE IMAGES

Figure C.1 and C.2 depicts the resin gaps of the selected top 5 specimens from side A and B respectively. The found crack lengths from both sides are depicted in figure C.3 and C.4. On some of the specimens extra inspections were made after polishing off ∼1 mm of material, the observations are depicted in figure C.5.

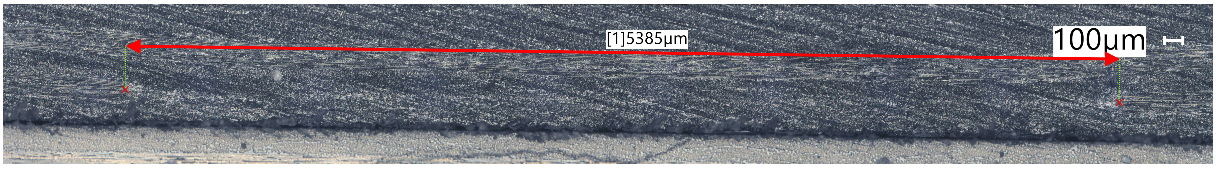

(a) Specimen 24 from side A.

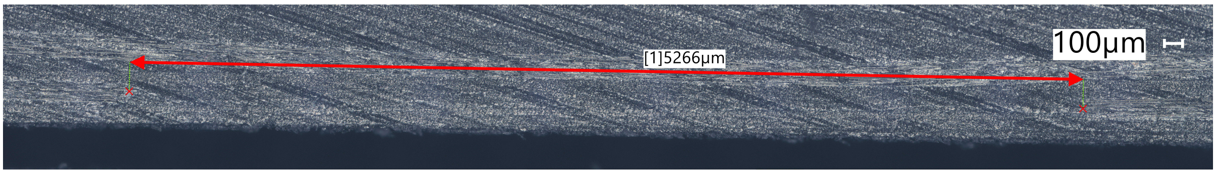

(b) Specimen 27 from side A.

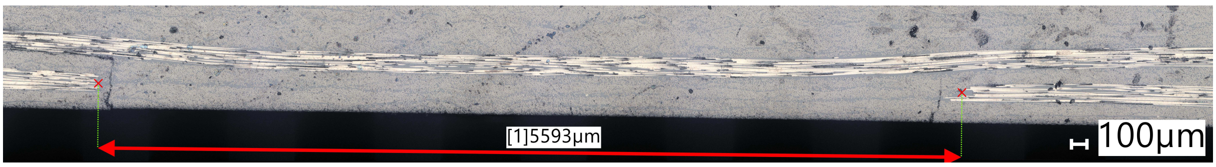

(c) Specimen 5 from side A.

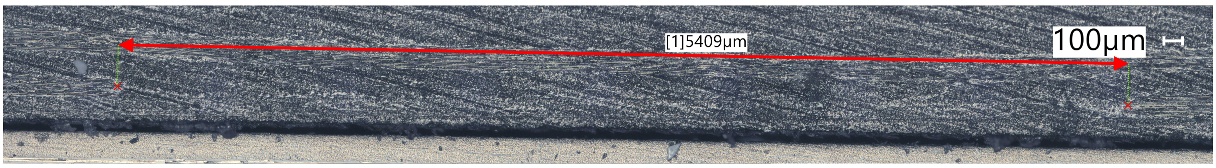

(d) Specimen 26 from side A.

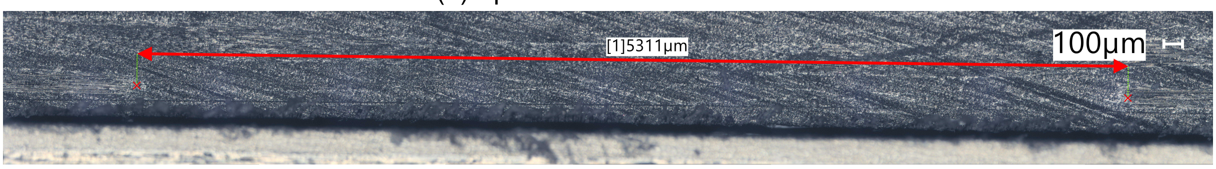

(e) Specimen 25 from side A.

Figure C.1: Cross section of top 5 Specimens Side A.

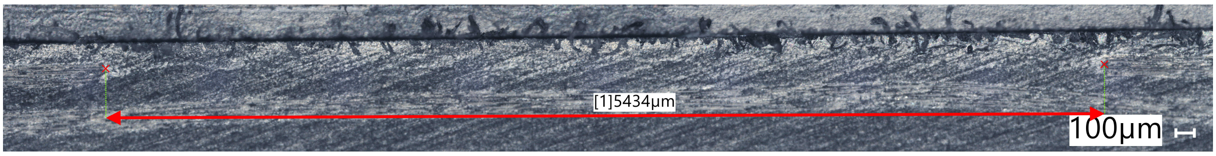

(a) Specimen 24 from side B.

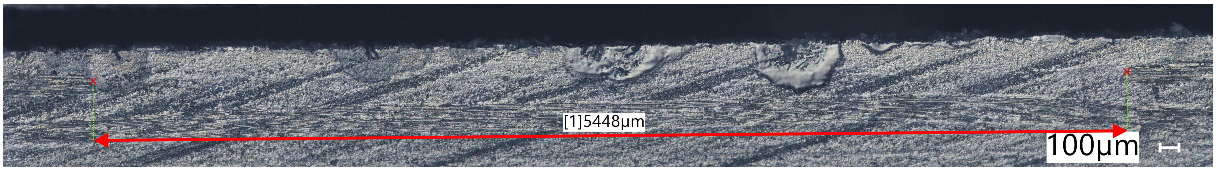

(b) Specimen 27 from side B.

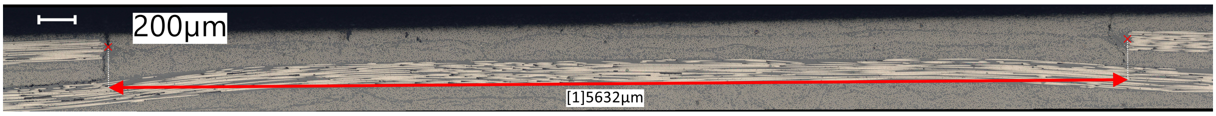

(c) Specimen 5 from side B.

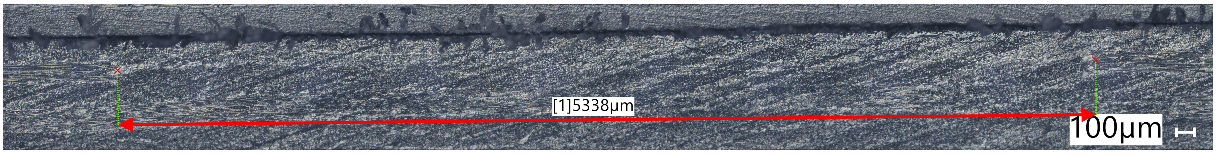

(d) Specimen 26 from side B.

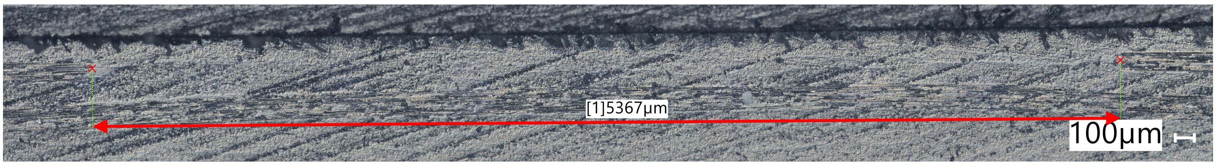

(e) Specimen 25 from side B.

Figure C.2: Cross section of top 5 Specimens Side B.

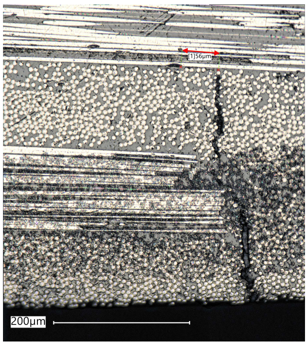

(a) Crack in Specimen 24 from side A.

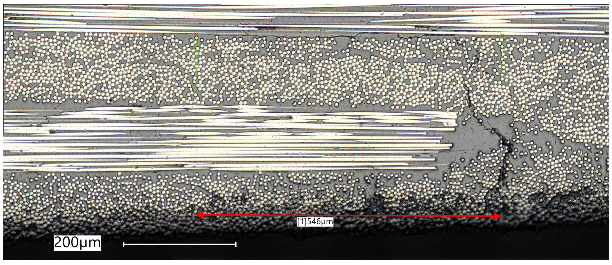

(b) Crack in Specimen 27 from side A.

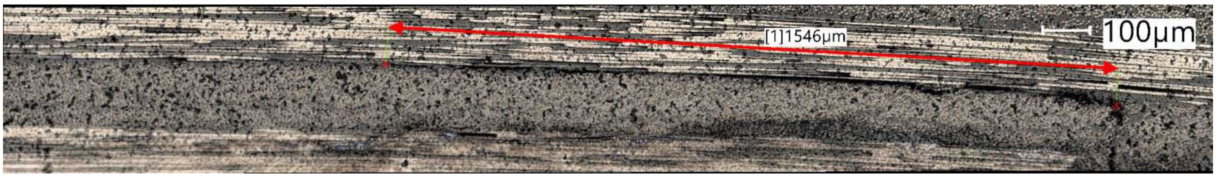

(c) Crack in Specimen 5 from side A.

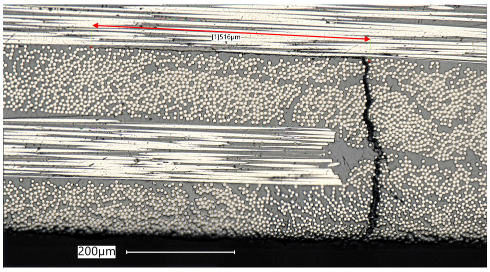

(d) Crack in Specimen 26 from side A.

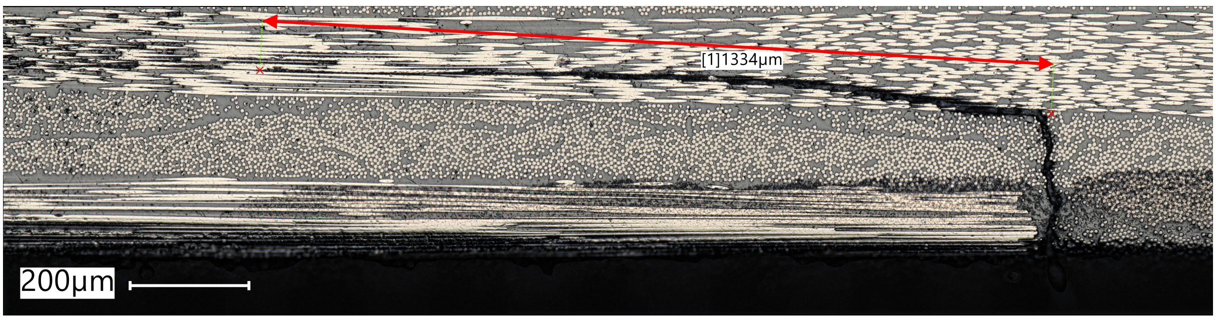

(e) Crack in Specimen 25 from side A.

Figure C.3: Cracks in top 5 Specimens Side A.

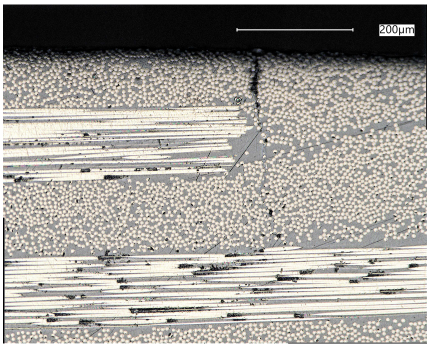

(a) Crack in Specimen 24 from side B.

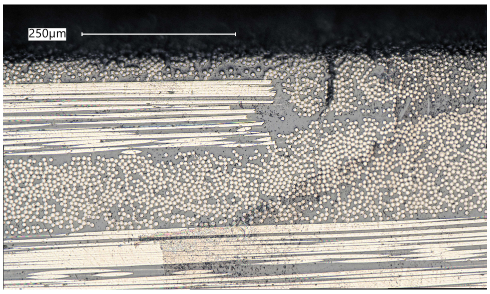

(b) Crack in Specimen 27 from side B.

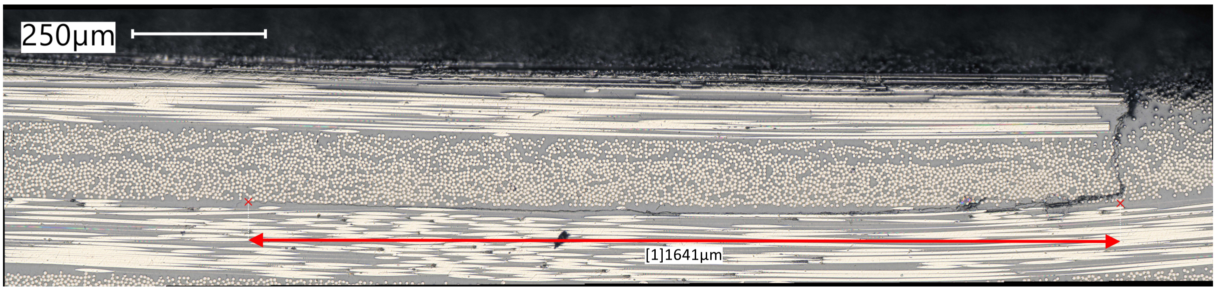

(c) Crack in Specimen 5 from side B.

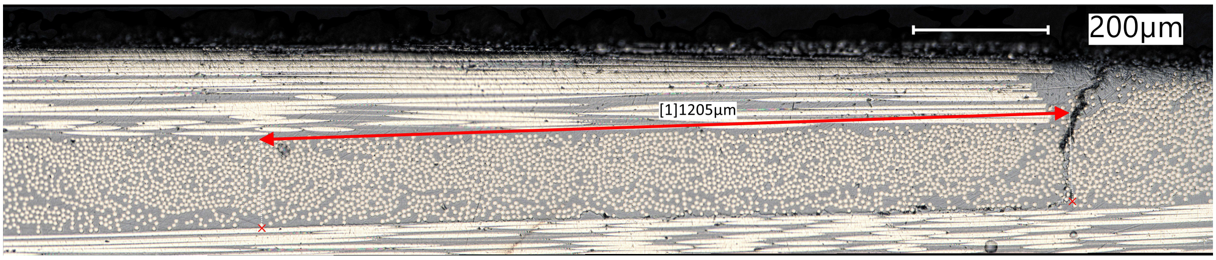

(d) Crack in Specimen 26 from side B.

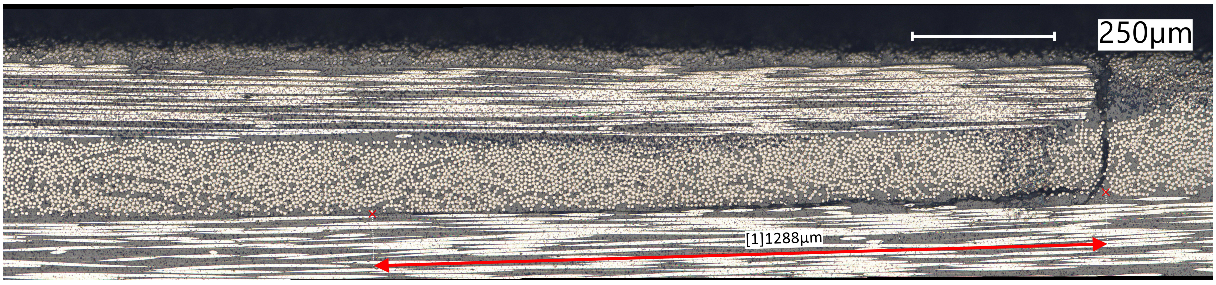

(e) Crack in Specimen 25 from side B.

Figure C.4: Cracks in top 5 Specimens Side B.

(a) Crack in Specimen 24 from side A $1mm$ into the specimen.

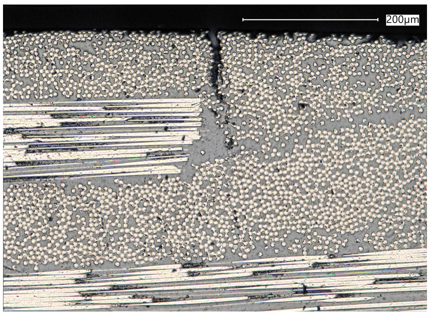

(b) Crack in Specimen 24 from side B $1mm$ into the specimen.

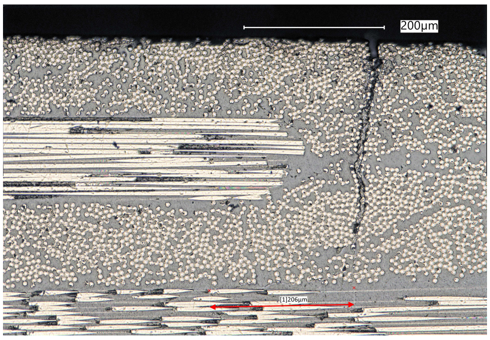

(c) Crack in Specimen 27 from side B $1mm$ into the specimen.

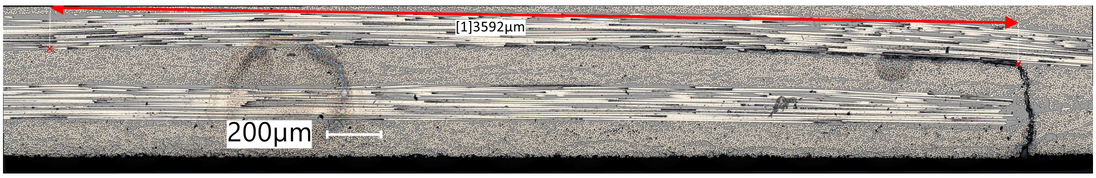

(d) Crack in Specimen 5 from side A $1mm$ into the specimen.

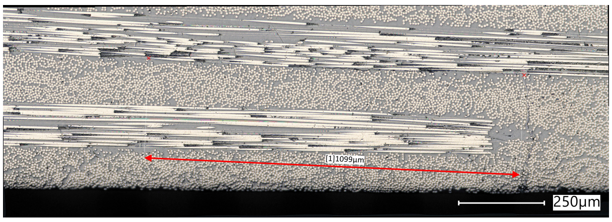

(e) Crack in Specimen 26 from side A $1mm$ into the specimen.

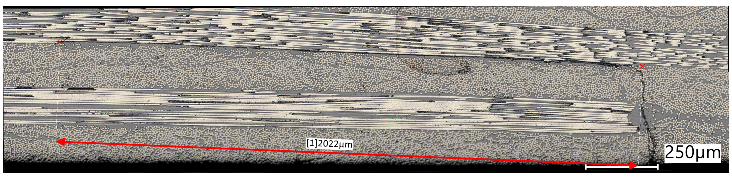

(f) Crack in Specimen 25 from side A $1mm$ into the specimen.

Figure C.5: Additional crack length inspections on the top 5 specimens.